GEOELECTRICAL SOUNDING AND ITS APPLICATION IN THE THEISTAREYKIR HIGH-TEMPERATURE AREA, NE-ICELAND

Domingo B. Layugan[+],
UNU Geothermal Training Programme,
National Energy Authority,
Grensásvegur 9, 108 Reykjavík,
Iceland

[+]Permanent address:
Philippine National Oil Company,
Energy Development Corporation,
Merritt Road, Fort Bonifacio,
Makati, Metro Manila,
Philippines

ABSTRACT

A brief review is given on the basic principles of the geoelectrical sounding method, the parameters that affect the resistivity of rocks and the various techniques of interpretation of resistivity data. An attempt is also made to discuss some limitations of the geoelectrical sounding method such as topographic effects, coastal effects, and the limits of resistivity modelling.

To get acquainted with the practical application of the method the author participated in the measurement of 7 D.C. Sclumberger soundings in the Theistareykir high temperature area, NE-Iceland. These soundings and 30 older soundings from the same area were interpreted to delineate areas of possible geothermal exploitation. Five of the latest soundings were designed for two-dimensional modelling, but other soundings were interpreted with an automatic one-dimensional modelling program. The role of geological concepts proved very valuable in the entire process of resistivity interpretation.

The interpreted resistivity models define a 6-8 km^2 low resistivity anomaly ($<15\Omega m$) and relatively highly resistive surrounding rocks ($\gtrsim 1000\Omega m$). These two resistivity features and the large contrast between them indicate the presence of a geothermal system in the Theistareykir area.

TABLE OF CONTENTS

LIST OF FIGURES

1 INTRODUCTION

The author was awarded a United Nations University Fellowship to attend the UNU Geothermal Training Programme at the National Energy Authority in Iceland for six months in 1981. The first month was devoted to a series of introductory lectures on a wide range of topics related to geothermal energy. After that the author received practical training in geophysical exploration with special emphasis on geoelectric methods. The author also participated in a two week field excursion to all the main geothermal fields in Iceland. He further participated in installing a microearthquake monitoring system in a high-temperature field and was introduced to the principal aspects of seismic monitoring of geothermal fields (2 weeks).

The author received specialized training in geophysical exploration with emphasis on the D.C. Schlumberger geoelectric sounding method. This included lectures and practical exercises on: 1) the theoretical aspects of geoelectrical sounding (2 weeks), 2) methods of interpretation of sounding data (2 weeks), and 3) case histories of geophysical exploration with electrical methods (1 week). The author participated in the measurement of 7 D.C. Schlumberger soundings with an exploration team from Orkustofnun (NEA) in the Theistareykir high-temperature area, N.E. Iceland, (2 weeks). These soundings as well as 30 older soundings from the area form the data base for the authors research project report. The author spent about two moths on interpreting the data and writing this report.

The report deals with the general aspects of the geoelectrical sounding method, and its application in the Theistareykir geothermal area, NE-Iceland.

2 GEOELECTRICAL SOUNDING IN GEOTHERMAL EXPLORATION

2.1 Introduction

The geoelectrical sounding method using the direct current resistivity techniques plays an important role in geothermal exploration and assessment. Its wide applicability to geothermal exploration has been successful because of the dependence of the electrical resistivity on the rock porosity and temperature and resistivity of the fluid in the rocks.

In recent years, advances have been made in the interpretation of sounding data to obtain quantitatively the resistivity distribution of the earth - from the graphical method employing curve matching techniques to the more recent numerical methods with the aid of computers.

There are other factors that influence the sounding measurements which are not the direct effect of the resistivity of rocks. Such factors as topographic and coastal effects should be included, when necessary, in the interpretation process of sounding data. Even with the use of modern-day computer techniques,which allows a comprehensive physical interpretation of resistivity measurements, there are still handicaps in resistivity modelling due to the fundamental limits of the resistivity method.

2.2 Basic principles of electrical resistivity

2.2.1 Ohm's law, resistivity and conductivity

Ohm's law defines the resistance of a specimen of a material to a current flow when a potential difference is applied across it. It is given by the relation:

$$V = I\,R \qquad (1)$$

where V = potential difference or voltage drop

I = current

R = resistance

Related to the resistance is the resistivity which is a characteristic of a material rather than that of a particular specimen. For a conducting cylinder which has a length L and a cross-sectional area A the resistance R is depentent on the resistivity ρ in the following way:

$$R = \rho \frac{L}{A} \qquad (2)$$

The unit of resistivity is usually given in ohm-meters (Ωm), while conductivity, the inverse of resistivity ($1/\rho$), is in siemens or in mho-meters.

2.2.2 Resistivity measurements; the Schlumberger electrode configuration

Consider that a direct current of strength I is introduced into a homogeneous and isotropic earth by means of two point electrodes A and B. The potential difference between the two points M and N on the surface is given by:

$$\Delta V = \frac{I\rho}{2\pi} \left\{ \left(\frac{1}{AM} - \frac{1}{BM}\right) - \left(\frac{1}{AN} - \frac{1}{BN}\right) \right\} \qquad (3)$$

where ρ is the resistivity of the ground. Thus, the resistivity of the homogeneous earth can be determined from the measurements on the surface.

Various electrode arrangements for A, B, M, and N have been suggested for the purpose. The ones more commonly used for resistivity (or geoelectric) sounding are: (1) symmetrical arrangement, and (2) dipole arrangement.

In the symmetrical arrangement, the points A, M, N, B are taken on a straight line such that the points M and N are symmetrically placed about the centre O of the "spread" AB. An example of this is the Schlumberger electrode configuration shown in Fig. 1. The current electrodes (A and B) are expanded away from the center of the array to force the current to penetrate deeper into the earth.

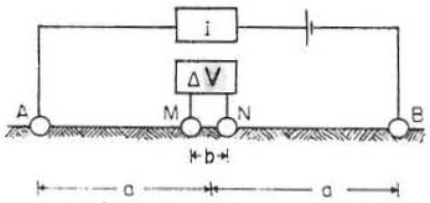

Fig. 1 The Schlumberger electrode configuration.

As stated above the true resistivity of a homogenous earth can be determined from (3). However, the earth is not homogenous and consists of different resistivity structures each having some arbitrary shape and resistivity. Then (3) gives the so-called apparent resistivity, ρ_a, which is dependent on the true resistivity distribution of the earth and also on the electrode separation. It is a resistivity which represents the medium probed with that particular electrode separation. It is not an average resistivity of the resistivity structures being probed but the concept of averaging is useful for the pictorial understanding of what happens.

In the case of Schlumberger configuration, (3) can be written as

$$\rho_a = \frac{\Delta V \cdot \pi}{I} \left(\frac{a^2}{b} - \frac{b}{4} \right) \qquad (4)$$

where ΔV = measured potential drop
I = amount of current transmitted
a = half the current electrode spacing (or AB/2)
b = the potential electrode spacing (or MN).

When $a >> b/4$ (in practice when $2a \geq 5b$) this can be simplified to:

$$a = \frac{\pi \cdot \Delta V a^2}{I\, b} \qquad (5)$$

The apparent resistivity data is plotted graphically (usually on a double logarithmic graph) as a function of half the current electrode spacing, AB/2. These graphs can then be interpreted either analytically or graphically to yield the true resistivity distribution of the earth.

2.2.3 Fundamentals of geoelectrical sounding

The purpose of resistivity sounding is to investigate the distribution of earth resistivities as a function of electrode separation and therefore of depth.

To appreciate the principles of geoelectrical sounding let us consider Fig. 2. It illustrates a two-layered geologic body having resistivities ρ_1 and ρ_2, where $\rho_2 >> \rho_1$. The two media are separated by a horizontal interface to a depth h.

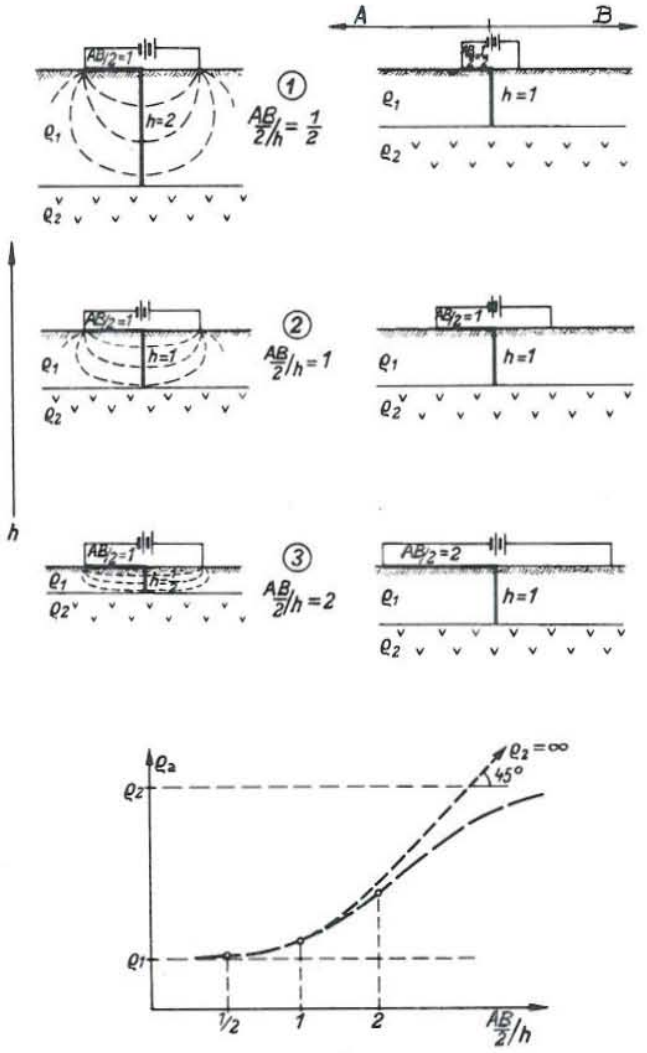

Fig. 2. The fundamental principle of electrical sounding (Flathe 1976).

On the left hand side of the figure (assuming $\rho_2 = \infty$, i.e. insulator) as h becomes small, while electrode separation AB remains constant, the current density j on the surface increases. A proportional relationship exists between j and the quotient AB/h. The potential difference ΔV, measured from the two potential electrodes located at the center of the electrode configuration, is proportional to j and also proportional to the apparent resistivity ρ_a. Apparent resistivity is related to the current density as a function of the quotient AB/h.

On the right hand side of the figure, depth, h, is fixed as the current arm, AB/2, is expanded. We obtain the same quotient AB/h on both sides of the figure which implies that from the change of current density, j, on the surface, expressed as the apparent resistivity, ρ_a, we can determine the depth, h, of the interface between layers of the given geologic body by the process of "pulling up the underground" when the current electrode separation is progressively enlarged. The graph (in a log-log scale) showing the apparent resistivity as a function of $\frac{AB}{2}/h$ (AB/2 is a convention from Schlumberger) presents this phenomenon. The apparent resistivity (given that $\rho_2 >> \rho_1$) increases when the quotient $\frac{AB}{2}/h$ is large. Conversely, where $\rho_1 > \rho_2$ the apparent resistivity of the second layer decreases gradually until at some great electrode separation, when most of the current will be flowing through the second layer, the apparent resistivity will asymptotically approach the resistivity of the second medium.

2.3 Factors affecting resistivity of rocks

The electrical resistivity of rocks depends on a number of parameters such as temperature, porosity and texture of rocks, salinity of the interstitial fluid and the degree of desaturation of the pore space. The combination of these factors or set of factors enhances the resistivity contrast between the rocks in the geothermal system and the surrounding rocks. However, some of these parameters may not contribute to the causes of anomalously low resistivities that often, but not always, characterize geothermal reservoirs. Thus, it is important to discriminate and separate, if possible, certain factors which are the direct causes of the low resistivity generally associated with geothermal environment.

2.3.1 Temperature

Electrical conductivity of electrolytes increases in an exponential fashion with temperature, at temperatures which are below about 250°C (Meidav 1980). It is notable that the mobility of ions is dependent on the temperature and concentration of electrolytes. A rise in the temperature of an electrolytic solution decreases the viscosity and hence leads to an increase in the mobility of ions. On the other hand, a high concentration of ions in a solution reduces the mobility due to the interaction between ions, i.e., the motion of ions will be influenced by the motion of ions close to it.

Fig. 3 shows the resistivity of a weak electrolyte as a function of temperature and pressure. An abrupt drop of resistivity of the solution is manifested for temperatures up to approximately 250°C. Near and above the critical temperature at 374°C the resistivity of the electrolyte increases with temperature. This is caused by the large decrease in the dielectric characteristics of water, causing reduction in polarization of the water molecules. High pressure would tend to compensate this phenomenon (Meidav 1980).

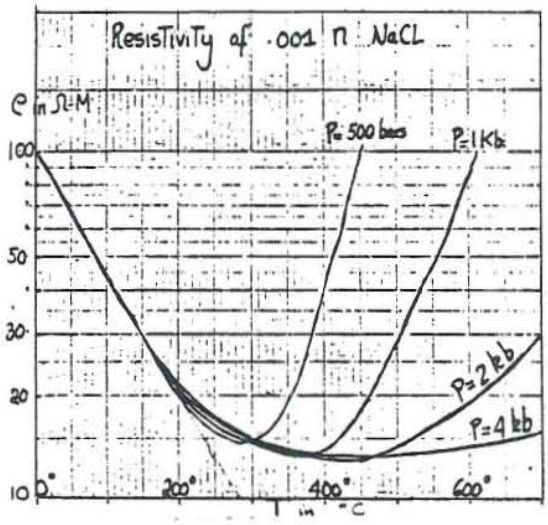

Fig. 3. The effect of temperature and pressure variations on the resistivity of a dilute electrolytic solution (Meidav 1980).

The relationship between the resistivity, ρ, of the rock saturated with an electrolyte, and temperature has been approximated by (Dakhnov 1962).

$$\rho = \frac{\rho_{18^\circ}}{1 + \alpha_t \, (t - 18^\circ C)} \qquad (6)$$

where ρ_{18° = resistivity in Ωm measured at the reference temperature

t = the ambient temperature in °C

α_t = the temperature coefficient of resistivity, usually 2.5%/°C for most electrolytes.

In geothermal systems the effect of temperature variations is greatest at low temperatures, less than 100°C, and becomes small above 200°C. Hence, porosity and salinity are the prevailing factors affecting resistivity rather than temperature in the deeper parts of a reservoir (Pálmason 1975).

2.3.2 Porosity and texture of rocks

Porosity occurs as intergranular, jointed, vesicular and vugular texture in hydrothermal environment. The pore space provided by these rock textures permits the storage of fluid saturating the rocks where electrical conduction is carried out.

The effect of porosity on resistivity of fluid saturated rocks has been described by an empirical function known as Archie's law which states that the resistivity varies approximately as the inverse power of porosity. This relationship is given by the equation

$$\rho = a \, \rho_w \, \Phi^{-m} \qquad (7)$$

where ρ = the bulk resistivity of rock

ρ_w = the resistivity of water (or fluid) filling the pore space

ϕ = fractional porosity

a = a number near unity

m = a constant which is nearly 2 in many rocks, but varies from 1.2-1.5 in noncemented, well-sorted sediments, to about 3.5 for older, well-cemented or crystalline rocks. It is sometimes called "the cementation factor" (Meidav 1980).

Equation (7) indicates that the ratio of bulk resistivity to water resistivity should be a constant for a given porosity and should not depend on the resistivity of the water in the rocks assuming constant temperature (Keller and Frischknecht 1966). This is referred to as the formation factor (F) as shown in the equation

$$F = \rho/\rho_w = a\,\Phi^{-m} \qquad (8)$$

According to Duba et al. (1978) this empirical formula is valid when the fluid resistivity is $\geq 1\Omega m$ but not for fluids with resistivity $\geq 100\Omega m$.

The above empirical formula has been translated by Meidav (1970) into a nomogram (Fig. 4) relating fractional porosity to formation factor, for any given value of m.

2.3.3 Salinity of the interstitial fluid

A relationship exists between the salinity of the electrolytic solution and its resistivity. Fig. 5 presents the effect of salinity of sodium chloride solution on resistivity at various temperatures. As the temperature is elevated from 0 to 140°C the conductivity of sodium chloride increases about sevenfold. (The higher temperatures in the range of 100-140°C are accompanied by sufficiently high pressures to keep water in liquid state.)

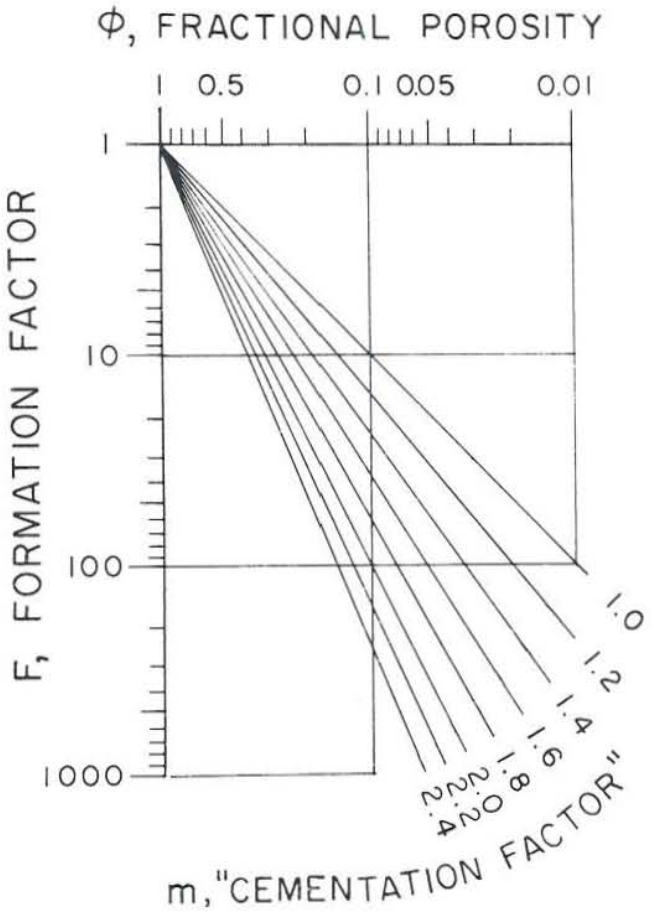

Fig. 4. Nomogram for determination of any of the three parameters which affect the electrical properties of the rock, when any two of these are known (Meidav 1970).

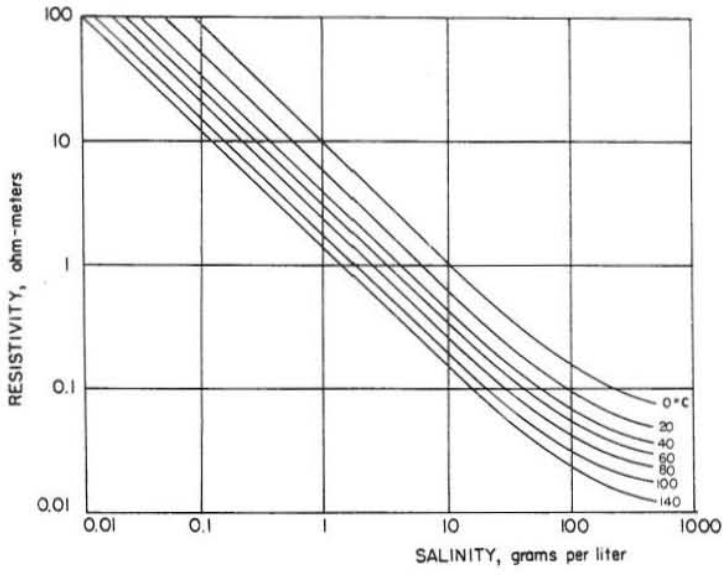

Fig. 5. The dependence of resistivity on salinity of sodium chloride at various temperatures (Keller and Frischknecht 1966).

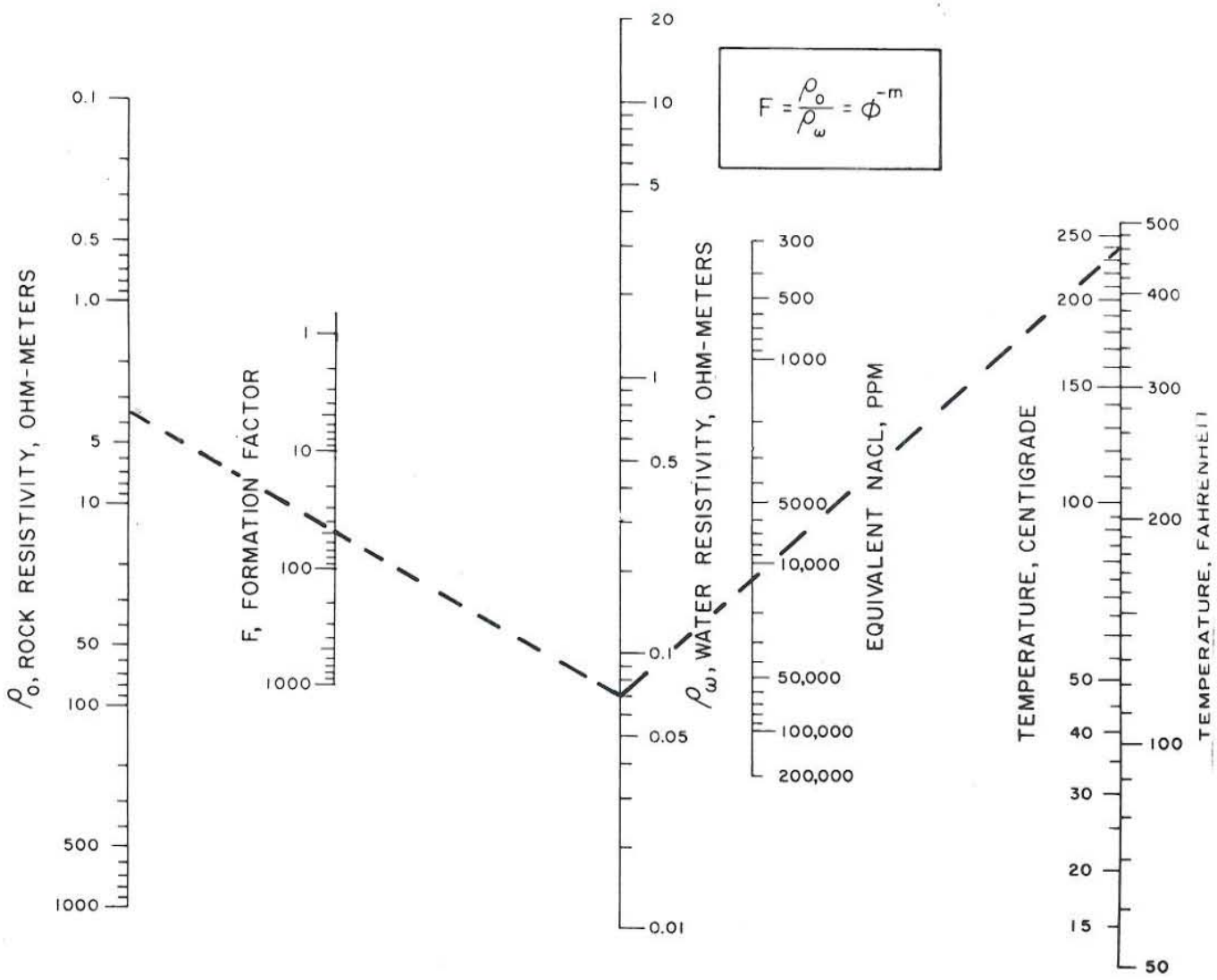

Fig. 6. Resistivity, formation factor, salinity, temperature nomogram. Anyone of these parameters may be determined if the other three are known. Dashed lines illustrate the use of the nomogram with values, as example, from measurements conducted in Svartsengi geothermal area (modified after Meidav 1970).

Graphical relationship between rock resistivity, temperature, porosity and salinity of pore fluid is shown in Fig. 6 (Meidav 1970). The nomogram (right-hand side) consists of the interaction between water resistivity, salinity and temperature. The three left-hand side scales relate rock resistivity, formation factor and resistivity of the saturating fluid. This figure is a nomographic solution of equations (6) and (7) when combined.

A typical example of the use of these equations/nomograms was illustrated by Georgsson (1979) in his resistivity measurements at the Svartsengi geothermal field located at the tip of southwestern Iceland (see Fig. 19). He demonstrated that the temperature drop from 240°C within the field to 40°C surrounding the field reflected resistivity contrast of 3.5 Ωm to 10 Ωm inside and outside the reservoir, respectively. From these calculations, he concluded that the true resistivity in the geothermal area is mainly dependent on salinity, temperature and porosity.

2.3.4 Desaturation effects

Vapor-dominated geothermal systems are characterized by higher resistivity than the surrounding, somewhat colder rocks. The relatively high resistivity values are attributed to the desaturation of pore space of rockgrains with dry steam. However, low resistivity anomalies are sometimes attributed to the caprock above the dry steam layer of the vapour dominated system, as in the case of the Kawah Kamojang geothermal field (Hochstein 1970).

2.3.5 Interaction of factors affecting the resistivity of rocks in a geothermal environment

Interaction of the above factors in a geothermal environment poses a difficult task on the part of the exploration geophysicist. How can he be able to isolate one factor or group of factors from the others with the help of his resistivity measurements in order to explain the amplified resistivity contrast between the reservoir and the relatively colder and fresher surrounding rocks ?
In the proven economic geothermal fields in the Tongonan, Wairakei,

Svartsengi, the Geysers, Kawah Kamojang etc., a remarkable correlation hasbeen revealed between the resistivity anomaly and the occurrence of of exploitable heat.

Meidav (1980) has summarized sets of conditions that characterize geothermal systems which are best detected by electrical resistivity surveys:

a) For a resistivity ratio greater than 1:5 between a geothermal reservoir (typically $\leq$ 5 Ωm) and the surrounding regions:

   1. the reservoir is liquid-dominated
   2. reservoir temperatures are often greater than 220°C
   3. the depth to the production zones is less than or equal to 2 km.

b) For higher resistivity of reservoir rocks against lower values related to the surrounding area:

   1. the reservoir is vapor-dominated
   2. temperature of reservoir approaches and/or surpasses the critical temperature, i.e. greater than 300°C.
   3. reduction of or considerable loss of porosity due to self-sealing.

The striking difference in the resistivity of geothermal and non-geothermal environment may be due to the following factors:

a. Salinity of the saturating fluid in reservoirs increases with elevated temperatures due to the greater dissolving power of hotter water. This phenomena is supported by the presence of large amounts of total dissolved solids in geothermal reservoirs.

b. Hot fluids dissolve some minerals and drive them away from the central portion of the reservoir resulting in a greater porosity in the heart of the convective geothermal system.

c. The enhancement of the overall conductivity of the rock mass can be explained by the hydrothermal alteration of igneous rocks into clays and zeolites.

2.4 Methods of interpretation of Schlumberger geoelectrical sounding curves

The aim of the interpretation of the geoelectrical sounding data is to determine the resistivity distribution of different layers from the study of the sounding field curves. The first phase of the interpretation is to convert the apparent resistivity versus the electrode spacing graph into a calculated resistivity and thickness of layers or the "true resistivity" distribution of the earth. This analytical and/or graphical interpretation of the field measurements into an electrical resistivity model of the subsurface which agrees with the observed apparent resistivity values at the earth's surface is then correlated with the geological structure of the area under investigation. The interpretation of the soundings is based on the assumption that the subsurface consists of a sequence of distinct layers of finite thickness (the deepest layer extends to infinite depth) separated by horizontal boundary planes; each of these layers is assumed to be electrically homogeneous and isotropic. For the above conditions, the method of interpretation is said to be one-dimensional and can be accomplished through whole curve matching, partial curve matching with the help of sets of auxiliary graphs, forward modelling and inverse modelling. For a two-dimensional interpretation technique, the modelling is based on the specification similar to that of a one-dimensional case except that the effects of lateral resistivity variations or vertical boundaries of different resistivities are considered, the third dimension of the geological body is assumed to extend infinitely.

2.4.1 Complete curve matching

The technique in the interpretation of the data is done by a visual comparison of the apparent resistivity data versus the electrode separation with the apparent resistivity curves computed for assumed models of stratification. When a good fit is found, the ratio of the thickness of layers with different resistivity and the ratio of the resistivity of layers can be read from the master curves. The resistivity of the first layer (which is the actual value read from the graph and considered as the true resistivity of the topmost layer at short electrode spacings) is multiplied to the ratio of the first-to-second layer to obtain the resistivity of the second layer. This process can be repeated between the second and the third layer. The same procedure is applied to determine the thickness of the layers.

Several albums of the three and four layer families of curves published by Orellana and Mooney (1966), the Netherlands Rijkswaterstaat 1968) and other earlier master curves have been available over the years. Example of a three-layer family of curves is shown in Fig. 7.

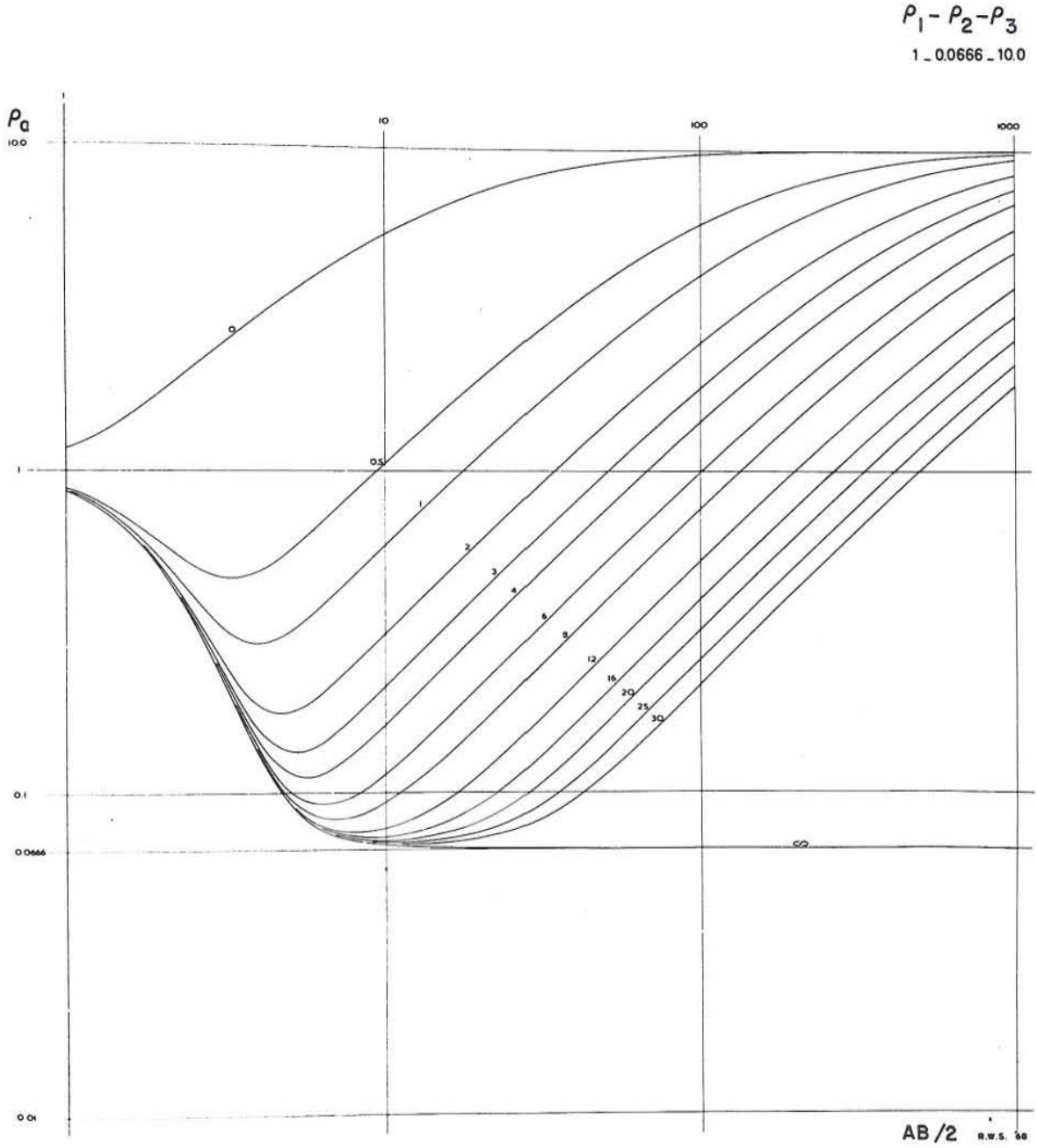

Fig. 7 Example of a three-layer family of curves used for complete curve matching. The parameter at each curve indicates the ratio between thickness of the second layer and the first layer. (The Netherland Rijkswaterstaat 1968).

2.4.2 Partial curve matching: the auxiliary point method

The method is based on the use of auxiliary curves (Fig. 9) in conjunction with two-layer resistivity model curves (Fig. 8). (The use of three-layer model curves is also found to be useful).

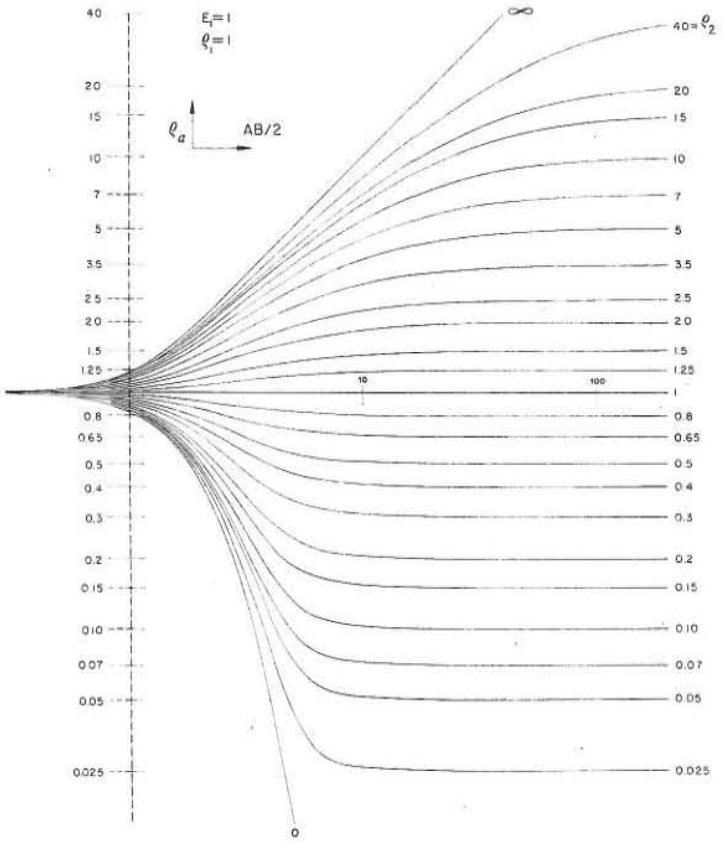

Fig. 8. Two-layer resistivity model curves (Orellana and Mooney 1966).

Since complete curve matching seldom works for more than three layer situations (due to the number of infinite permutations of different resistivities and thickness combinations), the auxiliary point method has been developed to decompose a graph of any number of layers into a set of sequential two-layers.

The set of auxiliary graphs (Fig. 9) are designed for each of the four possible combinations of resistivity layering in a three-layer case. The auxiliary curves are:

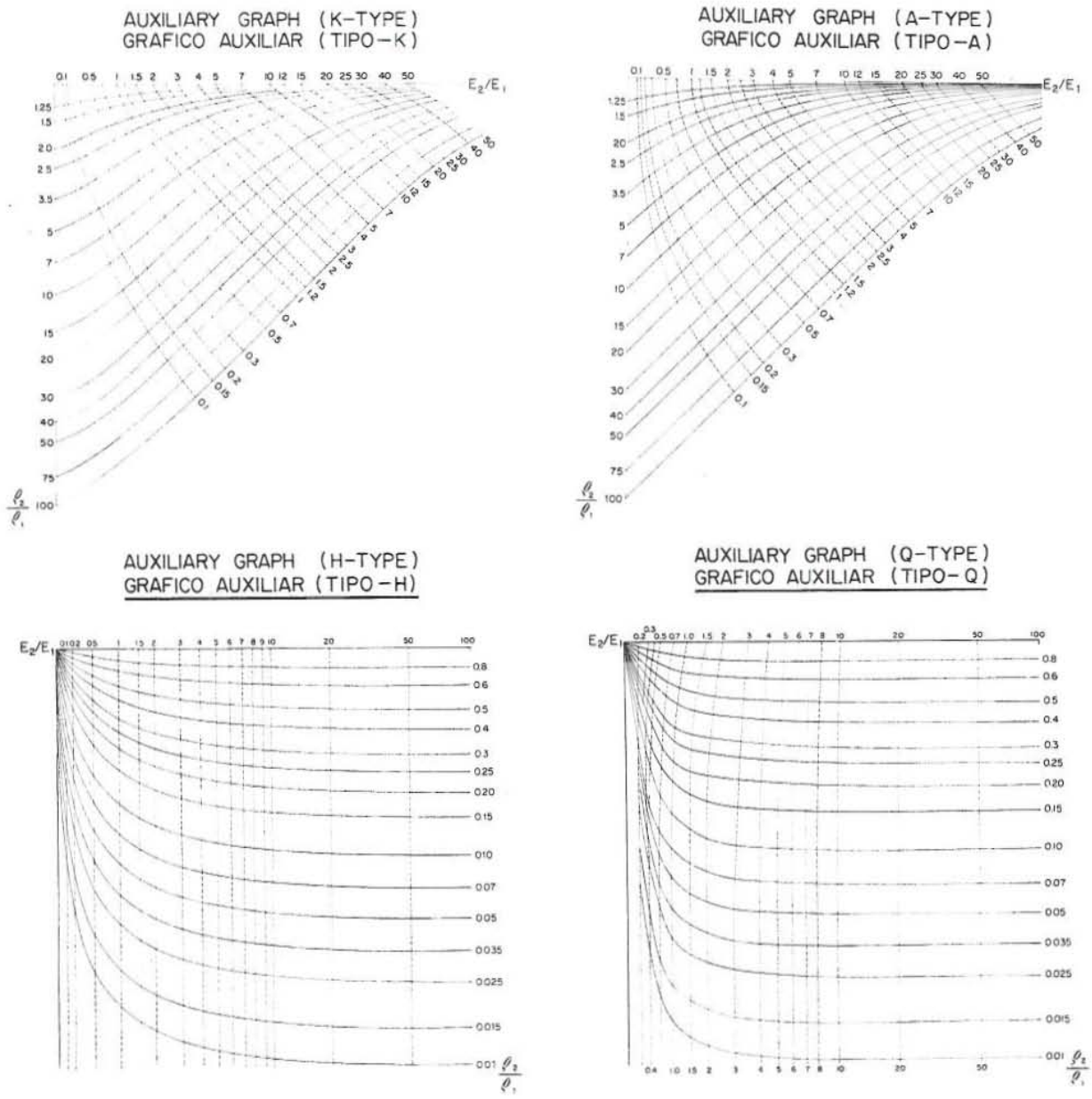

Fig. 9. The auxiliary graphs (Orellana and Mooney 1966).

K-type (maximum)	$\rho_1 < \rho_2 > \rho_3$
H-type (minimum)	$\rho_1 > \rho_2 < \rho_3$
A-type (double ascending)	$\rho_1 < \rho_2 < \rho_3$
Q-type (double descending)	$\rho_1 > \rho_2 > \rho_3$

The mechanics of using this method is discussed in the books by Orellana and Mooney (1966), Bhattacharya and Patra (1969), Koefoed (1979) and in other publications.

2.4.3 Forward modelling

The method is a trial-and-error approach where a geologically relevant starting model specifying the number of layers and the resistivity and thickness of these layers is fed into the computer. The resultant potential field is calculated from the starting model giving the theoretical apparent resistivity values which are compared with the field data. If the agreement between the two sets of data is unsatisfactory, then the parameters of the layer model are adjusted by the human interpreter. The process may require several iterations until a sufficient fit between the model data and the field data is attained. A graphic-display terminal can be used for visual comparison between the field curves and the calculated apparent resistivity values. A sample computer output of one-dimensional forward modelling is given in Appendix II. It shows an adjustment on the originally proposes model (based on curve matching techniques) to yield a satisfactory fit.

The curve matching techniques may be used to provide approximation of the thickness and resistivity parameters for the starting model. This helps to reduce the number of necessary iterations in the interpretation process. This starting procedure could also be applied to inverse modelling technique.

2.4.4 Inverse modelling

Unlike in the forward modelling technique, where the iterative process is done by the human interpreter, inverse modelling makes use of the computer to decide the adjustment of the layer parameters of the model. Based on the starting model from which theoretical apparent resistivity values are calculated, the computer does the comparison between the field data and the apparent resistivities derived from the model. The iterative process is continous until the overall difference between the sums of squares of deviations of the theoretical curve and the

field curve in the last two iterations is reduced by less than 0.1%. This stop criterion (difference < 0.1%) is determined by the human interpreter because electronic computers are unaware of reasonable limits on characterizing the physical parameters of the derived models.

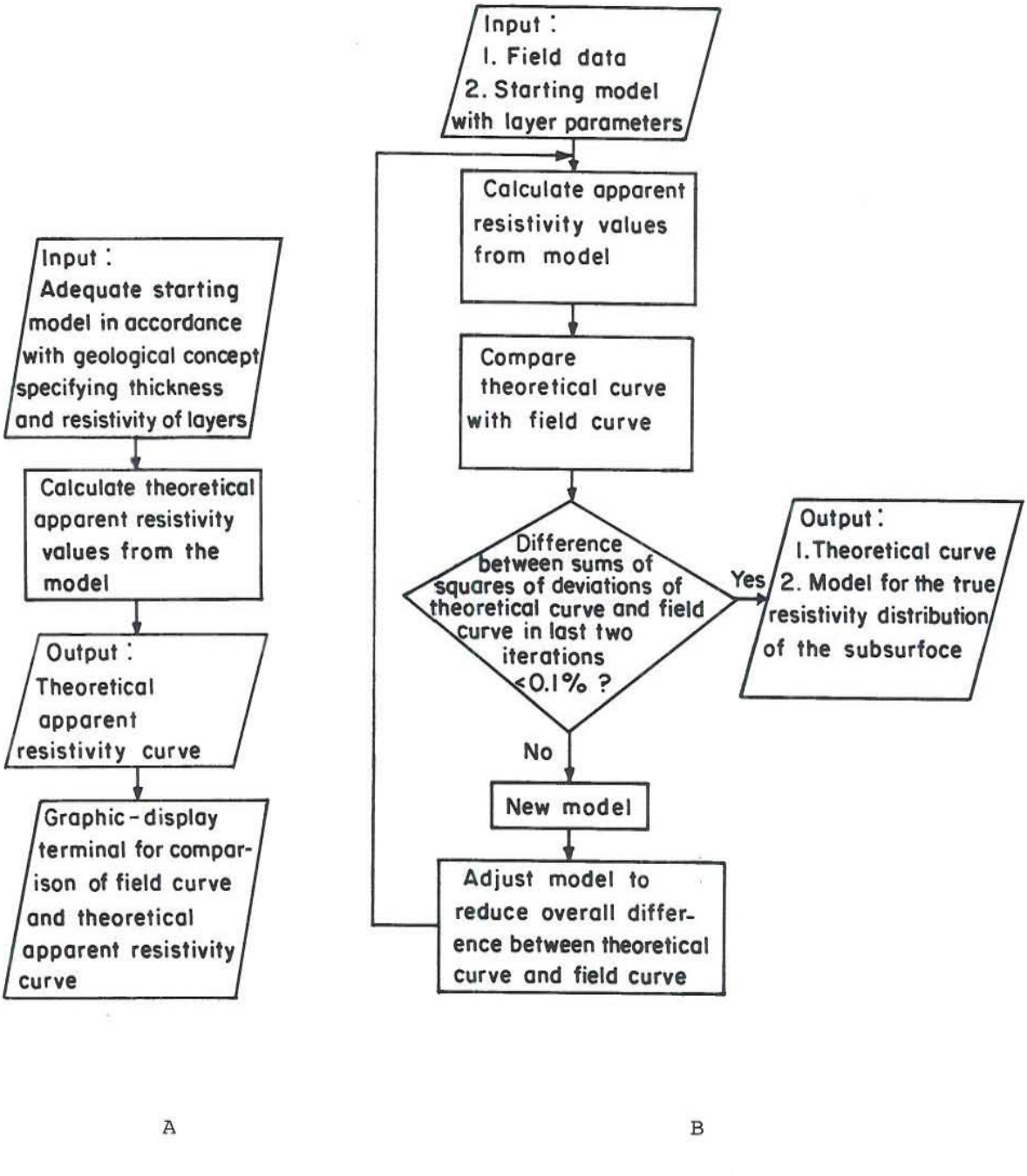

Fig. 10. A flow-chart showing A: the sequence of operations in forward modelling interpretation for one- and two-dimensional cases, B: the inverse modelling technique (Circle2 program) for one-one-dimensional case.

Fig. 10 shows the comparison between the sequence of operations employed in both forward modelling (one- and two-dimensional cases) and the inverse or automatic iterative interpretation for a one-dimensional situation.

2.4.5 Two-dimensional interpretation

In a two-dimensional case, the physical properties of the earth change in two dimensions but stay constant in the third dimension. The interpretation of the sounding field data makes it possible to determine lateral heterogeneities or vertical boundaries of different resistivities of the earth. Fig. 11 shows the values of resistivity ratios μ as a function of the azimuth angles at 0°, 45° and 90°. These apparent resistivity curves have been derived for Schlumberger sounding measurements near a vertical contact separating two media of distinct resistivities. The azimuth angle γ is the angle made by the sounding line and the surface trace of the vertical contact (Fig. 12). The theoretical sounding curves indicate that for a given azimuth angle, γ, the form of a sounding curve varies considerably more as a function of resistivity ratio when μ is less than unity than when μ is larger than unity. The sounding curves for a given value of γ are almost identical for values of $\mu \geq 20$. For values of $\mu << 1$, the theoretical sounding curves are significantly distinct from one another when μ is changed, especially at small values of γ.

Forward modelling techniques can be employed in the interpretation of two-dimensional earth structure. The technique is the same as described in chapter 2.4.3.

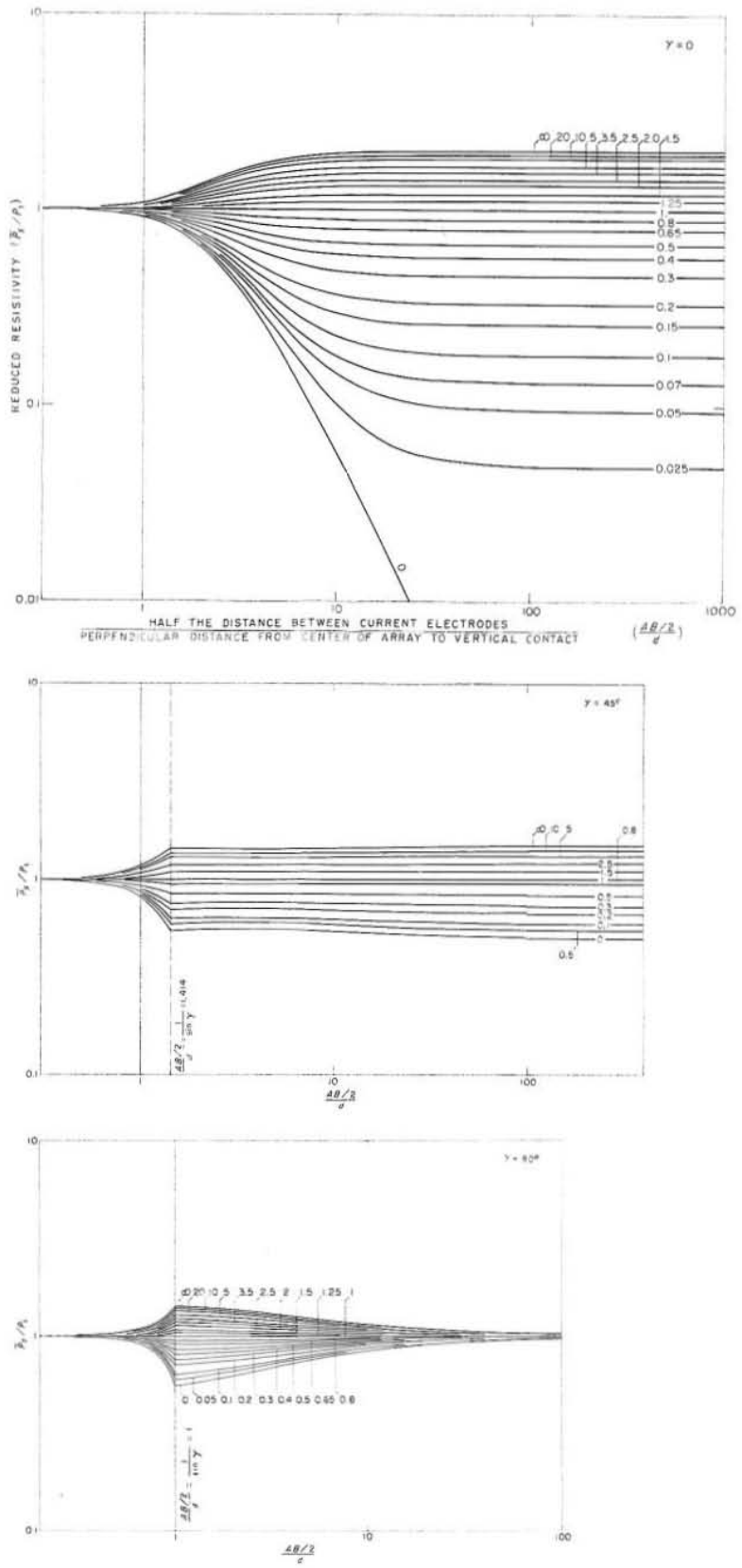

Fig. 11. Theoretical curves for Schlumberger soundings near a vertical contact for various values of resistivity ratios as a function of the azimuth angle (Zohdy 1970).

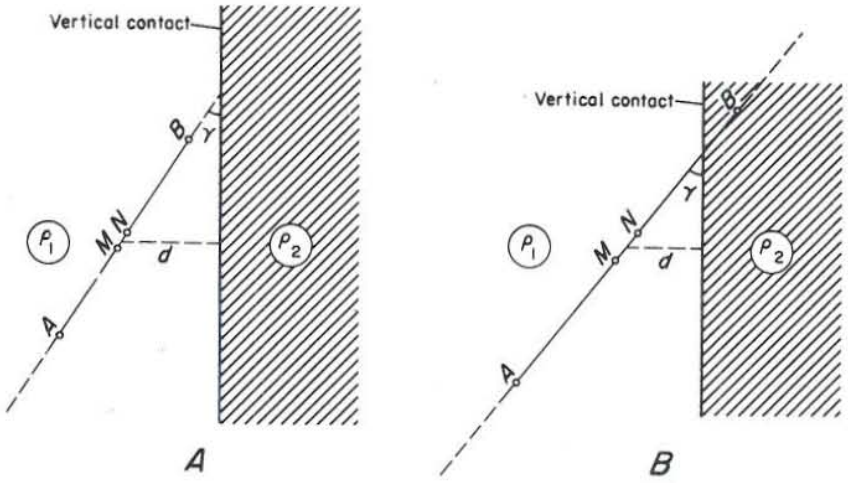

Fig. 12. Placement of electrodes (A, M, N, and B) in relation to a vertical contact separating two media (ρ_1 and ρ_2) of different resistivities; d, perpendicular distance from the center of the array to the vertical contact. A, All electrodes on same medium of resistivity (ρ_1); B, three electrodes on one medium of resistivity (ρ_1), and one electrode on second medium of resistivity (ρ_2) (Zohdy 1970).

2.5 Limitations of the resistivity sounding method

2.5.1 Topographic effects

Since most of the electrical resistivity surveys are conducted in mountainous terrains where most high-temperature geothermal areas occur (Philippine geothermal fields, Kawah Kamojang, the Geysers etc.), knowledge of the nature of these effects and their inclusion in the interpretation models are important. Treatment of the raw resistivity data obtained from these rugged areas could produce topographic-related anomalies that may lead to ambiguities in the interpretative models if one does not take into account the significance of topographic effects.

Topographic effects are geometric effects which are inherent to the relative locations of the current and potential electrodes and the nature of the terrain itself where resistivity survey lines are carried out. Because of these conditions, current flow lines are distorted

with corresponding effect on equipotential lines. This results in the alteration of the actual current and voltage readings which can be critical to field measurements and data interpretation.

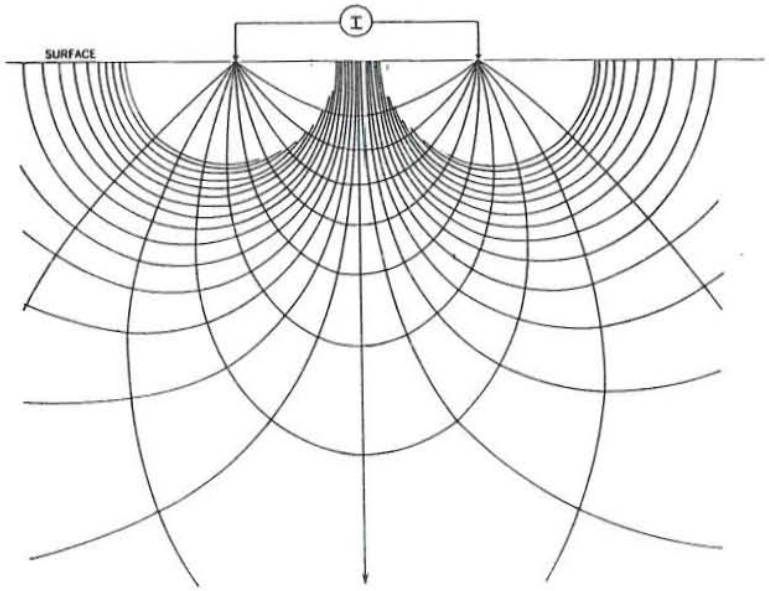

Fig. 13. Current flow and equipotential line configuration through a homogeneous flat earth created by a dipolar electric field.

Fig. 13 shows the undisturbed current flow and equipotential lines of a dipolar electric field for a homogeneous flat earth. The effect of a hill and a valley on the distribution of current flow and equipotential lines due to a distant current source in a homogeneous earth is shown in Fig. 14. Across a hill, a zone of current dispersion and a corresponding divergence of equipotential surfaces normal to the current flow are created, therefore producing a low apparent resistivity. On the other hand, current flow lines tend to concentrate beneath a valley, allowing equipotential surfaces to converge, thus the apparent resistivity will seem to be higher than the true resistivity.

Topographic effects are uniquely related to the particular electrode arrangement used.

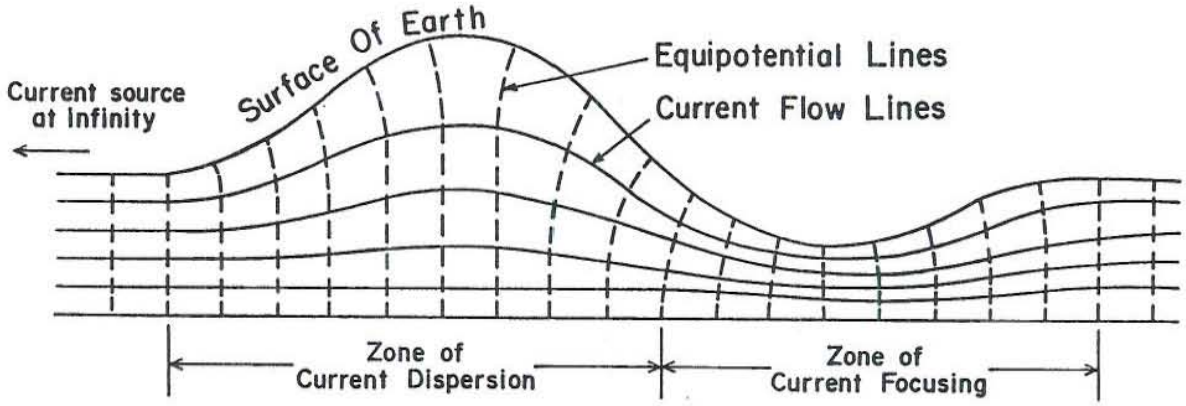

Fig. 14. Current flow and equipotential line distribution accross a hill and beneath a valley (Fox et al. 1978).

Fig. 15 shows an example of a high-angle ridge sloping downwards on both sides. Measurements for both dipole-dipole and Schlumberger arrays will result in different voltage readings at the given current electrode position. (In the case of a dipole-dipole survey, at receiving dipole where current focusing occurs, an increased potential difference V_1 arises. Conversely, potential difference V_2 decreases due to current dispersion. While in the Schlumberger electrode configuration, where the potential drop is measured at the center of the array, a relatively small effect on the voltage drop V is produced in this particular situation.)

The nature and significance of topographic effect - resistivity anomalies have been studied by Fox et al. (1978). In their experiments they used a two-dimensional, finite element computer technique for analysing the nature of these anomalies, correcting apparent resistivity data for topographic effects and incorporating topography in the interpretative models. They have published computer-generated models for various terrain situations on a valley, a ridge and a slope employing an inline dipole-dipole electrode array.

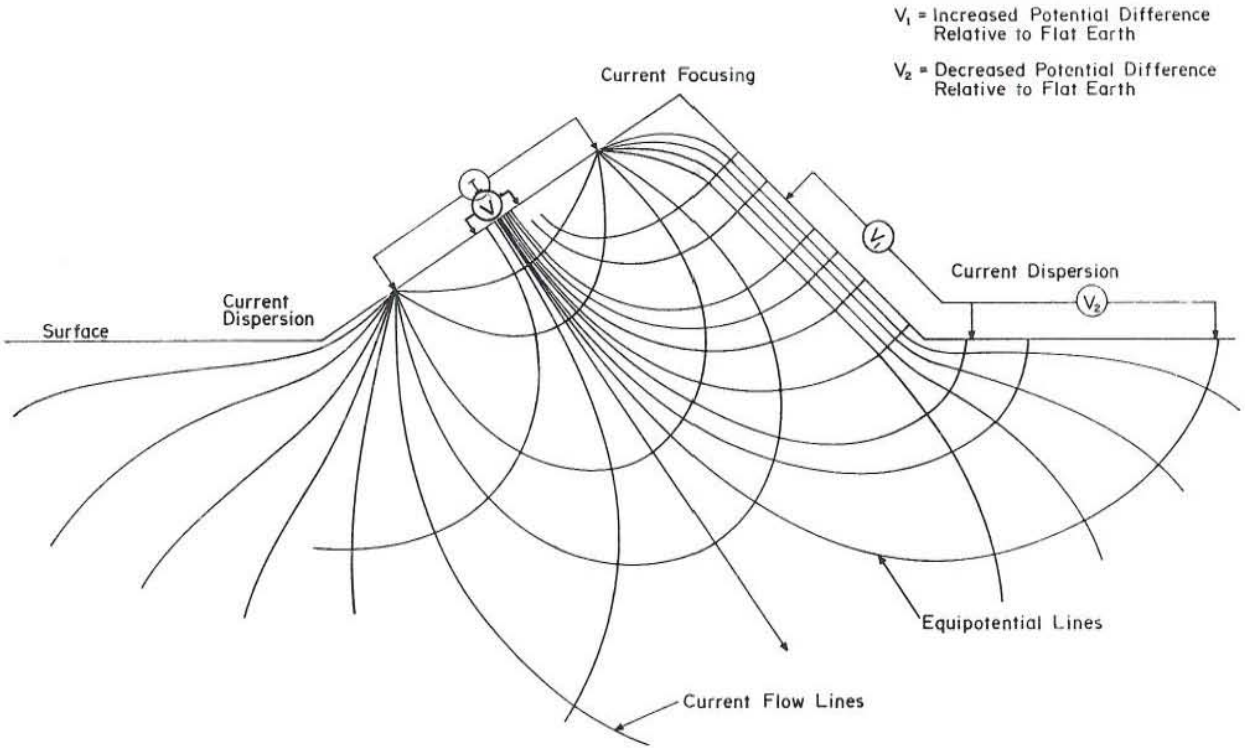

Fig. 15. Current focusing and dispersion produced on a ridge at a given current electrode position; V_1 and V_2 are voltage readings for dipole-dipole array, V for Schlumberger array (Modified after Fox et al. 1978).

2.5.2 Coastal effects

Geoelectrical resistivity soundings have been performed on land close to coastlines in Southern Africa along the Indian Ocean (Blohm et al. 1977), Maui Island, Hawaii (Mattice and Lienert 1980), Biliran Island, Philippines (Layugan 1981) and along fjords in Iceland (Georgsson, pers. comm.). Most of these vertical electrical soundings, either conducted parallel or perpendicular to the coastline, showed the influence of the highly conductive seawater (res. approx. 0.2 Ωm) on the resistivity field data. Therefore, it is worhwhile to correct these apparent resistivities before translating them into true resistivities of the rocks.

Mundey and Worzyk (1979) proposed a model consisting of a perfectly conducting, thin semi-infinite sheet, lying on the surface of a homogeneous earth (Fig. 16) to estimate the effect of the low resistivity ocean on a geoelectrical sounding measured near a coastline (the influence of seawater intrusion into the rocks is not considered in the model). They give model curves of the apparent resistivity for soundings located parallel or perpendicular to the edge of the coast. From these model curves it is possible to determine resistivity curves for other current and potential electrode arrangements. In a Schlumberger sounding configuration the corrected apparent resistivities, ρ_c, are given by (Mundrey and Worzyk 1979).

$$\rho_c = \frac{2\,\rho a}{\pi} \tan^{-1}(2b) + \frac{2b}{1+4b^2} \qquad (9)$$

for soundings parallel to the coast and;

$$\rho c = \frac{\rho a}{\pi} \tan^{-1}\left(\frac{\sqrt{b+1}+\sqrt{b-1}}{1-4b\sqrt{b^2-1}}\right) \frac{\sqrt{1-1/b}}{2b-1} + \frac{\sqrt{1+1/b}}{2b+1} \qquad (10)$$

for soundings perpendicular to the coast,

where ρa = the apparent resistivity

b = ratio of the distance, D, to the coast from the center of the array to AB/2 (Fig. 16).

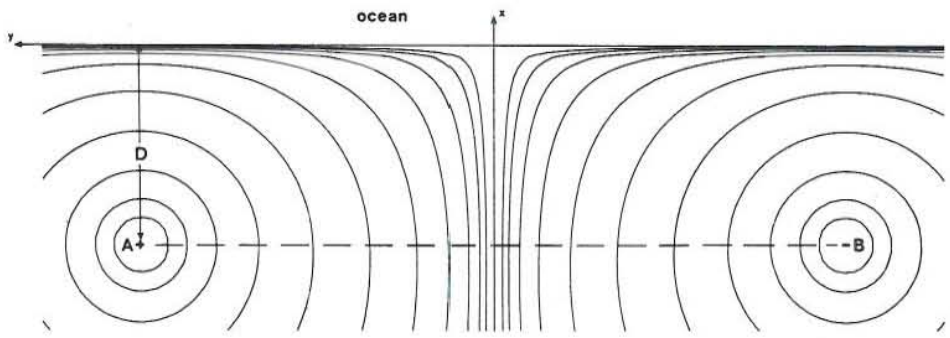

Fig. 16. Behavior of equipotential lines on the surface of the earth ($z = o$) for two current electrodes near an infinitely thin and infinitely conducting sheet ($x > o$) over a homogeneous half-space. The potential lines are disturbed considerably only immediately near the coast (Mundrey and Worzyk 1979).

2.5.3 Limits of resistivity modelling

Interpretation of a sounding field curve may yield several resistivity models of the earth. Fig. 17 shows a field curve which when seen at first glance seems to represent a four-layer case consisting of a dominating maximum and a double descending branch. However, this could also give an interpretation of three other models such as 5-, 6- and 12-layer cases. The deviation of the four theoretically calculated values of apparent resistivity from the measured data is ± 5%. This deviation is within the limits of the accuracy of the measured data.

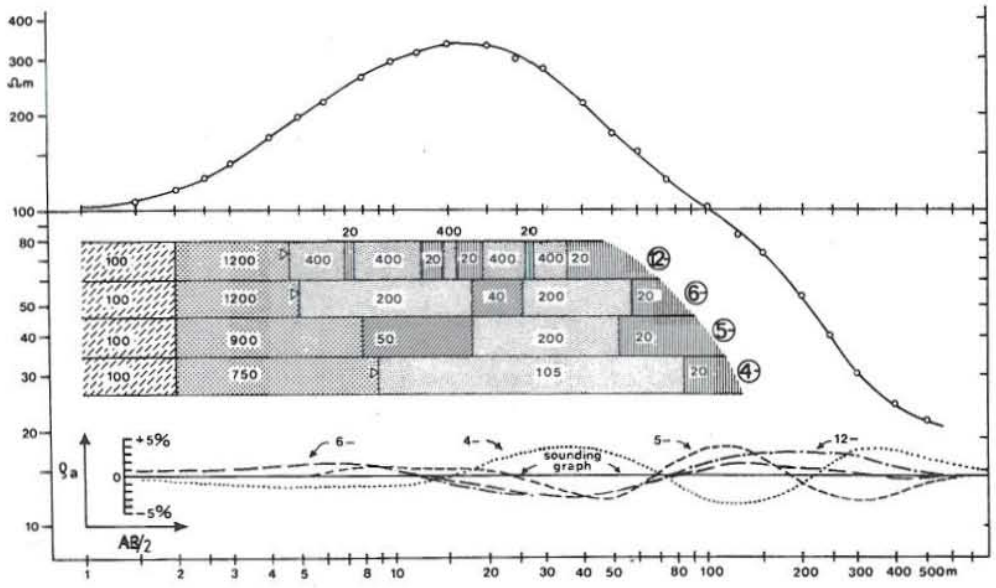

Fig. 17. Geoelectrical sounding graph ρ_a (AB/2).
The vertical profiles plotted in logarithmic scale (using the AB/2-scale as depth scale simultaneously) and provided with the layer resistivities in Ω m represent equivalent interpretations as 4-, 5-, 6- and 12-layer cases. The deviation of the theoretically calculated values of ρ_a from the measured data (in %) is given at the bottom of the diagram (Flathe 1976).

The above example illustrates the mathematical - physical aspect of the interpretation, i.e. from the field data to layer model parameters. The question arises: What would be the correct solution from among the four possible models ? To solve this problem the role of a geological concept is indispensible in translating the physical results into geological facts. The interpretation of sounding curves should not depend largely on the modern computer techniques. Rather the dialogue of the geophysicist and his computer should be replaced by the collaboration between the geophysicist and the geologist to overcome the difficulties arising from the fundamental limits of the resistivity interpretation.

3 D.C. SCHLUMBERGER RESISTIVITY SURVEY OF THE THEISTAREYKIR GEOTHERMAL AREA, NE-ICELAND

3.1 Introduction

Direct current Schlumberger resistivity data from the Theistareykir geothermal area in NE-Iceland, were collected in three separate field seasons. From the summers of 1972, 1973 and 1981 there are 17, 13 and 7 vertical electrical soundings, respectively. Areal coverage of the resistivity survey is approximately 100 km^2, mainly focused on the center of the active thermal area of Theistareykir and its vicinity. The location of the soundings and resistivity cross-sections are shown in Fig. 18.

The sounding measurements were performed to delineate areas of geothermal significance for more detailed exploration and for possible development and exploitation. Several other exploration methods have been applied in the area to date, such as detailed geological mapping (1973 and 1981), an aeromagnetic survey (1974), gravity measurements (1981) and chemical analyses of gas samples collected from the surface thermal manifestations present in Theistareykir (1972, 1973 and 1981).

This chapter deals with the interpretation of electrical sounding data from the Theistareykir area A resistivity model is presented and its geothermal implications discussed.

3.2 Geology

3.2.1 Regional geologic setting

Iceland is the exposed part of the northernmost extension of the Mid-Atlantic Ridge which is the boundary between the Eurasian and the American plates. It is composed of a thick pile of almost entirely Cenozoic basalts with some 10% of acid and intermediate rocks (Saemundsson 1979) that have been accumulated by the continuous volcanism from Miocene to the present. The most recent volcanic activity in the country

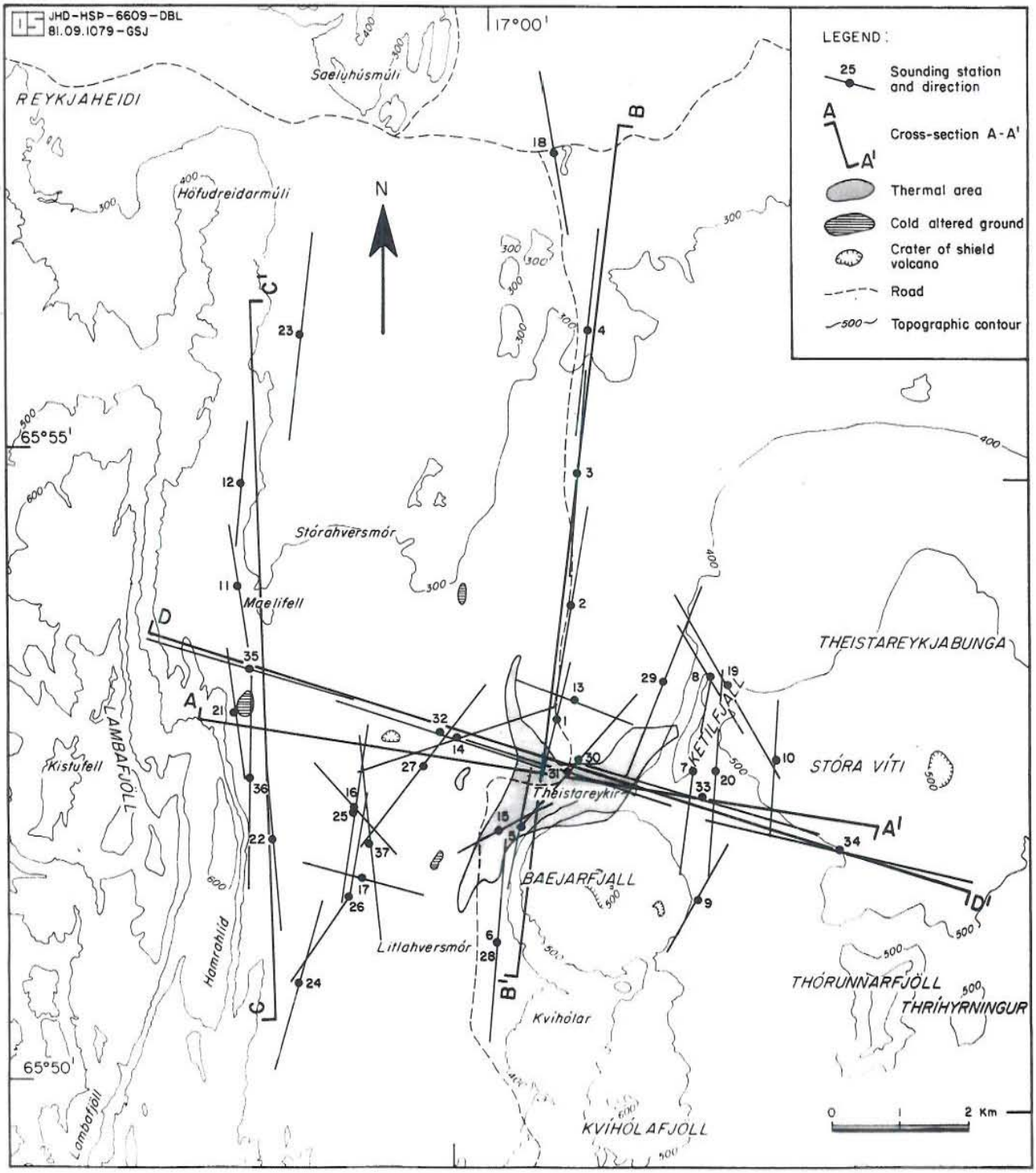

Fig. 18. Station location map of the geoelectrical soundings

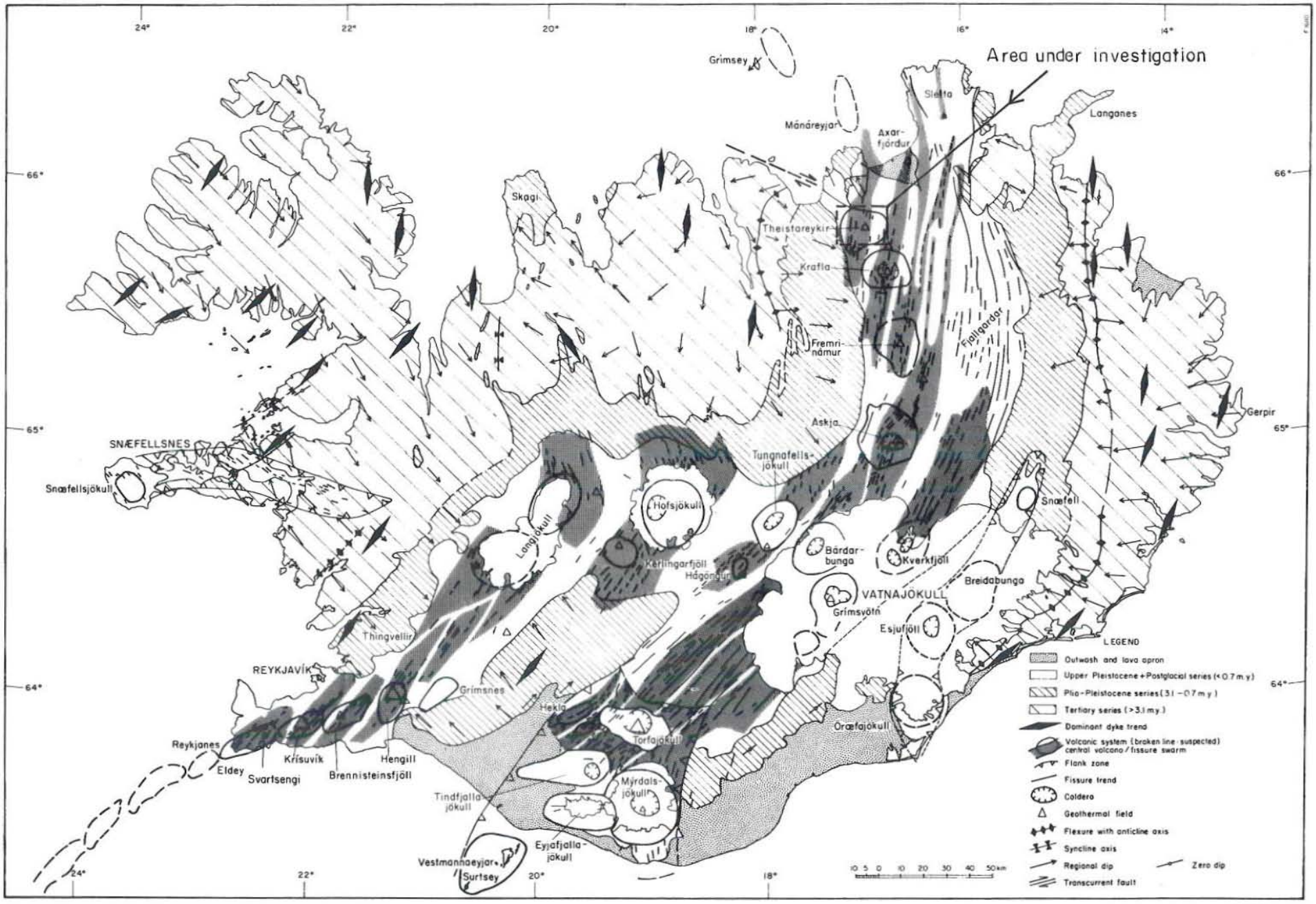

Fig. 19. Tectonic map of Iceland (Saemundsson 1979)

is exhibited in the Krafla geothermal area, NE-Iceland, where the current rifting episode has been active since 1975.

The active zone of rifting and volcanism, the so called Neovolcanic zone, crosses Iceland from the Reykjanes Ridge in the south-west to the Kolbeinsey Ridge in the north. The Neovolcanic zone is flanked by strips of Quarternary volcanics and below them are Tertiary flood basalts, which increase in age symmetrically away from the active zone (Saemundsson 1979). The Neovolcanic zone is predominantly characterized by fault- and fissure-swarms, and active volcanism. Central volcanoes are formed on the fault- and fissure-swarms where the lava production is highest. These sites are also commonly characterized by the presence of acid rocks and high-temperature geothermal fields (Saemundsson 1978). Fig. 19 presents a tectonic map of Iceland.

3.2.2 Local geologic setting

The Theistareykir geothermal area is situated in the northernmost part of the Neovolcanic zone (Fig. 19). The area under investigation is dominated by NNE-SSW striking tectonic and eruptive fissures which have been active in Upper Pleistocene (<0.7 m.y.) and Postglacial (last 9.000 to 13.000 years) time (Gronvold and Karlsdottir 1975). The Upper Pleistocene volcanic activity yielded early and late hyaloclastites of subglacial origin and interglacial lavas. A rhyolite dome (Maelifell) has been extruded during that time and is exposed about 6 km northwest of the Theistareykir thermal area. Unconsolidated deposits in the form of sand and gravel, found in the western part of the Theistareykir area, are of Late Pleistocene age. During Postglacial time lava shields produced basaltic lava flows. The youngest lava flow is younger than 2000 years, erupted from Stórihver volcano with extremely fresh lava surface and little soil cover, mostly moss. A map showing the geology of Theistareykir is presented in Fig. 20 (Gronvold and Karlsdottir 1975).

The surface manifestations of the active thermal area of Theistareykir (Fig. 18) are characterized by steaming vents, boiling mudpools and highly altered ground (Gronvold and Karlsdottir 1975). The thermally altered ground covers an area slightly less than 4 km^2. Spots of cold altered ground are also present in the vicinity of the area, especially in its western part.

3.3 Measurement Techniques and Methods of Instrumentation

The direct current geoelectrical sounding method using the Schlumberger electrode configuration was used in the resistivity surveys carried out in the Theistareykir area. Most of the 17 soundings performed in 1971 utilized a maximum current electrode arm (AB/2) of 900 m, and the measurement data points of each sounding were relatively dense. In the following year, the current electrode spacing was revised reaching to about AB/2 = 1500 m to achieve a greater depth penetration of the current into the ground; likewise the number of sampling points of resistivity data in a sounding was reduced. During the fieldwork in the summer of 1981, a maximum current arm of AB/2 = 1580 to 2000 m were applied with 10 measuring points spaced evenly on a logarithmic scale per each decade. This has been the standard procedure practiced in geoelectrical soundings conducted in Iceland during the last couple of years. Of the 7 soundings performed this year 5 were designed for two-dimensional interpretation. For this purpose sounding lines were positioned perpendicular to the general trend of the geologic structures present in Theistareykir area. All the field work has been conducted by exploration teams from the Geothermal Division of Orkustofnun (NEA). The author participated in the field work in 1981.

Any unreliable resistivity data recorded during the field measurements could impair the entire process of resistivity interpretation. Thus, obtaining good quality field data (at least within a reasonable range of error) is the most critical factor in the geoelectrical sounding process. The following are some practical points observed in the field that are worth considering while performing sounding measurements:

a. Care should be taken in the selection of location for the potential electrodes on the ground to avoid where near-surface in homogeneities may occur. The equipotential surfaces could be distorted by these, which would alter the voltage readings recorded during the entire measurements of the sounding.

   These inhomogeneities can be effectively detected if the sounding measurements are started at AB/2 = 100 m with different potential electrode spacings, say at 0.2 , 2.0 and 20 m (see Appendix I for sample of field data). If variations in the apparent resistivity

obtained at these different potential electrode spacings are small, then the sounding can proceed by restarting measurements at AB/2 = 1.00 m up to the desired maximum current electrode separation. Otherwise, another site should be selected for the center of the entire electrode system (near the intended location of the sounding station).

Flat grounds are preferable for positioning the potential electrode spread to avoid distortion of equipotential surfaces.

b. Once in a while during measurements a check of any appreciable current leakage in current wires should be made, especially when these wires are laid on wet ground. This is accomplished by disconnecting one of the current wires from its electrode. Current is then sent out and if a considerable amount of current is recorded, current leakage may be suspected (this procedure should be done for both electrodes A and B). In that case, current wires must be verified and repaired for any damage.

c. The contact between the cable reels containing the current wires and the ground (especially when wet) can also be a source of current leakage. The detection of this effect could be accomplished by the techniques mentioned in item b. Elimination of this problem could be done by insulating the cable reels with plastic bags (or any other insulating material) or by hanging these reels over wooden sticks.

d. Inhomogeneities may be formed by wire fences or objects that are not visible from the surface such as buried pipelines. Wire fences, owing to their high conductance distort current flow in the ground particularly when they are in good contact to the ground (for example wire fences with metal posts). These effects are reflected in the field curves.

e. While conducting the field measurements, the apparent resistivity recorded at every measuring point should be plotted at once on a double-logarithmic graphing paper. This aids in noting the trend of the sounding curves and at the same time assessing the quality of the data. When necessary during the measurements, these field curves can be interpreted in a preliminary manner by curve matching techniques for translation into layer parameters of the subsurface.

This helps in exercising some geological insights in the initial interpretation, especially when geological features are observed in the neighbourhood of the sounding station.

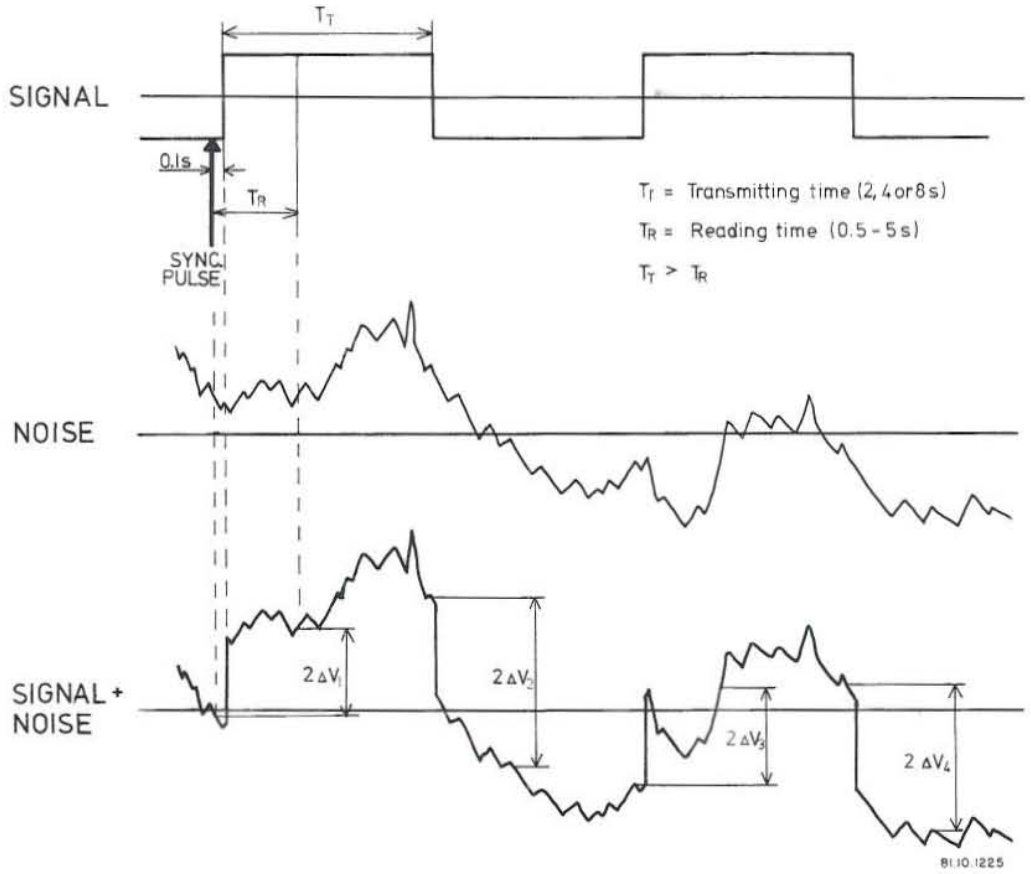

Fig. 21. The detection of the potential difference, ΔV, in no noise and noise cases, when the resistivity instruments are working automatically.

The instruments used in the 1981 survey were greatly improved from those utilized in the previous surveys. The instruments were designed and built at the Orkustofnun (NEA) electrical laboratory in Reykjavík. The set of instruments consists of a power transmitter, a voltage receiver and a data processor. The transmitter, with a maximum power output of 500 W and a maximum voltage of 1000 V, sends out regulated steady current square wave with 2, 4 or 8 seconds (T_T) between polarity changes. The voltage receiver, which can be operated manually or automatically, has a maximum sensitivity of approximately 1 μV and balances out self-potential variations. When operating in the automatic mode the transmitter sends

an optic signal to the receiver just (0.1 seconds) before changing polarity. The receiver's reading period can be varied but is usually kept slightly shorter than that of the transmitter's. Fig. 21 shows the reading period T_R and transmitting time T_T of an ideal no noise signal and a signal plus noise cases. The various voltage readings are automatically stacked in the data processor. The average and standard deviations of the voltage readings can be determined. This makes it possible to get meaningful results beyond the stage when the telluric noise exceeds the signal.

3.4 Modelling Programs

3.4.1 Program CIRCLE2 (One-dimensional case)

An iterative least squares program using singular value decomposition (Johansen 1977) was utilized to interpret the 37 Schlumberger sounding measurements obtained from the Theistareykir high-temperature area. The computer program can calculate the apparent resistivity values from a starting layer-model based on the assumption that the earth is horizontally stratified (see also Chapter 2.4.4). The sequence of operations in the execution of the program is shown in Fig. 10. A sample printout of one of the interpreted Theistareykir soundings (THK04) is given in Appendix II. The sample output includes the field data, the several iterations made to come out with the best solution of the layer model and the theoretical curve. It also shows the extreme parameter sets and the relevant information about the extent of the accuracy of interpreted final model.

One feature of the program is that a layer parameter, i.e. resistivity and/or thickness of any layer in a model can be fixed. The fixed parameter values determined by the human interpreter may be relevant with some geological concepts or simply the values are already known from other studies.

3.4.2 Program DIM-2 (Two-dimensional case)

A finite-difference program (Dey and Morrison 1976; Dey 1976) was used in the interpretation of 5 Theistareykir Schlumberger soundings designed for two-dimensional modelling. The program is capable of modelling resistivity variations in two dimensions with the third dimension assumed to

be infinite. It computes potentials at all nodal points within and on the surface of an arbitrary two-dimensional earth model. The grid network consists of 113 nodes in the x-direction and 16 nodes in the z-direction. A sample printout of a calculated apparent resistivity curve derived from the model of one sounding from Theistareykir (THK 33) is given in Appendix II. The output of the program includes the gridfile which gives information on the grid network, filterpoints, position of the current and potential electrodes, and the given model.

3.5 Interpretation of Resistivity Soundings

3.5.1 One-dimensional interpretation

The location of the resistivity cross-sections is shown in Fig. 18.

Cross-section A-A': The model (Fig. 22) is cut along a 10 km WNW-ESE trending section passing through the active thermal area of Theistareykir. This section includes 12 soundings with the current arm (AB/2) generally extending to 1500-1600 m.

The model defines an almost vertical resistivity "low" of <15Ωm from the top of the thermally altered ground down to a depth of more than 1000 m. The width of the low resistivity zone is about 3 km. A sharp contrast to the east delineates the eastern boundary of the anomaly. To the west, the prominent low to intermediate resistivity units are underlain by a relatively high resistivity formation. This high resistivity is likely to be caused by intrusive rocks which are suspected to be present in the western part of the area. Field curves of soundings 21, 32, 35 and 36 (Appendix I) reflect these resistive bodies as indicated by the increase of apparent resistivity values at depth. The "dry" lavas in the uppermost 100 m (above the groundwater table) are notable by their extremely high ($\gtrsim$ 5000 Ωm) resistivity results.

Cross-section B-B': The section (Fig. 23) runs across the thermal area with a SSW-NNE direction along a 12 km-line. Most of the 10 soundings which are concentrated in the central part of the section have a maximum current arm of about 900 m except for soundings 30 and 31 which reach out to about 1500 m.

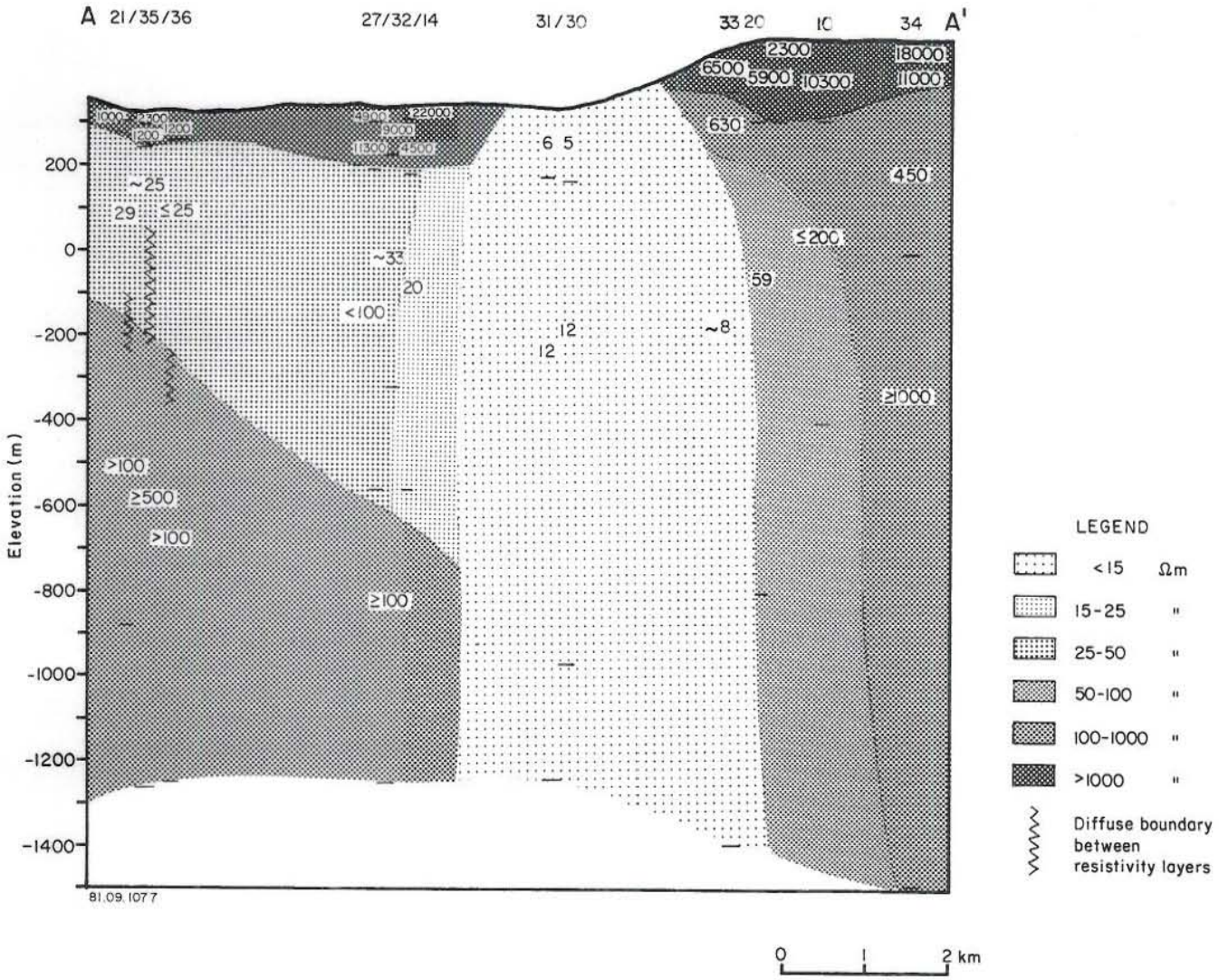

Fig. 22. Interpreted resistivity model along cross-section A-A'.

The low resistivity anomaly of <15Ωm defined in the model is slightly broader than in cross section A-A'. A transitional zone is noted to the north of the anomaly. This may be indicative of a gradual cooling of rocks towards this direction. This is supported by the fact that the general flow of groundwater in the area is towards north. The elongate resistivity pattern to the north also reflects the NNE striking fissures found in the northern part of the resistivity anomaly. This pattern is similarly manifested in the resistivity contour maps at 0 , 300 and 600 m below sea level (Fig. 25, 26 and 27). To the south of the anomaly, the resistivity changes to intermediate values although this boundary is considerably dependent on one sounding (28). However, sounding 6 measured at the same location as sounding 28 also reveals an intermediate to high

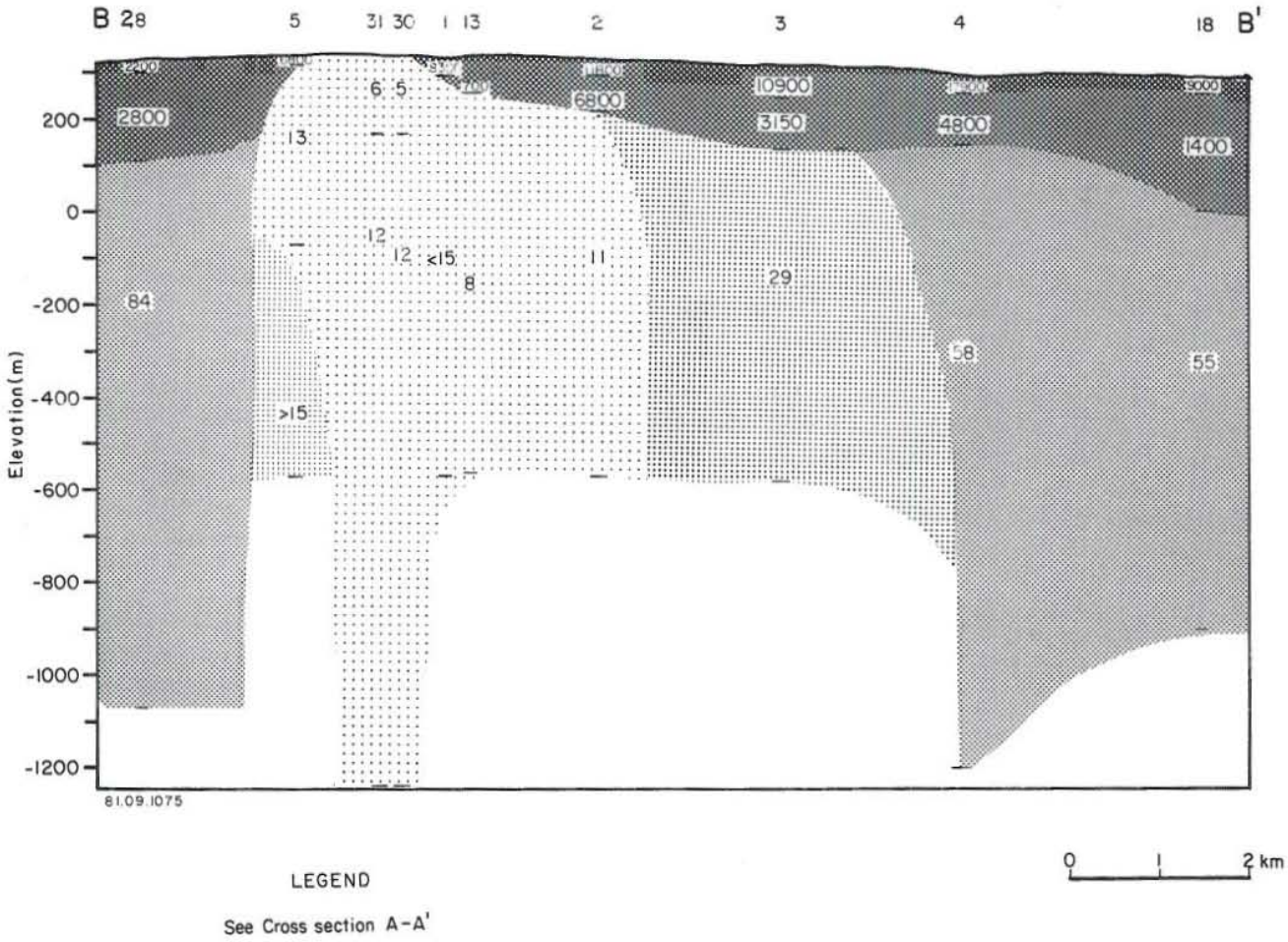

Fig. 23. Interpreted resistivity model along cross-section B-B'

resistivity layer of about 200 Ωm. The basaltic lavas in the uppermost 100 m are compatible with the highly resistive layer of >1000 Ωm.

Cross section C-C': This section (Fig. 24) extends almost parallel to the prevailing trend of faults and fissures in the western part of the area. Spots of cold altered ground are found along this line.

A localized resistivity "low" of about 25 Ωm coincides with the cold altered ground located near sounding 21. A trend of low to intermediate resistivity layers (25-50 Ωm) dip toward south. Diffuse boundaries are noted between these layers and the relatively high values at depth in soundings 21, 35 and 36. The behaviour of these soundings at depth and the likely cause of the relatively high resistivity was pointed out in the discussion of cross-section A-A'. Similarly, lavas of >1000 Ωm resistivity are prevalent on the surface.

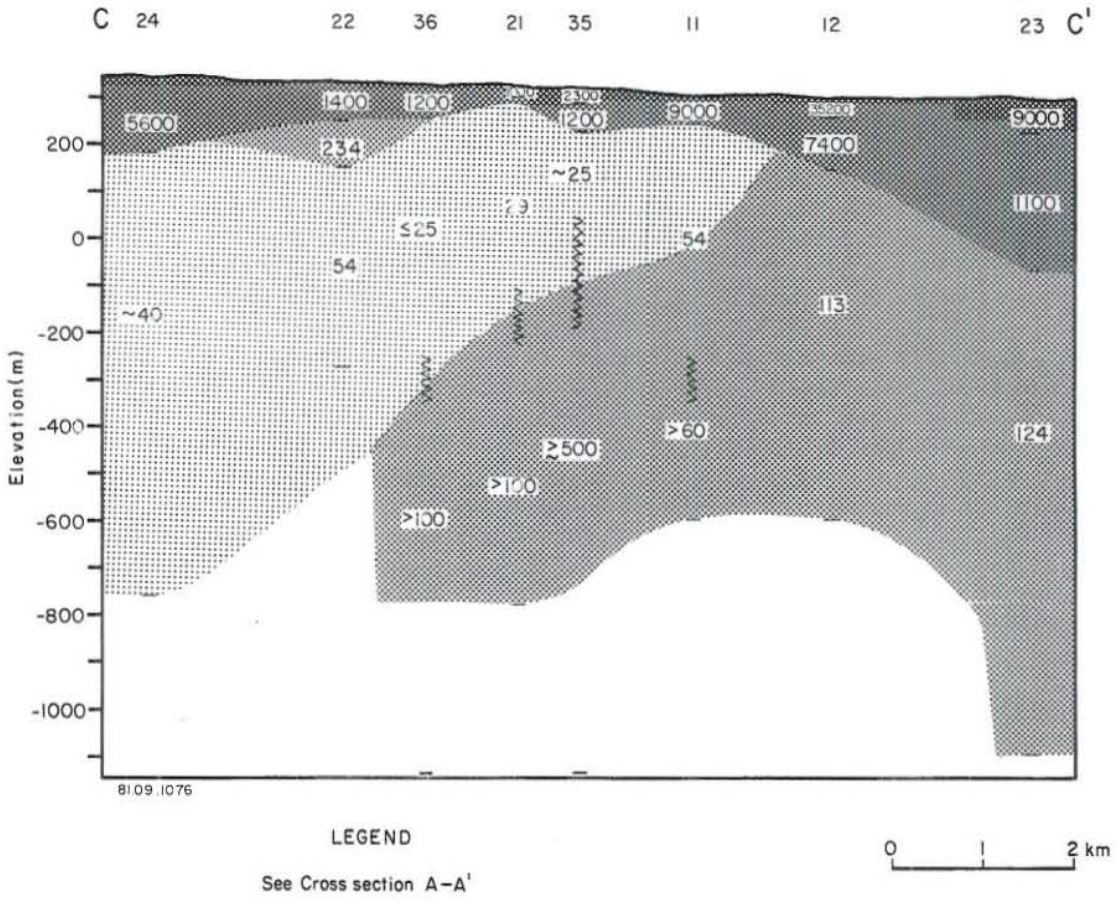

Fig. 24. Interpreted resistivity model along cross-section C-C'.

The isoresistivity maps: Three isoresistivity maps (Fig. 25, 26 and 27), were contoured at elevations of 0, 300 and 600 m below sea level. All of these display similar resistivity shapes and trends. The 15 Ωm closure defines a low resistivity anomaly which covers an area of approximately 6-8 km^2. At sea level, the 50 Ωm line encloses a broader area relative to the maps of greater depths. The enlargement of this resistivity contour line is mainly due to the localized low resistivity values in the western part of the geothermal area.

The field data of the group of soundings southwest of the thermal area are not in a good agreement. This is especially true for soundings 16, 25 and 37 (Appendix I). Data of these soundings at depth (with maximum AB/2 of 900 m except sounding 37 at 1580 m) appear to be disturbed by lateral inhomogeneities and/or vertical boundaries. This is suggestive of a complex geological structure of the area where these soundings are located. The young lava shield (Stórihver) which is to the west and north

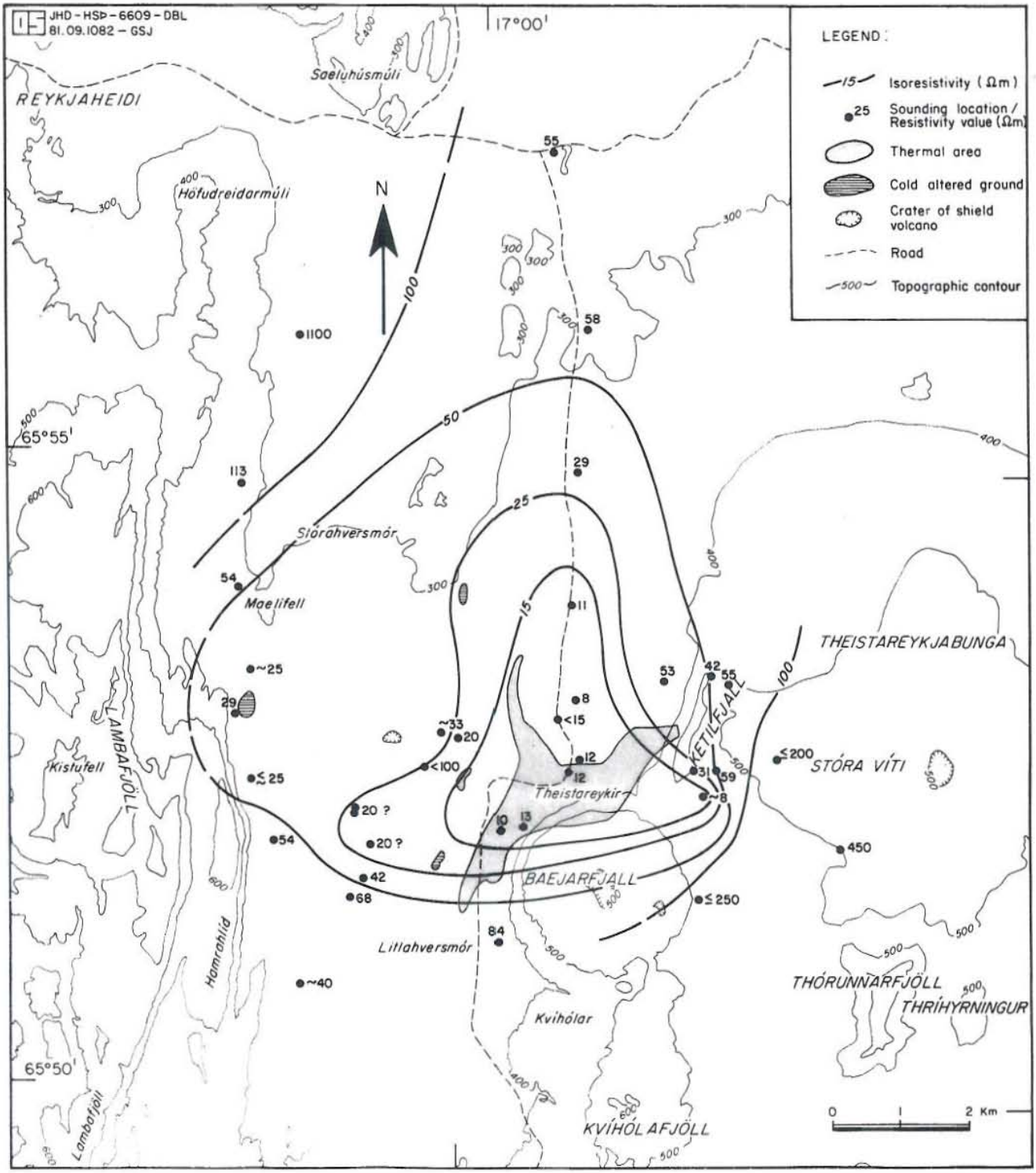

Fig. 25. Isoresistivity map at sea level.

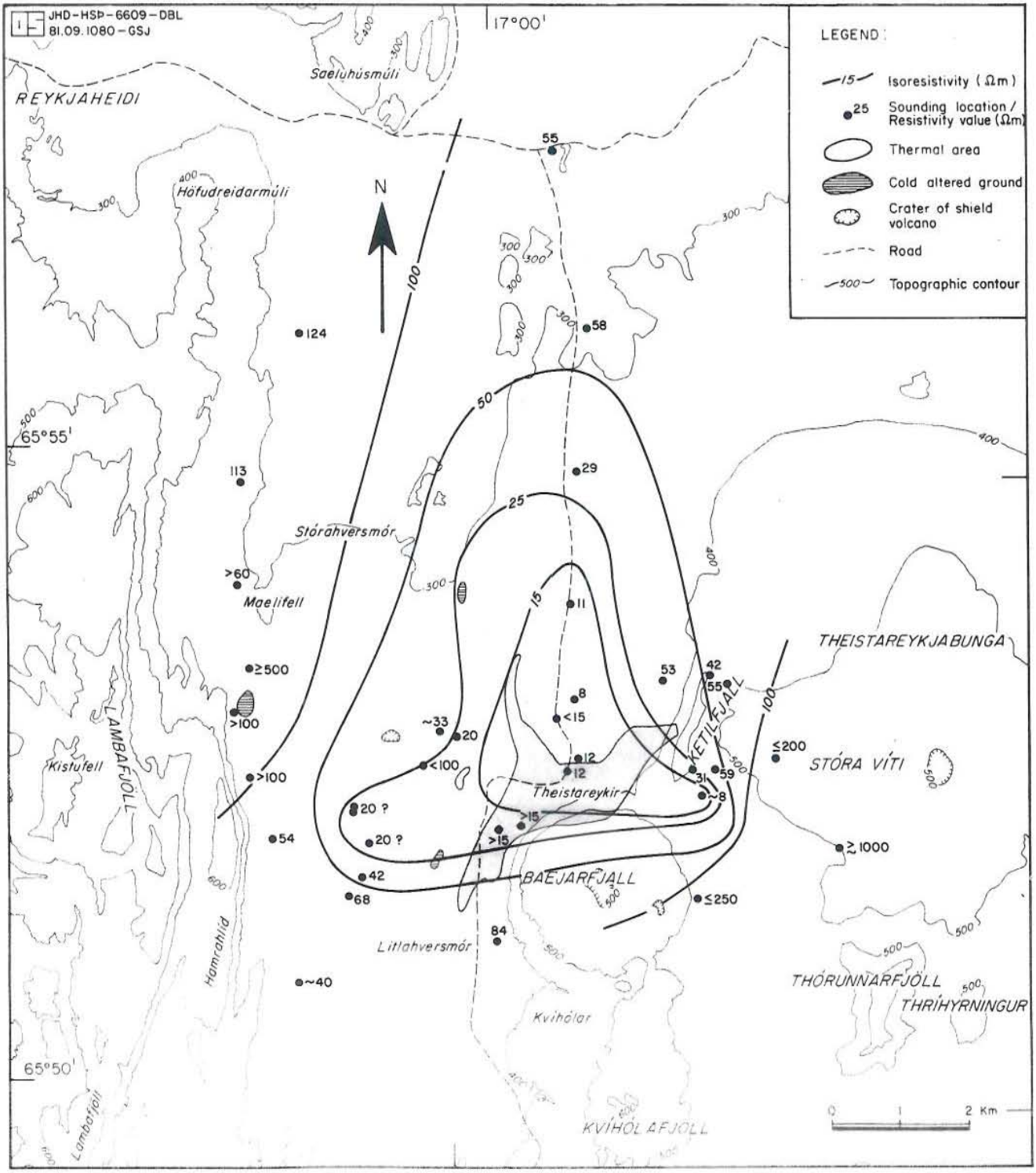

Fig. 26. Isoresistivity map at 300 m below sea level

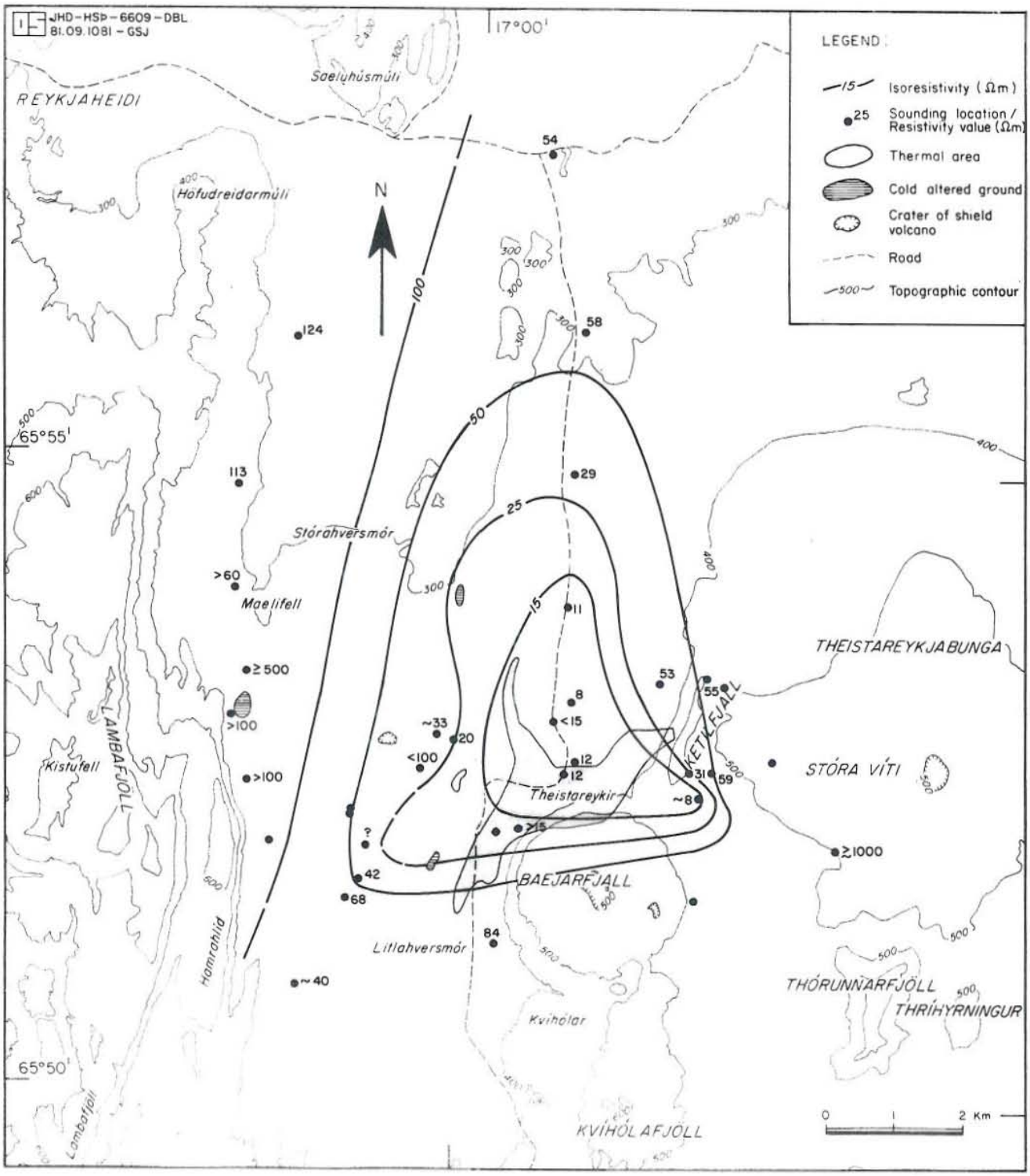

Fig. 27. Isoresistivity map at 600 m below sea level. Stations with no resistivity values assigned indicate that the interpreted soundings do not reach down to 600 m b.s.l.

of this group of soundings, may play a role in these effects. Field data obtained in areas like this can be exceptionally difficult to interpret quantitatively. The southwestern portion of the 25 Ωm isoresistivity line is therefore not well-defined as shown in the countour maps. However, inspection of the field curves discloses a downward trend that might justify the doubtful resistivity values of 20 Ωm assigned to these soundings.

3.5.2 Two-dimensional interpretation

Five D.C. Schlumberger soundings with a maximum current electrode spacing (AB/2) of 1580-2000 m were used for the two-dimensional modelling of the resistivity structure of the Theistareykir area. These soundings, generally trending in one direction, cut approximately a 13 km section extending from WNW-ESE; its mid-section crosses the Theistareykir thermal area (cross-section D-D′ in Fig. 18). These soundings, spaced approximately 2000 m apart, generally overlap each other for about 1700-2000 m, except for soundings 32 and 35 which overlap for about 300 m. There were no problems of terrain effects on field resistivities since the topography in the area is essentially flat.

Fig. 28 shows from top to bottom the two pseudosections for both the field data sets and the model-generated data sets, and the two-dimensional resistivity model. The apparent resistivities of the field data sets are plotted, by convention, below the centers of the sounding arrays. The 11 plotted measuring points of the field data sets, were selected at various AB/2 at the first few hundred meters (where data is dense) to faciliate contouring and convenient presentation. For example, the first measuring point is plotted at AB/2 = 10 m while the last point is at AB/2 = 1580 or 2000 m depending on the maximum current electrode separation. On the other hand, the calculated apparent resistivities derived from the model, consist of ten sampling points starting from AB/2 = 300 m down to 2100 m with an interval of 200 m. The number of sampling points and their location in terms of units, is determined in the gridfile of the modelling program used (see Appendix II). Therefore the near-surface resistivities in the calculated apparent resistivity pseudosection are averaged in contrast to the apparent resistivities plotted in the field resistivity pseudosection.

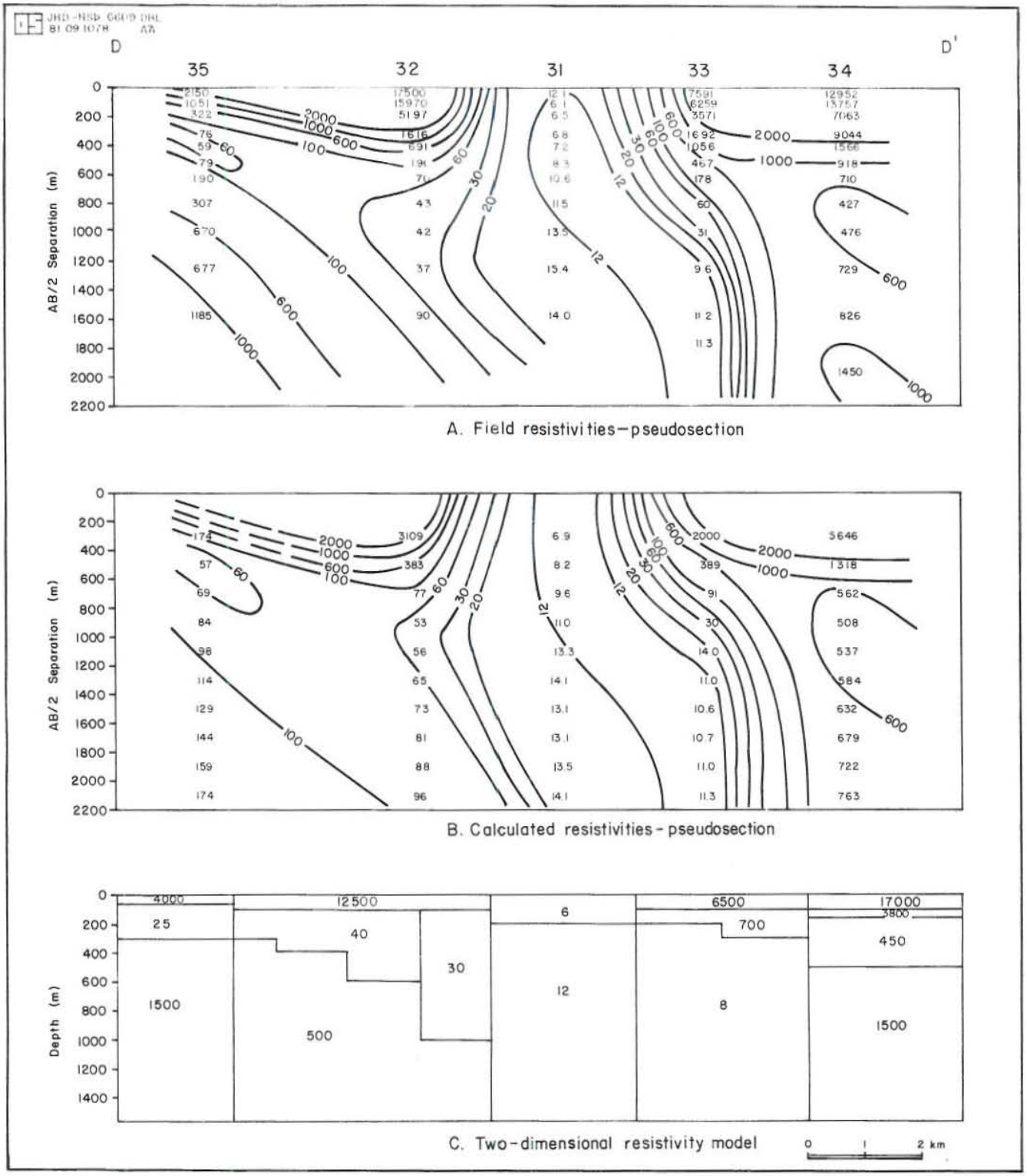

Fig. 28. Two-dimensional interpretation of resistivity soundings. A: Field data pseudosection, B: Model-generated data, C: Two-dimensional model.

The approximate location of the lateral and vertical boundaries in the model was based on the behaviour of the field curves and on the surface geology and structures in the area. These two factors seem to agree quite well. The abrupt rise of the field curves at greater electrode separations can be both attributed to vertical boundaries and to high resistivity formations at depth. This characteristic of the curves is evident particularly in soundings 32, 34 and 35 (see Appendix I). On the other hand the behaviour of the curves of soundings 31 and 33 is interpreted to be the sole effect of vertical boundaries.

The assignment of resistivity units for the initial two-dimensional models was based on the field resistivity pseudosection, some complimentary information from the one-dimensional models and the knowledge of the geological structures of the area. For example, the resistivity units of 30 and 40 Ωm below sounding 32 were based on its one dimensional interpretation and the other interpreted soundings close to it.

Several adjustments of the model were necessary to fit the field data and the calculated apparent resistivities. Generally the comparison between these indicates a good to excellent agreement. This is especially true for soundings 31, 33 and 34. The encouraging result is appreciated since the low resistivity anomaly (<15 Ωm) depends considerably on the interpretation of these soundings.

Since soundings 32 and 35 overlap for only 300 m, the resolution of vertical boundaries in the model affected by these soundings is relatively weak. Furthermore, the field curve of sounding 35 rises steeply starting at AB/2 = 400 m up to its maximum current electrode spacing. Hence it would be impossible to match this part of the field curve to a theoretically acceptable calculated curve. It is also doubtful whether this sounding can be interpreted two-dimensionally with any accuracy, because of complex geological structures in its vicinity. The data of sounding 32 are on the other hand scattered at depth. However, it can be noted that the resistivity pattern at the left side of both pseudosections appears to agree fairly well.

The resistivity values contained in each block and the lateral and vertical boundaries in the model should not be considered exact. For instance, in cases of monotonically increasing or decreasing resistivity

units, the range of acceptable models may be quite large because of the equivalence of the models. The contrast between 8 and 1500 Ωm units is considered as extremely high and stretches the program of interpretation to its limits.

3.6 The Resistivity Model and its Geothermal Implications

At first glance the section shown in Fig. 29 could be regarded as a new version of the two-dimensional model. However this resistivity model, cut from east to west, is the result of the complementary interpretations of both the one- and two-dimensional models.

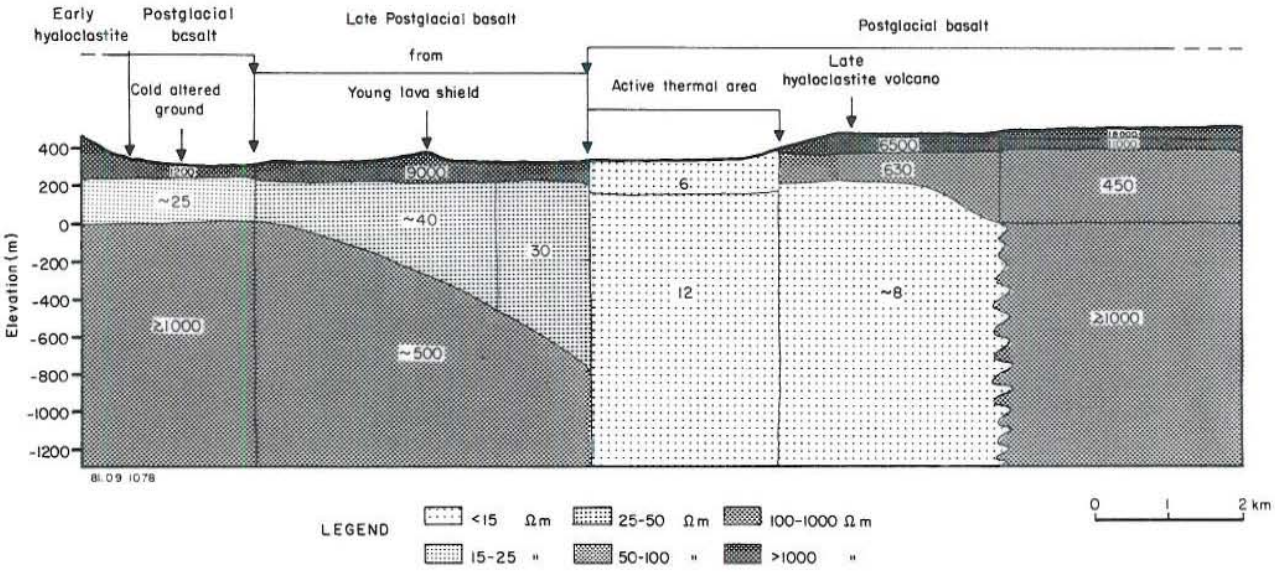

Fig. 29. Resistivity model based on one- and two-dimensional interpretations.

The highly resistive surface layers of >5000 Ωm correspond to about 100 m of "dry" (above the groundwater table) Postglacial (younger than ∿10.000 years) basaltic lava flows extruded from the lava shields present in the Theistareykir area (Fig. 20). This thickness of the top layer was confirmed by surface geological mapping in the area (Torfason 1981, pers. comm.). Exception to this top layer is the low resistivity unit of 6 Ωm which is confined within the active thermal area. This is to be expected since thermally altered ground is characterized by the presence of clay and other alteration minerals which are generally very conductive.

A conductive body is represented by the anomalously low resistivity of <15 Ωm. This low resistivity body, with a width of about 5 km along this section, is indicative of the upwelling zone of the Theistareykir geothermal system. A sharp boundary is evident to the east of the conductive zone. This boundary may reflect a buried fault or faults which would serve as a hydrological barrier for the hot fluids in the geothermal system. This inferred fault is not found on the surface. The NNE-trend of the hyaloclastite ridge (Fig. 20) north of the anomaly may suggest the presence of faults which may be the northward extension of the faults present south of the Baejarfjall volcano. H. Torfason has recognized surface traces of faults on top of the volcano. The high resistivity unit of $\gtrsim$1000 Ωm in the eastern part of the area could be interpreted as colder and fresher rock formation unaffected by the hot fluids of the geothermal system. However, as indicated in cross-section A-A′, a transitional zone of about 1.5 km of intermediate resistivity exists between the conductive and the resistive formations. It could therefore be noted that the boundary between these two units is more diffuse than the model in Fig. 29 indicates.

To the west of the conductive zone, units of low to intermediate resistivities (30-40 Ωm) may be attributed to a horizontal flow of hot water from the central part of the geothermal system. Steam coming out in the western flanks of the young Stórihver lava shield could attest to this. The high resistivity layer at depth may be attributed to intrusive bodies such as dykes, sheets and other intrusions with a very low porosity. The presence of such intrusive rocks is common in central volcanic systems located within the Neovolcanic zone in Iceland.

The aeromagnetic map in Fig. 30 (flown by Prof. T. Sigurgeirsson, University of Iceland in 1974) shows a prominent negative magnetic anomaly (<51,000-51,500γ) that coincides with the upwelling zone as defined by the low resistivity anomaly. An interesting feature of the magnetic map is the E-W trend of the magnetic anomaly. This feature may resemble the pattern of low to intermediate resistivity units at shallow depth as described above, and is a further indication of outflow of hot water to the west from the central part of the geothermal system.

Preliminary interpretation of geochemical analyses of gas samples collected from the active thermal area of Theistareykir suggests a similar location of the upflow zone as indicated by the resistivity and magnetic anomalies (G. Gislason 1981, per. comm.).

The Theistareykir geothermal area is characterized by a low resistivity body and a large contrast between the resistivity within the body and that of the surrounding rocks. Applying the rules of thumb described by Meidav (1980 ; see also Chapter 2.3.5) these resistivity signatures are indicative of a liquid-dominated system with a reservoir temperature $\geq 220^{\circ}C$ and a depth to the reservoir of ≤ 2 km. The low resistivity anomaly of $<15\ \Omega m$ manifested in Theistareykir against the relatively high resistivity of the surrounding rocks may be the effect of the combination of factors such as temperature, porosity and salinity of the saturating fluids in the reservoir rocks.

The heat source of the possible geothermal system in Theistareykir probably comes from some recent intrusive rocks (or even a magma chamber) associated with the Theistareykir volcanic system. Pore space that permits the storage of hydrothermal fluids may be provided by the relatively high porous hyaloclastites and the contact between these rocks and the layers of subaerial lavas as is considered common in Icelandic geothermal systems (Fridleifsson 1979). The presence of faults and fissures in the area may render these rock units permeable for the formation of acquifers.

3.7 Conclusions

1. The D.C. Schlumberger sounding measurements delineate a low resistivity anomaly ($<15\ \Omega m$) of about 6-8 km^2. This anomaly is correlated with the upwelling zone of the Theistareykir geothermal system.

2. The low resistivity formation and the large contrast in resistivity between it and the highly resistive surrounding rocks are characteristic of a typical high-temperature geothermal system.

3. The sharp boundary of the conductive body to the east may be explained by the presence of a buried NNE-SSW striking fault(s). This

fault may act as a hydrologic barrier for the hot fluids in the geothermal system towards the east.

4. The relatively high resistivity at depth in the western part of the area is attributable to intrusive rocks.

5. Two-dimensional modelling allowed the possibility of detecting lateral inhomogeneites and vertical boundaries of the resistivity structure in the Theistareykir geothermal area. One-dimensional modelling worked well in most cases, but some of the soundings are distorted by surficial heterogeneities and vertical boundaries.

6. The role of geological concepts is valuable in the entire process of resistivity interpretation.

3.8 Recommendations

1. Further D.C. Schlumberger soundings should be conducted northwest of the thermal area to fill a gap which is as yet devoid of resistivity measurements.

2. Good sounding data that can be obtained west of the thermal area (where field curves do not agree quite well with each other) may prove to be very helpful in resolving the complex geological structure suspected to occur locally in this area.

3. Fill-in soundings are proposed in between the measurements along cross-section D-D'. A high data density obtained along this line may make it possible to detect the vertical boundaries in detail.

4. Sounding lines are recommended in the northern and southern part of the low resistivity anomaly for two-dimensional interpretation. This is intended to model a more realistic two-dimensional structure of the Theistareykir geothermal area.

ACKNOWLEDGEMENTS

I wish to express my profound gratitude to my supervisor, Mr. Ludvik S. Georgsson, who offered a wealth of ideas; his unceasing support and guidance were truly overwhelming. Special thanks are due to Mr. Halldor Halldorsson for providing notes on computer programs, and to Mr. Asmundur Jakobsson for his generous assistance on operating computer systems.

My sincere gratitude is due to Dr. Hjalti Franzson and Ms. Solveig Jonsdottir for their continuous assistance during my stay in Iceland. I am grateful to Ms. Ragna Karlsdottir and the resistivity crew of Orkustofnun for their practical instructions on measurement techniques during the field work in Theistareykir. I owe my thanks to Ms. Sigridur Valdemarsdottir for patiently typing the text and to the drawing staff of the National Energy Authority of Iceland who painstakingly drew most of the figures.

My warmest thanks to Dr. Ingvar B. Fridleifsson, Prof. Sveinbjörn Björnsson and Mr. Ólafur Flóvenz who critically reviewed the manuscript.

I am deeply honoured by having attended the UNU Geothermal Training Programme at Orkustofnun in Iceland and grateful to the United Nations University for the Fellowship. Lastly I am greatly indebted to the Energy Development Corporation of the Philippine National Oil Company for the support and encouragement to pursue overseas training.

REFERENCES

Bhattacharya, P.K. and Patra, H.P. 1968: Direct current geoelectrical sounding. Elsevier, Amsterdam, 135 p.

Blohm, E.K., Worzyk, P., and Scriba, H. 1977: Geoelectrical deep soundings in Southern Africa using the Cabora Bassa power line. J. Geophys., vol. 43, 665-679.

Dakhnov, V.N., 1962: Geophysical well logging. Quart. Colorado Sch. Mines, vol. 57, no. 2, 445 p.

Dey, A. 1976: Resistivity modelling for arbitrarily shaped two-dimensional structures. Part II: User's guide to FORTRAN algorithm RESIS2D. Lawrence Berkeley Laboratory, Berkeley, LBL-5283, 56 p.

Dey, A. and Morrison, H.F. 1976: Resistivity modelling for arbitrarily two-dimensional structures. Part I: Theoretical formulation. Lawrence Berkeley Laboratory, Berkeley, LBL-5223, 18 p.

Duba, A., Piwinskii, A.J., Santor, M. and Weed, H.C. 1978: The electrical conductivity of sandstone, limestone and granite. Geophys. J.R. astr. Soc., vol. 53, 583-597.

Flathe, H. 1976: The role of a geological concept in geophysical research work for solving hydrological problems. Geoexploration, vol. 14, 195-206.

Fox, R.C., Hohmann, G.W. and Rijo, L. 1978: Topographic effects in resistivity surveys. Earth Sciences Laboratory, Salt Lake City, Utah, 99 p.

Fridleifsson, I.B. 1979: Geothermal activity in Iceland. Jökull, vol. 29, 47-56.

Georgsson, L.S. 1979: Svartsengi. Electrical resistivity survey at Svartsengi on western Reykjanes Peninsula (in Icelandic). Orkustofnun, OS 79042/JHD 20, 100 p.

Gronvold, K. and Karlsdottir, R. 1975: Progress report on surface investigations of the Theistareykir geothermal area (in Icelandic). Orkustofnun, OS-JHD-7501, 37 p.

Hochstein, M.P. 1975: Geophysical exploration of the Kawah Kamojang field, West Java. Second U.N. Symposium on the Development and Use of Geothermal Resources, San Francisco, USA. Proc., vol. 2, 1049-1058.

Johansen, H.K., 1977: A man/computer interpretation system for resistivity soundings over a horizontally stratified earth. Geophys. Prosp., vol. 25, 667-691.

Keller, G.V. and Frischknecht, F.C. 1966: Electrical methods in geophysical prospecting. Pergamon Press, New York, 519 p.

Koefod, O. 1979: Geosounding principles 1 - Resistivity sounding measurements. Elsevier, Amsterdam, 276 p.

Layugan, D.B. 1981: Geothermal implications of the D.C. Schlumberger resistivity survey over the entire Biliran Island. Paper presented in the third annual PNOC-EDC geothermal workshop and geoscientific conference, Tongonan, Leyte (January 1981), 17 p.

Mattice, M.D. and Lienert, B.R. 1980: Schlumberger survey of Maui Island, State of Hawaii. Geothermal Resources Council, Transactions, vol. 4, 85-88.

Meidav, T. 1970: Application of electrical resistivity and gravimetry in deep geothermal exploration in the Imperial Valley. Geothermics, Sp. Issue 2, vol. 2, 303-310.

Meidav, T. 1980: D.C. resistivity methods in Geothermal exploration. In: Geophysical exploration methods for geothermal resources. Geothermal Resources Council, techn. train. course no. 2, 28 p.

Mundrey, E. and Worzyk, P. 1979: On the coastal effect on geoelectrical soundings. J. Geophys., vol. 45, 329-336.

Orellana, E. and Mooney, H.M. 1966: Master tables and curves for vertical electrical sounding over layered structures. Intersciencia, Madrid, 193 p.

Palmason, G. 1975: Geophysical methods in geothermal exploration. Second U.N. Symposium on the Development and Use of Geothermal Resources, San Francisco, USA, Proc., vol. 2, 1175-1184.

Rijkswaterstaat, The Netherlands 1968: Standard graphs for resistivity prospecting.

Saemundsson, K. 1978: Fissure-swarms and central volcanoes of the neo-volcanic zone of Iceland. In: Bowes, D.R. and Leake, B.E. (ed). Crustal evolution in Northwestern Britain and adjacent regions, Geol. J., Spec. issue, vol. 10, 415-432.

Saemundsson, K. 1979: Outline of the geology of Iceland. Jökull, vol. 29, 7-28.

Zohdy, A.A. 1970: Variable azimuth Schlumberger resistivity sounding and profiling near a vertical contact. Geol. Survey Bull. 1313-A, 22 p.

A P P E N D I X I

1. The interpreted resistivity models of the D.C. Schlumberger soundings performed in Theistareykir geothermal area.

2. Sample of field data.

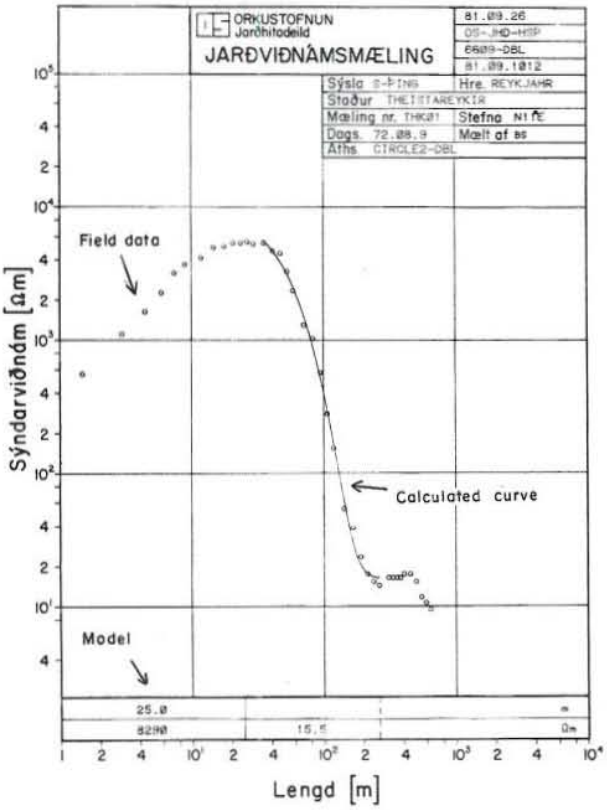
ORKUSTOFNUN
Jarðhitadeild
JARÐVIÐNÁMSMÆLING
81.09.26
OS-JHD-HSÞ
6609-DBL
81.09.1012
Sýsla S-ÞING
Hre. REYKJAHR
Staður THEISTAREYKIR
Mæling nr. THK01
Stefna N1°E
Dags. 72.08.9
Mælt af ss
Aths. CIRCLE2-DBL
Field data
Calculated curve
Model
Sýndarviðnám [Ωm]
Lengd [m]
25.0
8290
15.5
m
Ωm

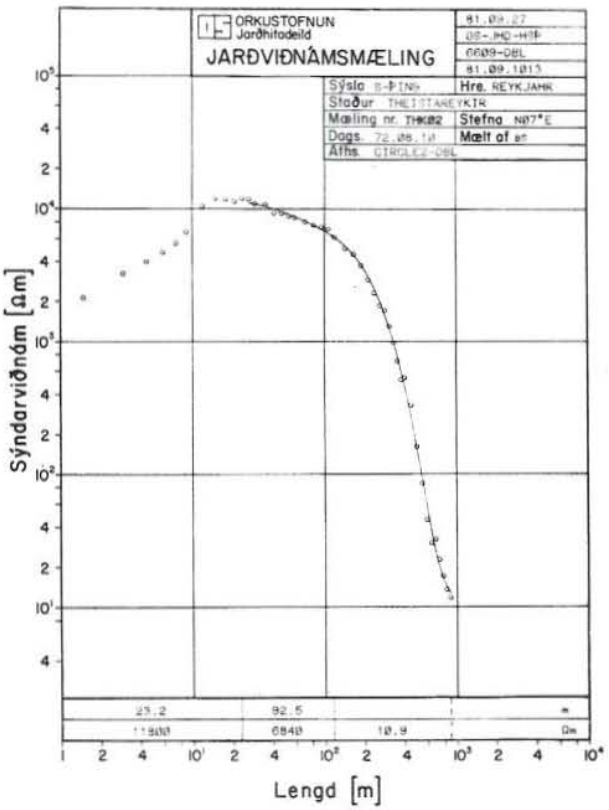
ORKUSTOFNUN
Jarðhitadeild
JARÐVIÐNÁMSMÆLING
81.09.27
OS-JHD-HSÞ
6609-DBL
81.09.1013
Sýsla S-ÞING
Hre. REYKJAHR
Staður THEISTAREYKIR
Mæling nr. THK02
Stefna N97°E
Dags. 72.08.10
Mælt af ss
Aths. CIRCLE2-DBL
Sýndarviðnám [Ωm]
Lengd [m]
23.2
92.5
11900
6840
10.9
m
Ωm

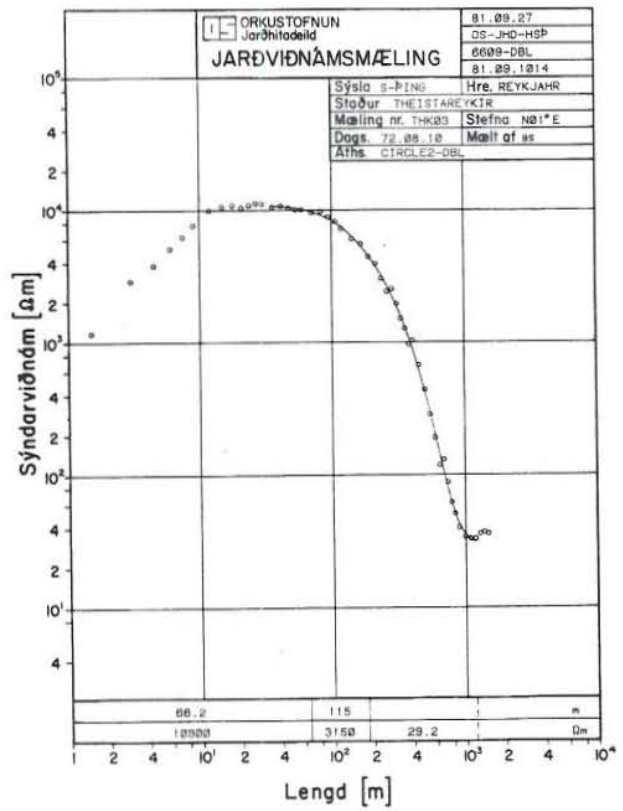
ORKUSTOFNUN
Jarðhitadeild
JARÐVIÐNÁMSMÆLING
81.09.27
OS-JHD-HSÞ
6609-DBL
81.09.1014
Sýsla S-ÞING
Hre. REYKJAHR
Staður THEISTAREYKIR
Mæling nr. THK03
Stefna N81°E
Dags. 72.08.10
Mælt af ss
Aths. CIRCLE2-DBL
Sýndarviðnám [Ωm]
Lengd [m]
66.2
115
18000
3150
29.2
m
Ωm

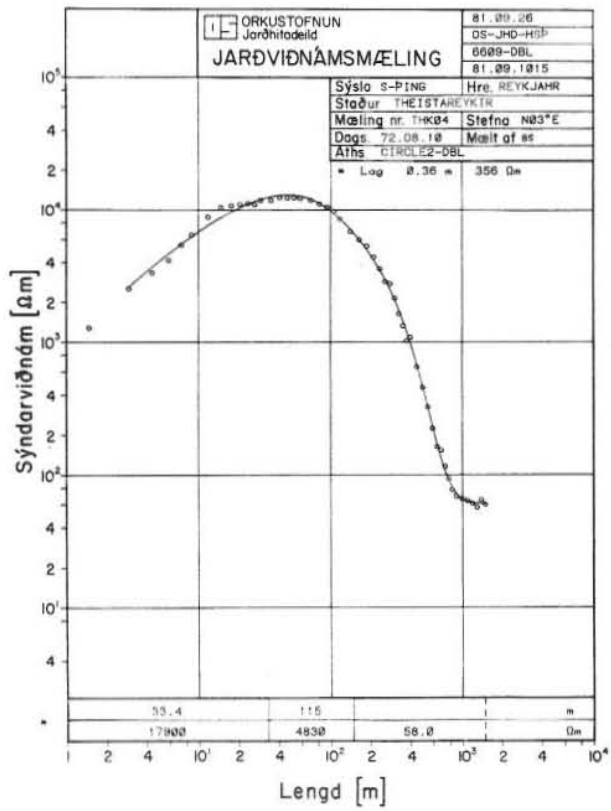
ORKUSTOFNUN
Jarðhitadeild
JARÐVIÐNÁMSMÆLING
81.09.26
OS-JHD-HSÞ
6609-DBL
81.09.1015
Sýsla S-ÞING
Hre. REYKJAHR
Staður THEISTAREYKIR
Mæling nr. THK04
Stefna N83°E
Dags. 72.08.10
Mælt af ss
Aths. CIRCLE2-DBL
* Lag 0.36 m 356 Ωm
Sýndarviðnám [Ωm]
Lengd [m]
33.4
115
17900
4830
58.0
m
Ωm

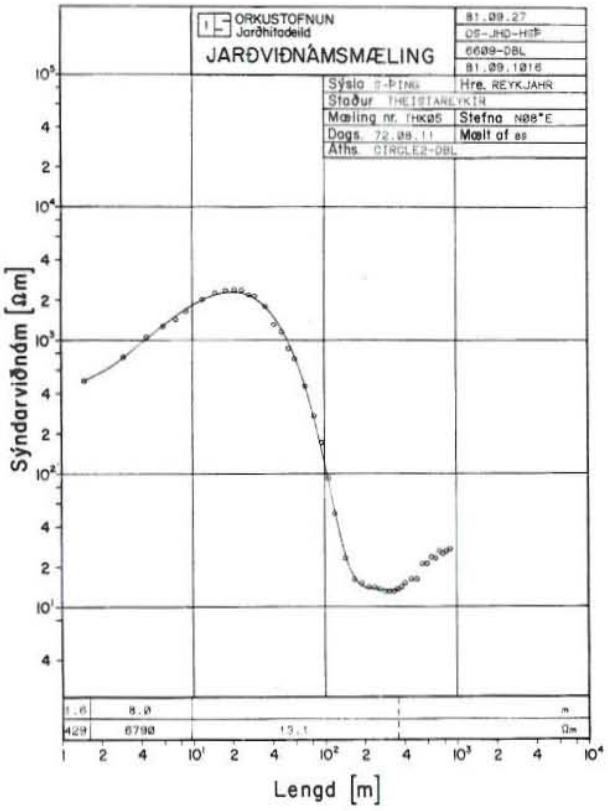
ORKUSTOFNUN
Jarðhitadeild
JARÐVIÐNÁMSMÆLING
81.09.27
OS-JHD-HSÞ
6009-DBL
81.09.1016
Sýsla S-ÞING
Hre. REYKJAHR
Staður THEISTAREYKIR
Mæling nr. THK05
Stefna N08°E
Dags. 72.08.11
Mælt af ss
Aths. CIRCLE2-DBL
Sýndarviðnám [Ωm]
Lengd [m]
1.6 8.0 m
429 6790 13.1 Ωm

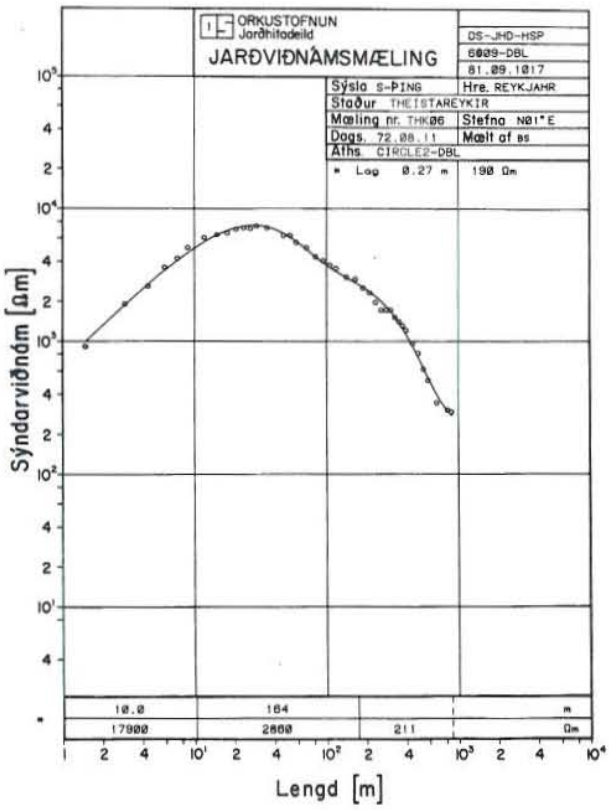
ORKUSTOFNUN
Jarðhitadeild
JARÐVIÐNÁMSMÆLING
OS-JHD-HSP
6009-DBL
81.09.1017
Sýsla S-ÞING
Hre. REYKJAHR
Staður THEISTAREYKIR
Mæling nr. THK06
Stefna N01°E
Dags. 72.08.11
Mælt af ss
Aths. CIRCLE2-DBL
* Lag 0.27 m 190 Ωm
Sýndarviðnám [Ωm]
Lengd [m]
10.0 164 m
17900 2860 211 Ωm

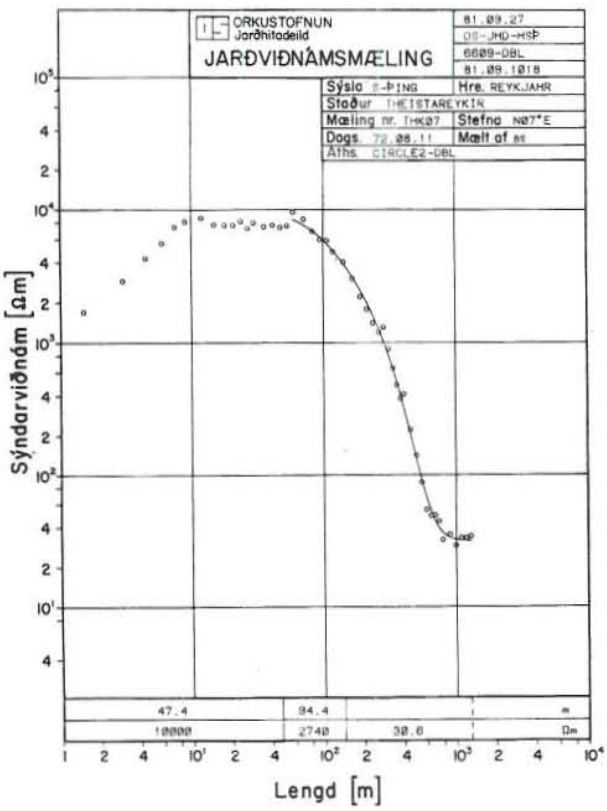
ORKUSTOFNUN
Jarðhitadeild
JARÐVIÐNÁMSMÆLING
81.09.27
OS-JHD-HSÞ
6009-DBL
81.09.1018
Sýsla S-ÞING
Hre. REYKJAHR
Staður THEISTAREYKIN
Mæling nr. THK07
Stefna N07°E
Dags. 72.08.11
Mælt af ss
Aths. CIRCLE2-DBL
Sýndarviðnám [Ωm]
Lengd [m]
47.4 94.4 m
10000 2740 30.6 Ωm

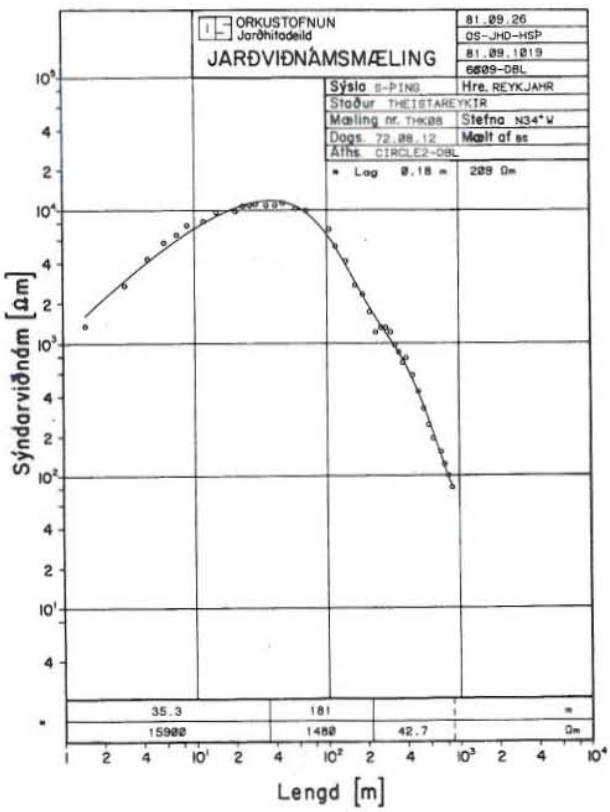
ORKUSTOFNUN
Jarðhitadeild
JARÐVIÐNÁMSMÆLING
81.09.26
OS-JHD-HSÞ
81.09.1019
6009-DBL
Sýsla S-ÞING
Hre. REYKJAHR
Staður THEISTAREYKIR
Mæling nr. THK08
Stefna N34°W
Dags. 72.08.12
Mælt af ss
Aths. CIRCLE2-DBL
* Lag 0.18 m 209 Ωm
Sýndarviðnám [Ωm]
Lengd [m]
35.3 181 m
15900 1460 42.7 Ωm

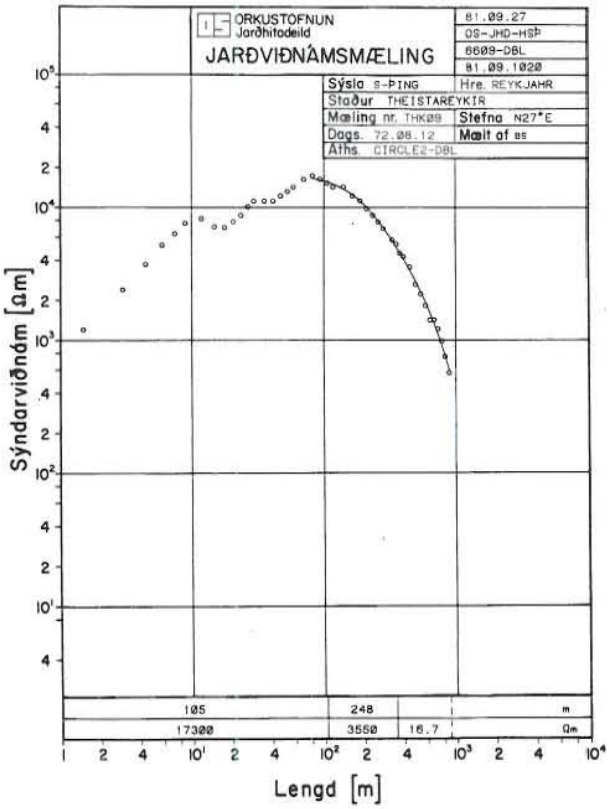
ORKUSTOFNUN
Jarðhitadeild
JARÐVIÐNÁMSMÆLING
81.09.27
OS-JHD-HSÞ
6609-DBL
81.09.1020
Sýsla S-ÞING
Hre. REYKJAHR
Staður THEISTAREYKIR
Mæling nr. THK09
Stefna N27°E
Dags. 72.08.12.
Mælt af BS
Aths. CIRCLE2-DBL
105 248 m
17300 3550 16.7 Ωm
Sýndarviðnám [Ωm]
Lengd [m]

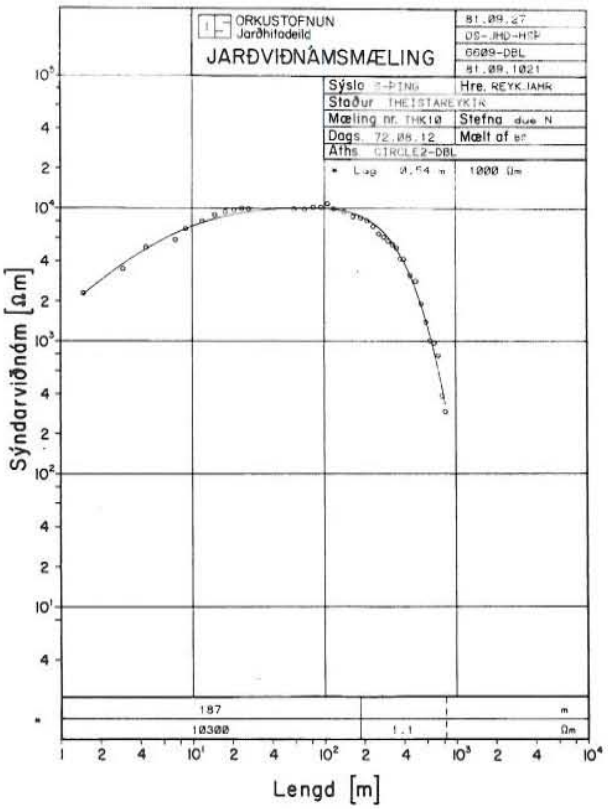
ORKUSTOFNUN
Jarðhitadeild
JARÐVIÐNÁMSMÆLING
81.09.27
OS-JHD-HSÞ
6609-DBL
81.09.1021
Sýsla S-ÞING
Hre. REYKJAHR
Staður THEISTAREYKIR
Mæling nr. THK10
Stefna due N
Dags. 72.08.12.
Mælt af BS
Aths. CIRCLE2-DBL
* Lag 0.54 m 1000 Ωm
187 m
10300 1.1 Ωm
Sýndarviðnám [Ωm]
Lengd [m]

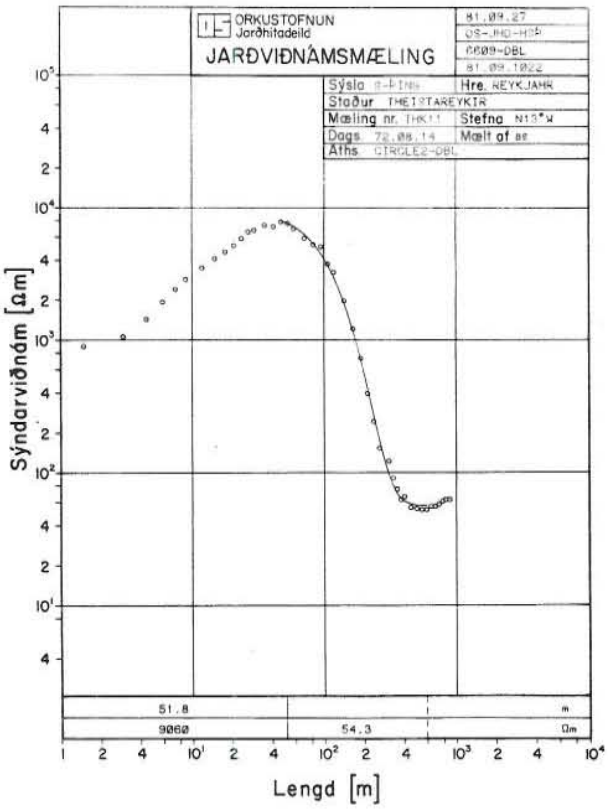
ORKUSTOFNUN
Jarðhitadeild
JARÐVIÐNÁMSMÆLING
81.09.27
OS-JHD-HSÞ
6609-DBL
81.09.1022
Sýsla S-ÞING
Hre. REYKJAHR
Staður THEISTAREYKIR
Mæling nr. THK11
Stefna N13°W
Dags. 72.08.14
Mælt af BS
Aths. CIRCLE2-DBL
51.8 m
9060 54.3 Ωm
Sýndarviðnám [Ωm]
Lengd [m]

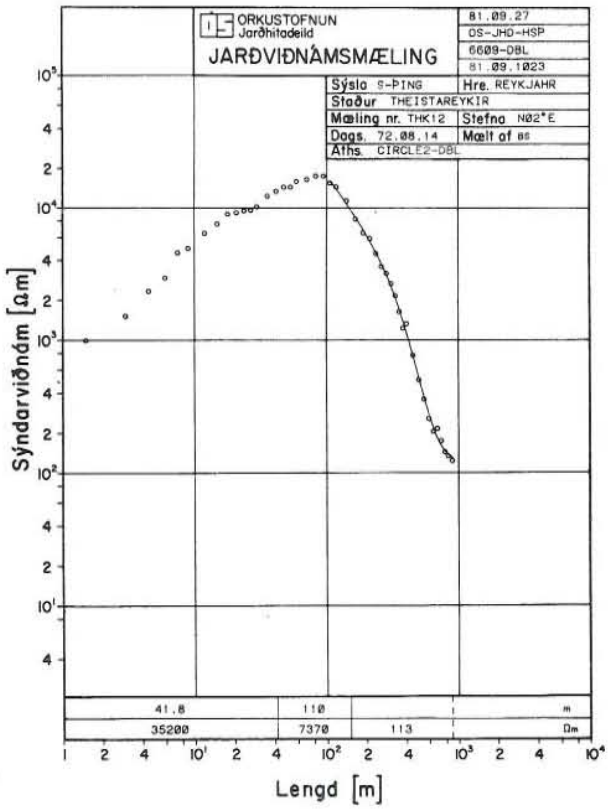
ORKUSTOFNUN
Jarðhitadeild
JARÐVIÐNÁMSMÆLING
81.09.27
OS-JHD-HSÞ
6609-DBL
81.09.1023
Sýsla S-ÞING
Hre. REYKJAHR
Staður THEISTAREYKIR
Mæling nr. THK12
Stefna N02°E
Dags. 72.08.14
Mælt af BS
Aths. CIRCLE2-DBL
41.8 110 m
35200 7370 113 Ωm
Sýndarviðnám [Ωm]
Lengd [m]

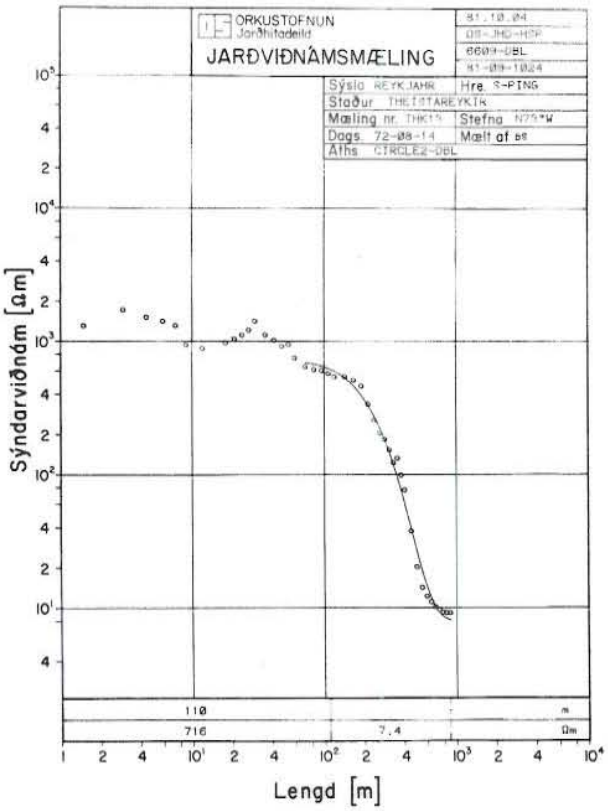
ORKUSTOFNUN
Jarðhitadeild
JARÐVIÐNÁMSMÆLING
81.10.04
OS-JHD-HSP
6609-DBL
81-09-1024
Sýsla REYKJAHR
Hre. S-ÞING
Staður THEISTAREYKIR
Mæling nr. THK13
Stefna N75°W
Dags. 72-08-14
Mælt af ss
Aths. CIRCLE2-DBL
Sýndarviðnám [Ωm]
Lengd [m]
110
716
7.4
m
Ωm

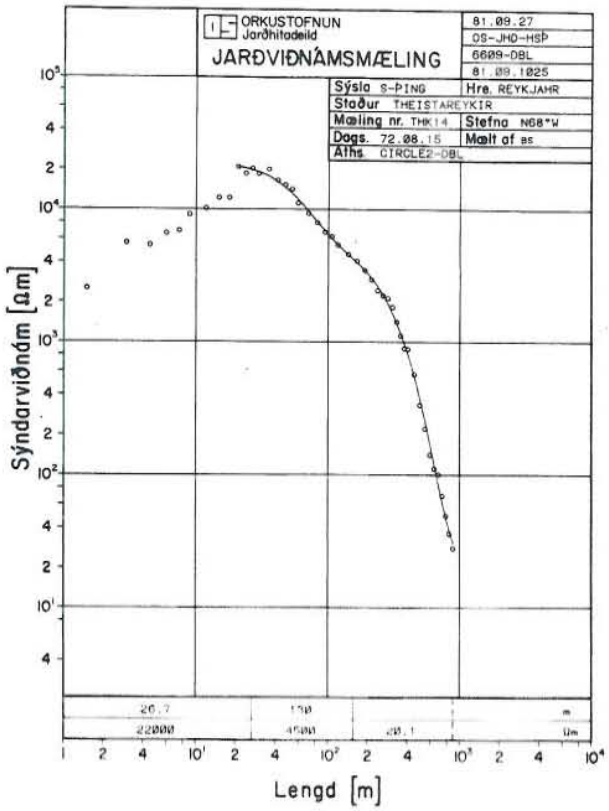
ORKUSTOFNUN
Jarðhitadeild
JARÐVIÐNÁMSMÆLING
81.09.27
OS-JHD-HSP
6609-DBL
81.09.1025
Sýsla S-ÞING
Hre. REYKJAHR
Staður THEISTAREYKIR
Mæling nr. THK14
Stefna N68°W
Dags. 72.08.15
Mælt af ss
Aths. CIRCLE2-DBL
Sýndarviðnám [Ωm]
Lengd [m]
26.7
22000
170
4500
m
Ωm

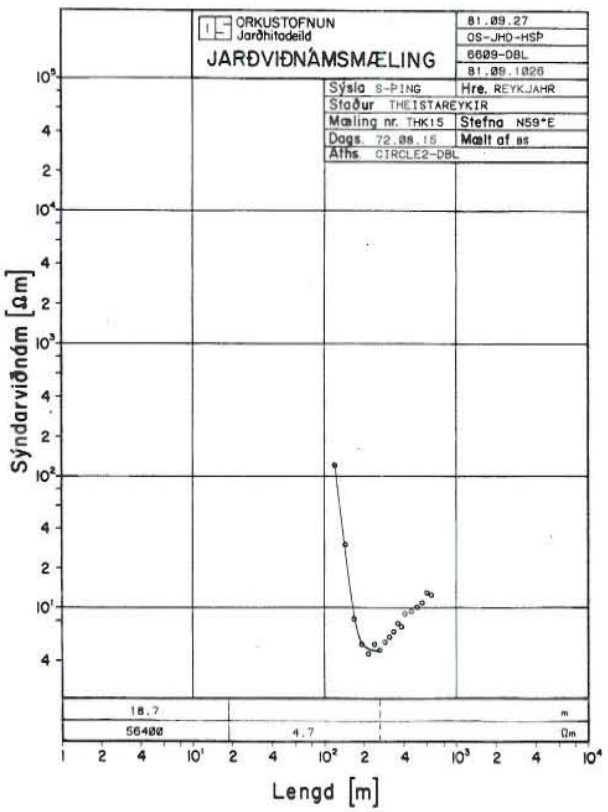
ORKUSTOFNUN
Jarðhitadeild
JARÐVIÐNÁMSMÆLING
81.09.27
OS-JHD-HSP
6609-DBL
81.09.1026
Sýsla S-ÞING
Hre. REYKJAHR
Staður THEISTAREYKIR
Mæling nr. THK15
Stefna N59°E
Dags. 72.08.15
Mælt af ss
Aths. CIRCLE2-DBL
Sýndarviðnám [Ωm]
Lengd [m]
18.7
56400
4.7
m
Ωm

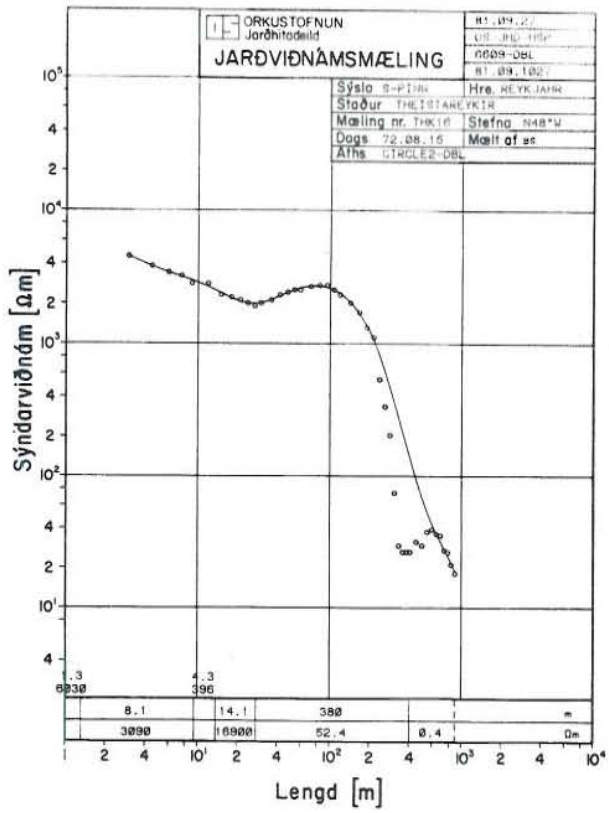
ORKUSTOFNUN
Jarðhitadeild
JARÐVIÐNÁMSMÆLING
6609-DBL
Sýsla S-ÞING
Hre. REYKJAHR
Staður THEISTAREYKIR
Mæling nr. THK16
Stefna N48°W
Dags. 72.08.15
Mælt af ss
Aths. CIRCLE2-DBL
Sýndarviðnám [Ωm]
Lengd [m]
1.3
6830
4.3
396
8.1
3090
14.1
16800
380
52.4
0.4
m
Ωm

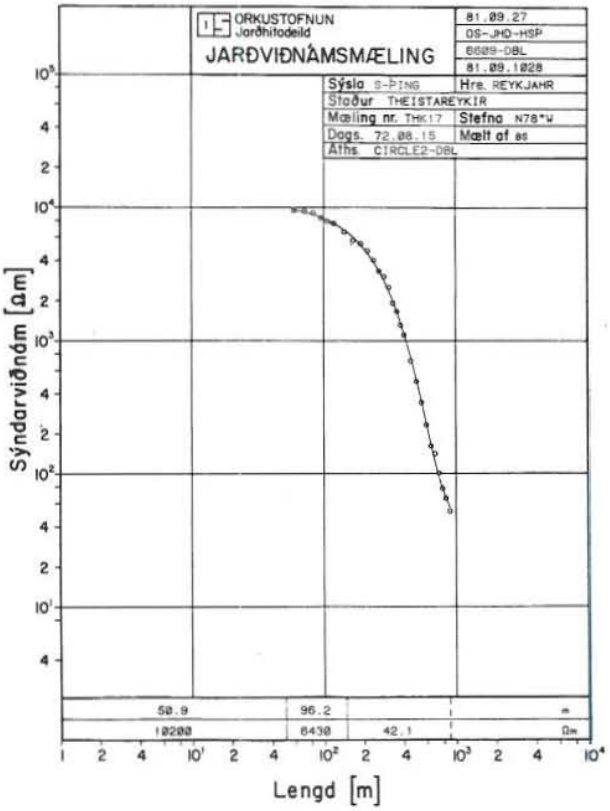
ORKUSTOFNUN
Jarðhitadeild
JARÐVIÐNÁMSMÆLING
81.09.27
OS-JHD-HSÞ
6609-DBL
81.09.1028
Sýsla S-ÞING
Hre. REYKJAHR
Staður THEISTAREYKIR
Mæling nr. THK17
Stefna N78°W
Dags. 72.08.15
Mælt af ss
Aths. CIRCLE2-DBL
Sýndarviðnám [Ωm]
Lengd [m]
50.9
96.2
m
10200
6430
42.1
Ωm

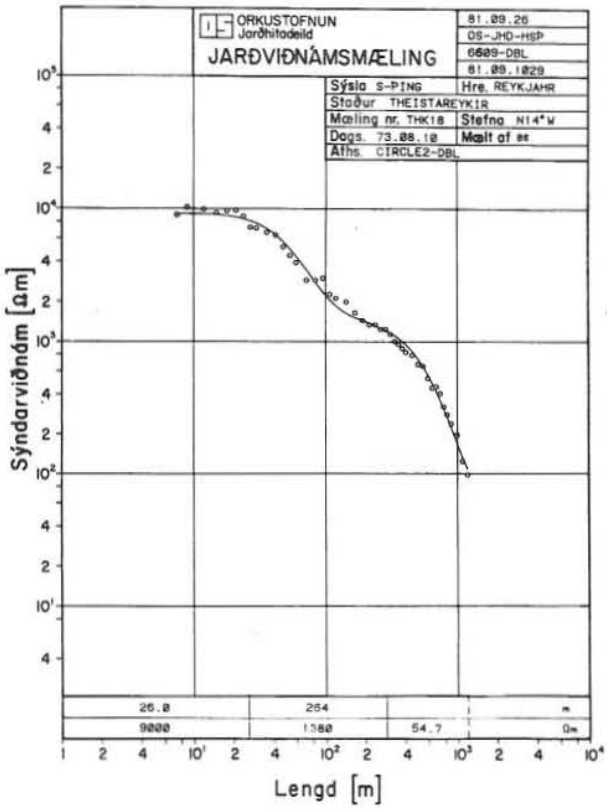
ORKUSTOFNUN
Jarðhitadeild
JARÐVIÐNÁMSMÆLING
81.09.26
OS-JHD-HSÞ
6609-DBL
81.09.1029
Sýsla S-ÞING
Hre. REYKJAHR
Staður THEISTAREYKIR
Mæling nr. THK18
Stefna N14°W
Dags. 73.08.10
Mælt af ss
Aths. CIRCLE2-DBL
Sýndarviðnám [Ωm]
Lengd [m]
26.0
254
m
9000
1380
54.7
Ωm

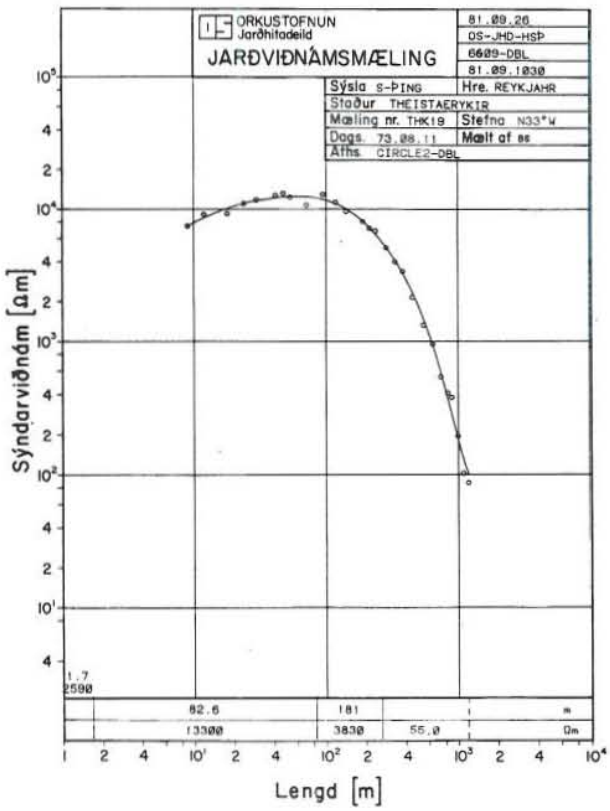
ORKUSTOFNUN
Jarðhitadeild
JARÐVIÐNÁMSMÆLING
81.09.26
OS-JHD-HSÞ
6609-DBL
81.09.1030
Sýsla S-ÞING
Hre. REYKJAHR
Staður THEISTAERYKIR
Mæling nr. THK19
Stefna N33°W
Dags. 73.08.11
Mælt af ss
Aths. CIRCLE2-DBL
Sýndarviðnám [Ωm]
Lengd [m]
1.7
2590
82.6
181
m
13300
3830
55.0
Ωm

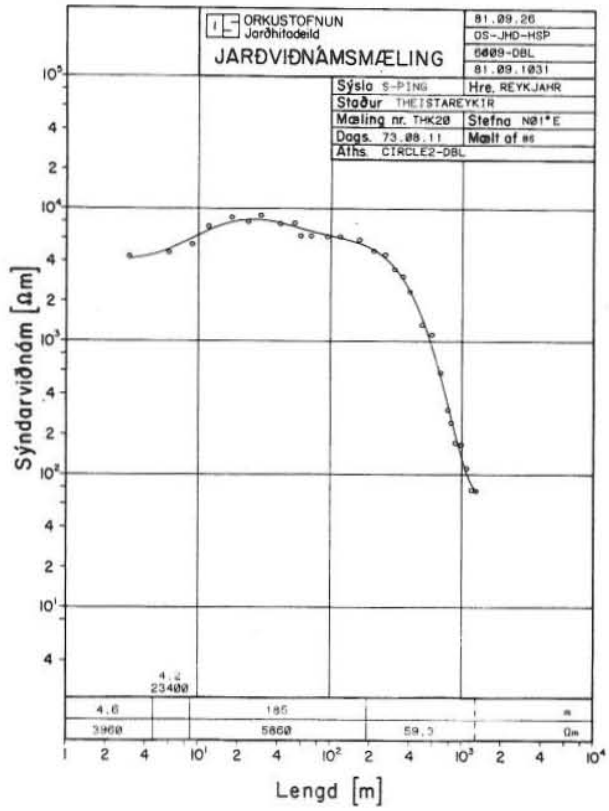
ORKUSTOFNUN
Jarðhitadeild
JARÐVIÐNÁMSMÆLING
81.09.26
OS-JHD-HSÞ
6609-DBL
81.09.1031
Sýsla S-ÞING
Hre. REYKJAHR
Staður THEISTAREYKIR
Mæling nr. THK20
Stefna N01°E
Dags. 73.08.11
Mælt af ss
Aths. CIRCLE2-DBL
Sýndarviðnám [Ωm]
Lengd [m]
4.4
23400
4.6
185
m
3960
5860
59.0
Ωm

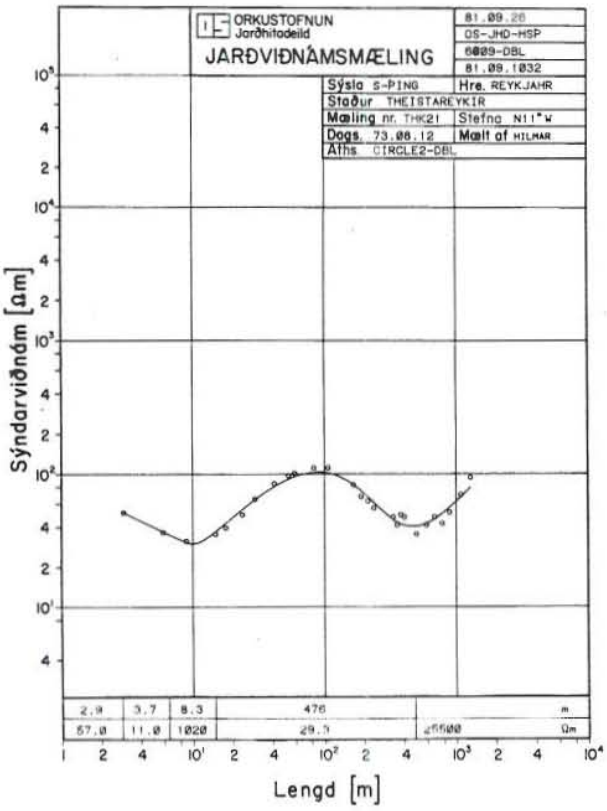
ORKUSTOFNUN
Jarðhitadeild
JARÐVIÐNÁMSMÆLING
81.09.26
OS-JHD-HSP
6009-DBL
81.09.1032
Sýsla S-ÞING
Hre. REYKJAHR
Staður THEISTAREYKIR
Mæling nr. THK21
Stefna N11°W
Dags. 73.08.12
Mælt af HILMAR
Aths. CIRCLE2-DBL
Sýndarviðnám [Ωm]
Lengd [m]

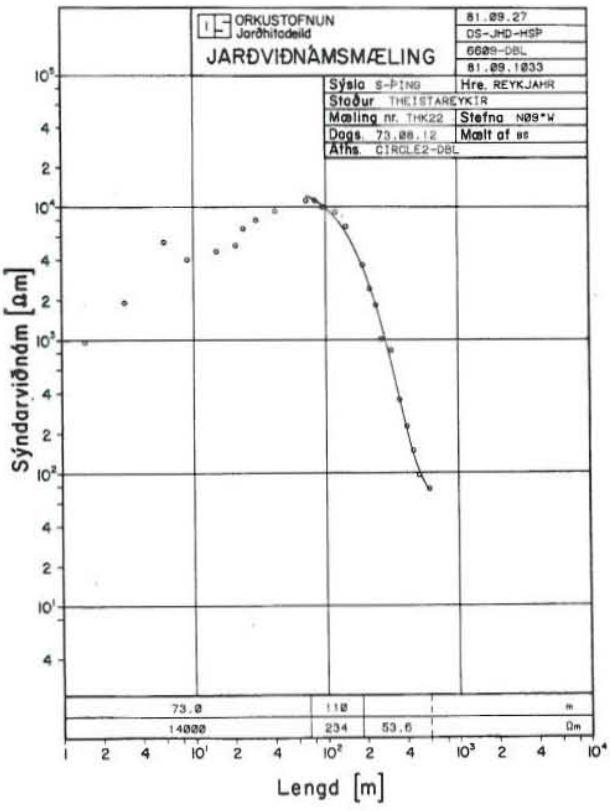
ORKUSTOFNUN
Jarðhitadeild
JARÐVIÐNÁMSMÆLING
81.09.27
OS-JHD-HSP
6009-DBL
81.09.1033
Sýsla S-ÞING
Hre. REYKJAHR
Staður THEISTAREYKIR
Mæling nr. THK22
Stefna N09°W
Dags. 73.08.12
Mælt af BS
Aths. CIRCLE2-DBL
Sýndarviðnám [Ωm]
Lengd [m]

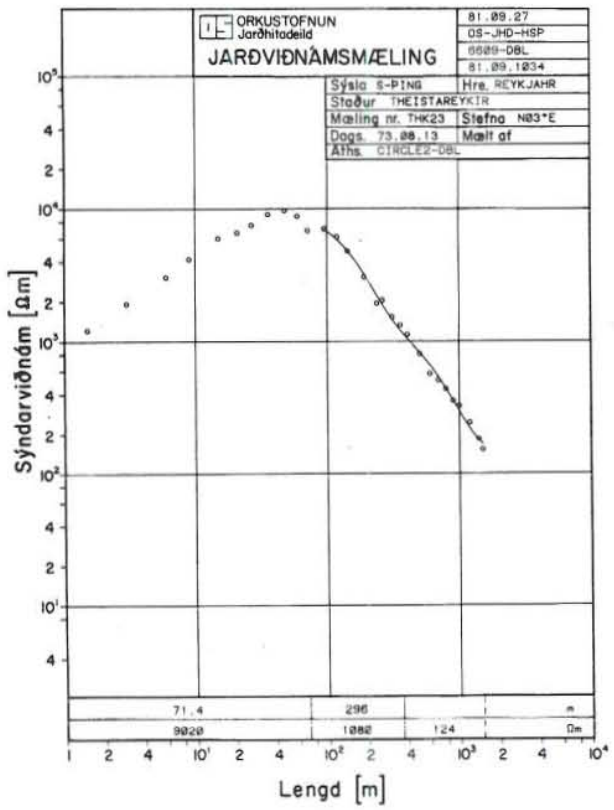
ORKUSTOFNUN
Jarðhitadeild
JARÐVIÐNÁMSMÆLING
81.09.27
OS-JHD-HSP
6009-DBL
81.09.1034
Sýsla S-ÞING
Hre. REYKJAHR
Staður THEISTAREYKIR
Mæling nr. THK23
Stefna N03°E
Dags. 73.08.13
Mælt af
Aths. CIRCLE2-DBL
Sýndarviðnám [Ωm]
Lengd [m]

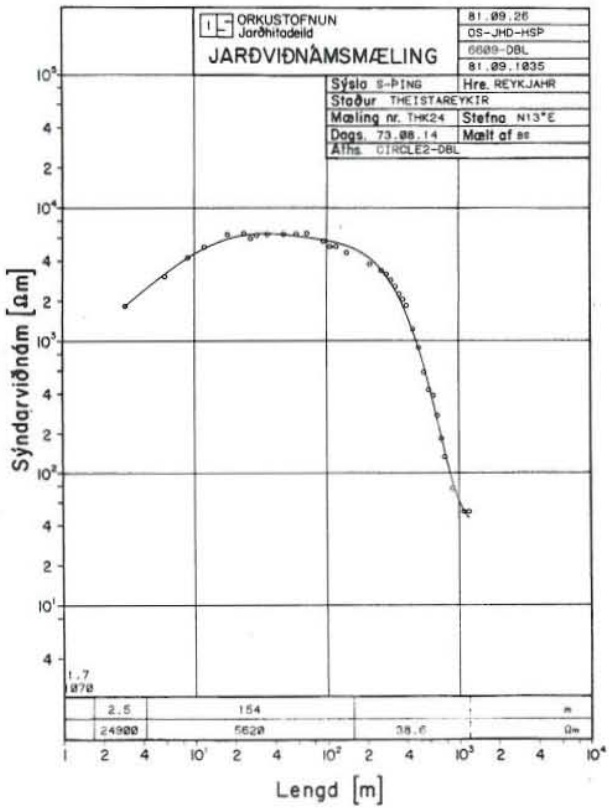
ORKUSTOFNUN
Jarðhitadeild
JARÐVIÐNÁMSMÆLING
81.09.26
OS-JHD-HSP
6009-DBL
81.09.1035
Sýsla S-ÞING
Hre. REYKJAHR
Staður THEISTAREYKIR
Mæling nr. THK24
Stefna N13°E
Dags. 73.08.14
Mælt af BS
Aths. CIRCLE2-DBL
Sýndarviðnám [Ωm]
Lengd [m]

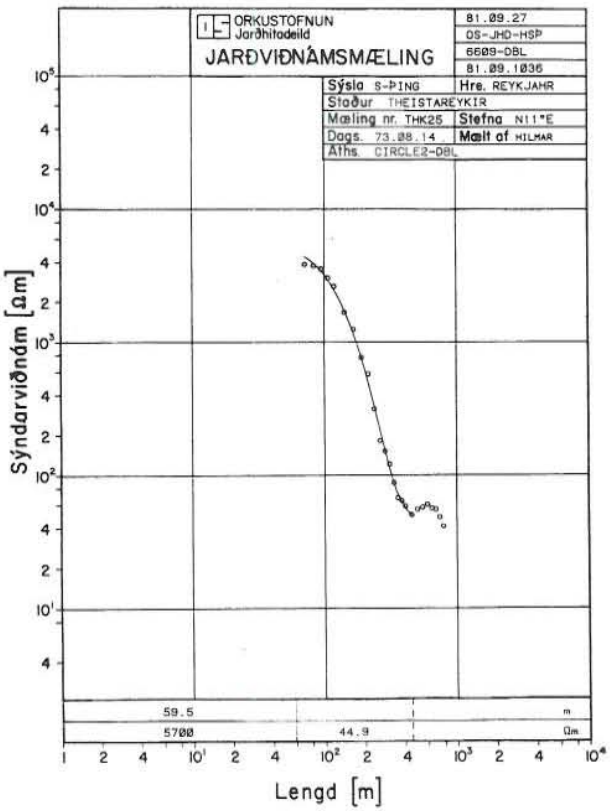
ORKUSTOFNUN
Jarðhitadeild
JARÐVIÐNÁMSMÆLING
81.09.27
OS-JHD-HSÞ
6609-DBL
81.09.1036
Sýsla S-ÞING
Hre. REYKJAHR
Staður THEISTAREYKIR
Mæling nr. THK25
Stefna N11°E
Dags. 73.08.14
Mælt af HILMAR
Aths. CIRCLE2-DBL
Sýndarviðnám [Ωm]
Lengd [m]
59.5
m
5700
44.9
Ωm

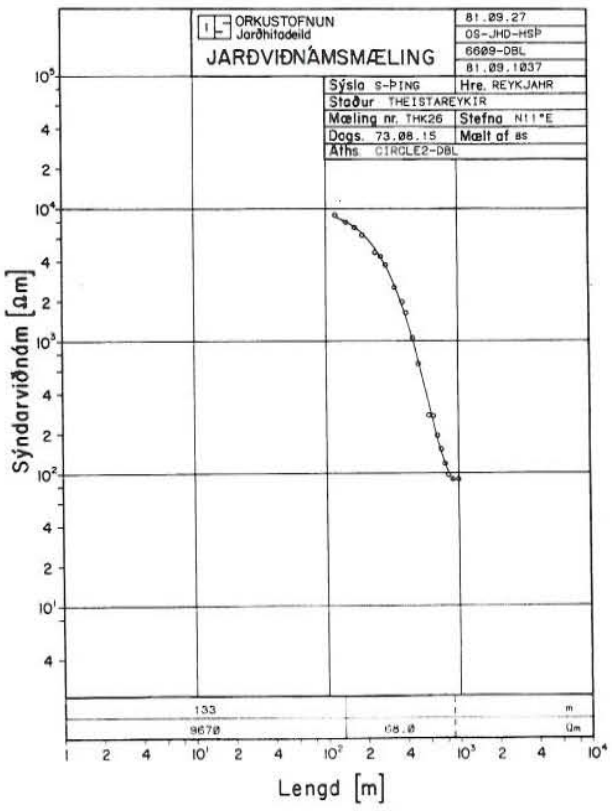
ORKUSTOFNUN
Jarðhitadeild
JARÐVIÐNÁMSMÆLING
81.09.27
OS-JHD-HSÞ
6609-DBL
81.09.1037
Sýsla S-ÞING
Hre. REYKJAHR
Staður THEISTAREYKIR
Mæling nr. THK26
Stefna N11°E
Dags. 73.08.15
Mælt af BS
Aths. CIRCLE2-DBL
Sýndarviðnám [Ωm]
Lengd [m]
133
m
9670
65.0
Ωm

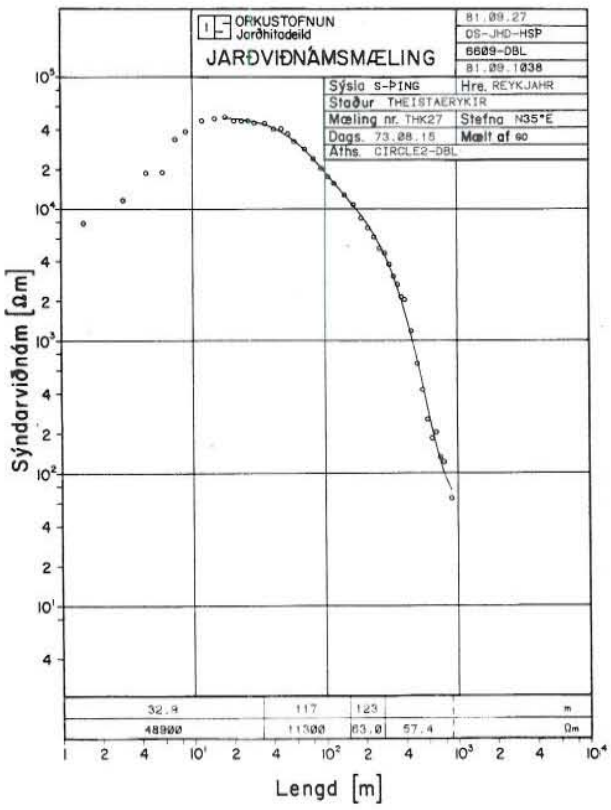
ORKUSTOFNUN
Jarðhitadeild
JARÐVIÐNÁMSMÆLING
81.09.27
OS-JHD-HSÞ
6609-DBL
81.09.1038
Sýsla S-ÞING
Hre. REYKJAHR
Staður THEISTAERYKIR
Mæling nr. THK27
Stefna N35°E
Dags. 73.08.15
Mælt af GO
Aths. CIRCLE2-DBL
Sýndarviðnám [Ωm]
Lengd [m]
32.9
117
123
m
48800
11300
63.0
57.4
Ωm

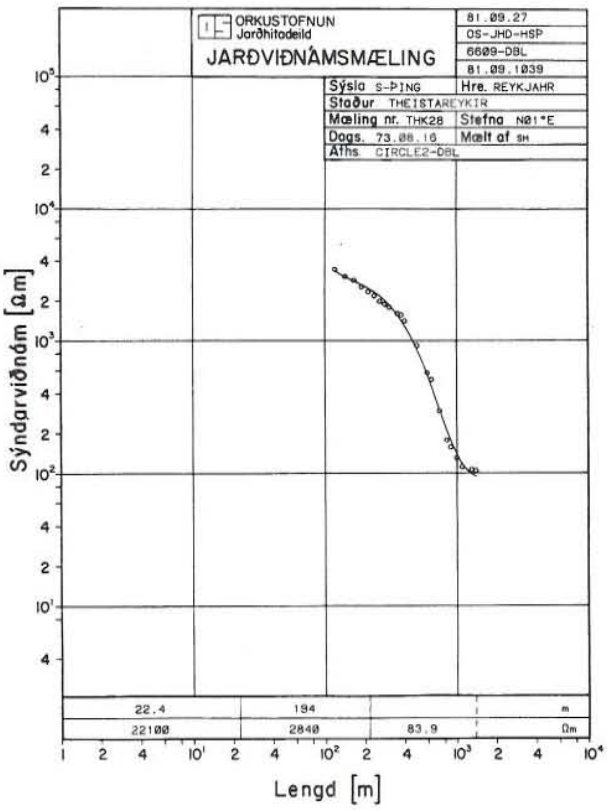
ORKUSTOFNUN
Jarðhitadeild
JARÐVIÐNÁMSMÆLING
81.09.27
OS-JHD-HSÞ
6609-DBL
81.09.1039
Sýsla S-ÞING
Hre. REYKJAHR
Staður THEISTAREYKIR
Mæling nr. THK28
Stefna N01°E
Dags. 73.08.16
Mælt af SH
Aths. CIRCLE2-DBL
Sýndarviðnám [Ωm]
Lengd [m]
22.4
194
m
22100
2840
83.9
Ωm

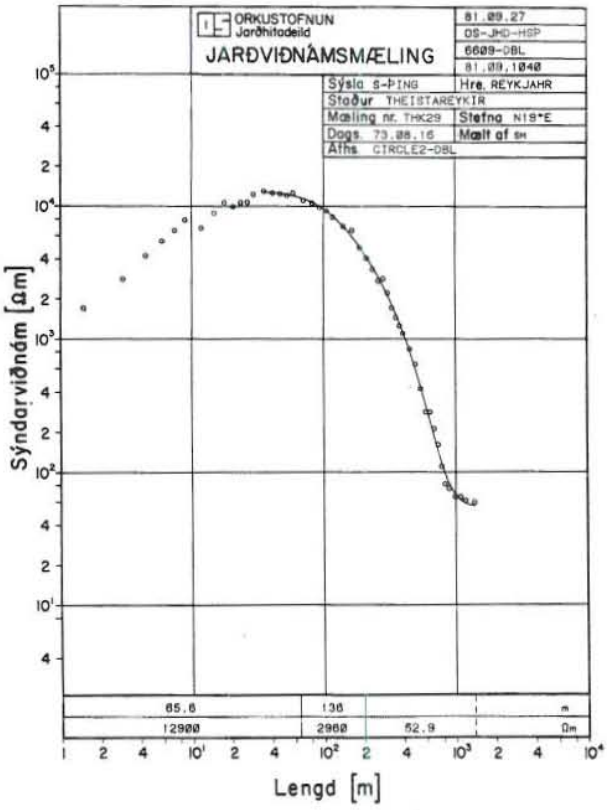
ORKUSTOFNUN
Jarðhitadeild
JARÐVIÐNÁMSMÆLING
81.09.27
OS-JHD-HSÞ
6609-DBL
81.09.1040
Sýsla S-ÞING
Hre. REYKJAHR
Staður THEISTAREYKIR
Mæling nr. THK29
Stefna N19°E
Dags. 73.08.16
Mælt af SH
Aths. CIRCLE2-DBL
Sýndarviðnám [Ωm]
Lengd [m]

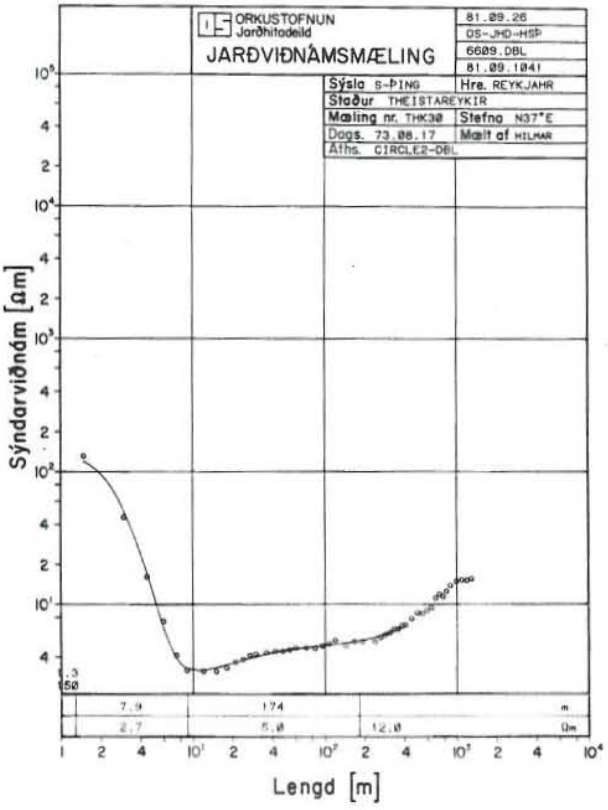
ORKUSTOFNUN
Jarðhitadeild
JARÐVIÐNÁMSMÆLING
81.09.26
OS-JHD-HSÞ
6609.DBL
81.09.1041
Sýsla S-ÞING
Hre. REYKJAHR
Staður THEISTAREYKIR
Mæling nr. THK30
Stefna N37°E
Dags. 73.08.17
Mælt af HILMAR
Aths. CIRCLE2-DBL
Sýndarviðnám [Ωm]
Lengd [m]

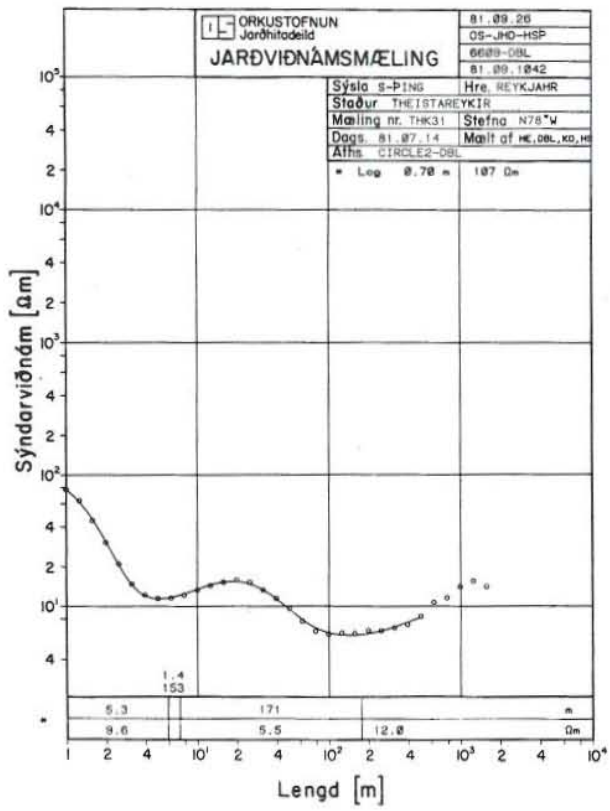
ORKUSTOFNUN
Jarðhitadeild
JARÐVIÐNÁMSMÆLING
81.09.26
OS-JHD-HSÞ
6609-DBL
81.09.1042
Sýsla S-ÞING
Hre. REYKJAHR
Staður THEISTAREYKIR
Mæling nr. THK31
Stefna N78°W
Dags. 81.07.14
Mælt af HE,DBL,KO,HS
Aths. CIRCLE2-DBL
Sýndarviðnám [Ωm]
Lengd [m]

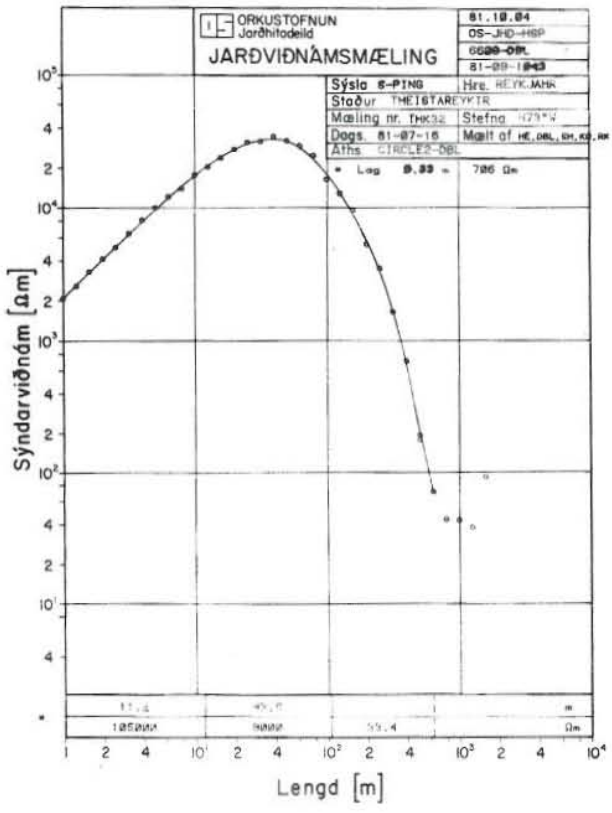
ORKUSTOFNUN
Jarðhitadeild
JARÐVIÐNÁMSMÆLING
81.10.04
OS-JHD-HSÞ
6609-DBL
81-09-1043
Sýsla S-ÞING
Hre. REYKJAHR
Staður THEISTAREYKIR
Mæling nr. THK32
Dags. 81-07-15
Aths. CIRCLE2-DBL
Sýndarviðnám [Ωm]
Lengd [m]

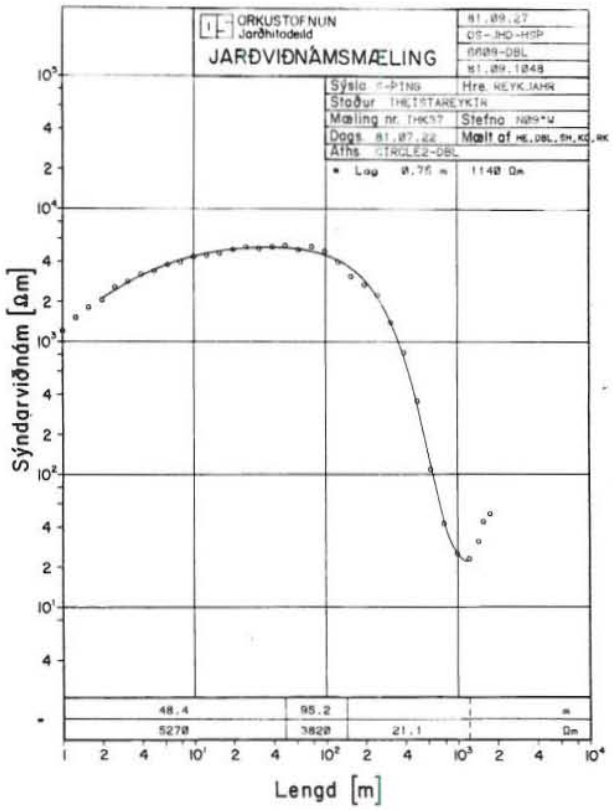
ORKUSTOFNUN
Jarðhitadeild
JARÐVIÐNÁMSMÆLING
81.09.27
OS-JHD-HSP
0009-DBL
81.09.1048
Sýsla Á-PING
Hre. REYKJAHR
Staður HEISTAREYKIR
Mæling nr. HK17
Stefna NW-W
Dags 81.07.22
Mælt af HE,DBL,SH,KG,RK
Áths CIRCLE2-DBL
Lag 0.75 m
1140 Ωm
48.4
95.2
m
5270
3820
21.1
Ωm
Sýndarviðnám [Ωm]
Lengd [m]

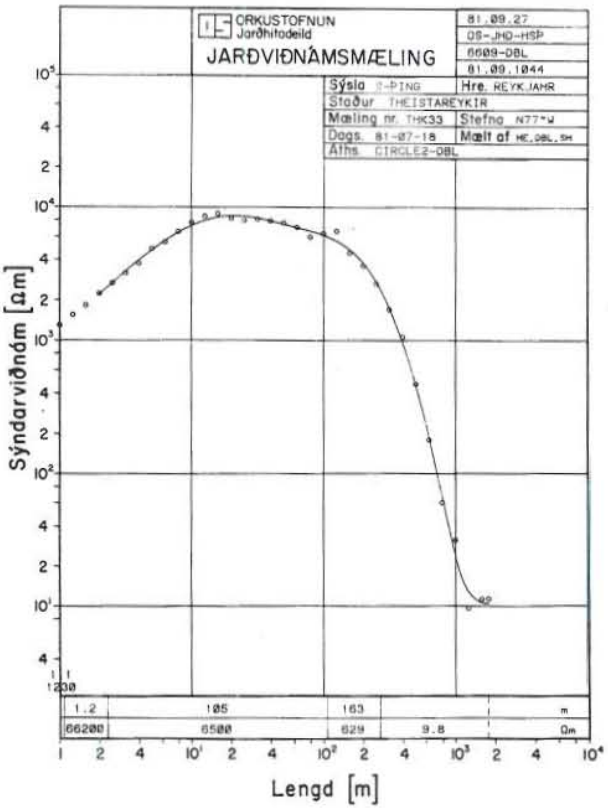
ORKUSTOFNUN
Jarðhitadeild
JARÐVIÐNÁMSMÆLING
81.09.27
OS-JHD-HSP
6609-DBL
81.09.1044
Sýsla S-ÞING
Hre. REYKJAHR
Staður THEISTAREYKIR
Mæling nr. THK33
Stefna N77°W
Dags. 81-07-18
Mælt af HE,DBL,SH
Aths. CIRCLE2-DBL
Sýndarviðnám [Ωm]
Lengd [m]
1.2 105 163 m
66200 6500 629 9.8 Ωm

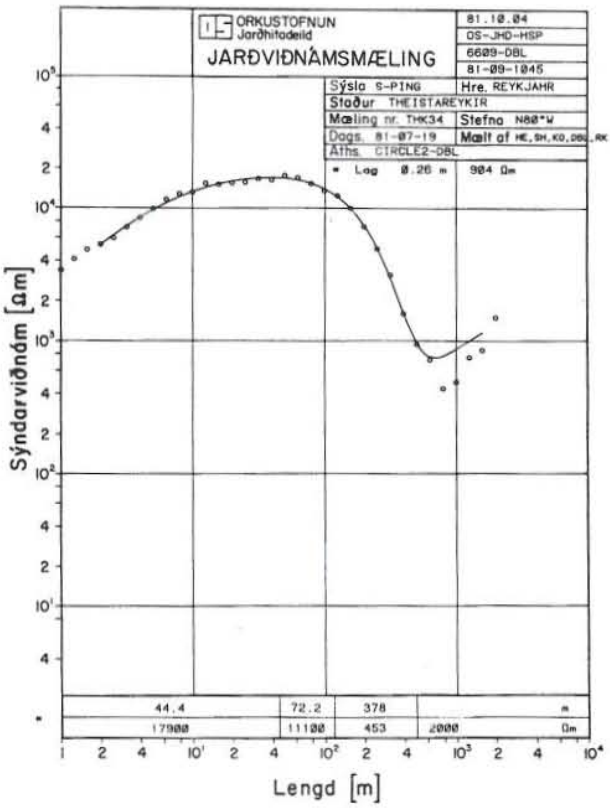
ORKUSTOFNUN
Jarðhitadeild
JARÐVIÐNÁMSMÆLING
81.10.04
OS-JHD-HSP
6609-DBL
81-09-1045
Sýsla S-ÞING
Hre. REYKJAHR
Staður THEISTAREYKIR
Mæling nr. THK34
Stefna N80°W
Dags. 81-07-19
Mælt af HE,SH,KD,DBL,RK
Aths. CIRCLE2-DBL
* Lag 0.26 m 904 Ωm
Sýndarviðnám [Ωm]
Lengd [m]
44.4 72.2 378 m
17900 11100 453 2000 Ωm

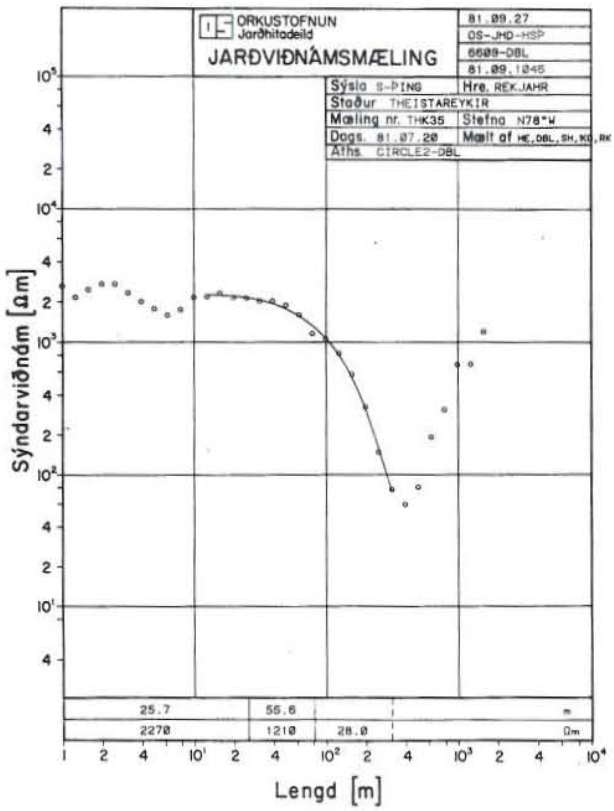
ORKUSTOFNUN
Jarðhitadeild
JARÐVIÐNÁMSMÆLING
81.09.27
OS-JHD-HSP
6609-DBL
81.09.1045
Sýsla S-ÞING
Hre. REYKJAHR
Staður THEISTAREYKIR
Mæling nr. THK35
Stefna N78°W
Dags. 81.07.20
Mælt af HE,DBL,SH,KD,RK
Aths. CIRCLE2-DBL
Sýndarviðnám [Ωm]
Lengd [m]
25.7 55.6 m
2270 1210 28.0 Ωm

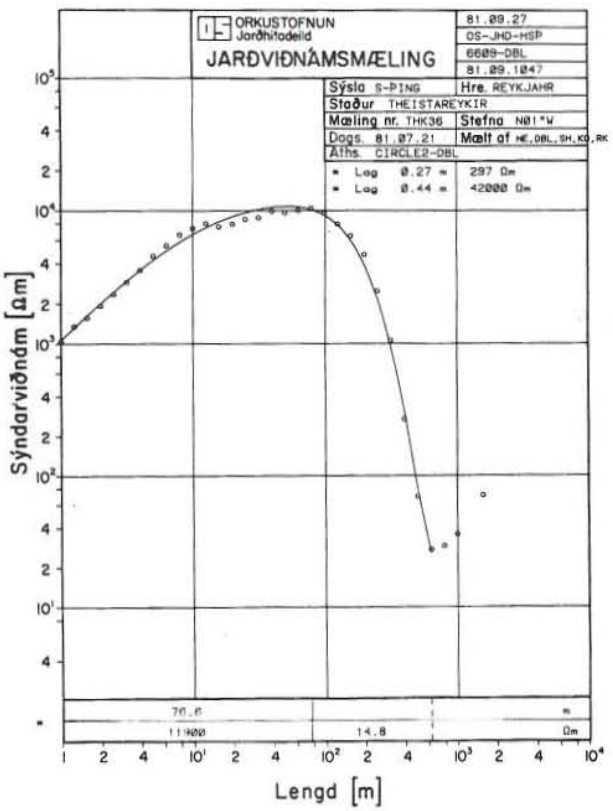
ORKUSTOFNUN
Jarðhitadeild
JARÐVIÐNÁMSMÆLING
81.09.27
OS-JHD-HSP
6609-DBL
81.09.1047
Sýsla S-ÞING
Hre. REYKJAHR
Staður THEISTAREYKIR
Mæling nr. THK36
Stefna N01°W
Dags. 81.07.21
Mælt af HE,DBL,SH,KD,RK
Aths. CIRCLE2-DBL
* Lag 0.27 m 297 Ωm
* Lag 0.44 m 42000 Ωm
Sýndarviðnám [Ωm]
Lengd [m]
76.6 m
11900 14.8 Ωm

ORKUSTOFNUN
JARÐHITADEILD

VIÐNÁMSMÆLINGAR

Sýsla, kaupstaður:	Hreppur:
S-Þingeyjarsýsla	REYKJAHREPPUR
Staður: ÞEISTAREYKIR	**Mæling nr.:** THK-32
Dagsetning: 16/7 '81 / 15/7 1981	**Stefna línu:** N113°A
Mælitæki:	**Mælt af:** SH. HE. KJÓ. DL

S m	P m	K	I mA	ΔV mV	ϱ Ωm	Aths.	S m	P m	K	I mA	ΔV mV	ϱ Ωm	Aths.
~~100~~	0.2	~~78500~~	100	~~30.75~~	12070		63.1	2	5120	5	92.5	28860	/
—	2.0	~~7850~~	—	407	15970	/	—	0.2	31300	5	8.4	~~26290~~	
—	20.0	754	—	3800	14330		79.4	2	4950	5	49,5	24500	
—	39.4	332	—	9020	14970		126	—	12500	-	10.0	12500	
							158	-	19600	20	19.2	9408	
1.00	0.2	7.54	5	2730	2068		200	—	31400	—	6,62	5197	
1.26	-	12.2	-	2100	2562		251	—	49500	20	2,85	3527	
1.58	-	19.3	-	1700	3281		316	—	78100	50	2,75	2156	
2.00	-	31.1	—	1320	4105		—	~~398~~	3880	—	5.0	1980	útleiðsla endurt. 16/7
2.51	-	49.2	—	1020	5018		398	—	6190	40	31.5	2437	
3.16	-	78.1	—	81x3	6349		—	2	124000	—	16.5	2557	
3.98	-	124	—	64x5	8000		501	39.8	9840	100	19	4728	
5.01	-	197	-	50x5	9940	Endað 16/7	316	2	78400	140	10.1	2828	n=50, 5=5% útl
6.31	-	312	-	38,5	12010		—	398	3880	—	260	3603	n=40; 5=6%
7.94	-	495	—	28,0	13860		251	2	19500	130	18.5	3522	3432
10.0	-	785	—	22,3	17500		—	398	2420	—	359	3341	
12.6	—	1250	—	16x1	20130		316	2	78400	140	5.51	1542	1616
15.8	—	1960	—	12x0	23520		-	398	3880	—	122	1690	
20.0	-	3140	—	8x76	27320		398	398	6190	100	22.6	699	
25.1	-	~~4950~~	—	~~5,9~~	~~29200~~		—	2	124000	-	2.25	1395	691
—	2	192	—	63.0	30990	/	—	20	12400	-	11.0	682	5=2‰
316	02	7840	-	3,65	28610		501	398	9840	100	3.49	172	190
—	2	781	-	4,00	31240		—	79.4	1840	100	8.62	208	
39.8	—	1240	-	275	34100		631	398	15700	140	0.420	23.5	n=30 5=10%
—	0.2	12400	-	23.0	~~28520~~		—	79.4	7750	—	1.13	31.2	20- 6%
50.1	0.2	19760	—	14.7	~~29160~~		794	—	12300	130	~~0.272~~	36.5	60- 11%
—	2	1970	—	160	31520	/	—	—	—	—	0.839	396	~~meðal: 4~~ ~~n=40 — 5=9%~~

Aths.: Úrvinnslutaki gapt upp. (Problem in instruments)
Rigning og súld; útleiðsla og hætt í 501m. (Leakage in 501m)
Haldið áfram daginn eftir með viðg. úr og nýtt úrvinnslutaki
Bras. og * Hundaveður (Continued next day)
Rain - bad weather

ORKUSTOFNUN
JARÐHITADEILD

VIÐNÁMSMÆLINGAR

Sýsla, kaupstaður:	Hreppur:

Staður:	Mæling nr.:
Þeistareykir	THK-32

Dagsetning:	Stefna línu:	Mælitæki:	Mælt af:
15.-16.7 '81	N 113°A	GLS-7208 SLM-7701 URV-7707	HE, SH, KJÓ, DL, RK

S m	P m	K	I mA	ΔV mV	ϱ Ωm	Aths.	S m	P m	K	I mA	ΔV mV	ϱ Ωm	Aths.
794	39.8	21800	130	0,0406	3.87	send.14; mæl 3 n=6 - σ=44%							
–	–	–	131	0,034	12,7	send 2; mæl 12 22 16%							
–	–	–	130	0,266	25,3	s=4 m:3 20 20%							
–	–			0,635	60,5								
–	–			0.476	45.4	s/m = 2/1.2							
–	–			0.450	42.9	s/m 4/3 ~5%							
–	–			0.419	39.9	s/m 8/5 n:14 σ: 7%							
–	79.4	12300		1.46	69.6	s/m 2/1.2 20 – 2%							
				1.43	67.6	s/m 4/3 10 2%							
631	79.4	7750	100	2.34	90.6	40 – 5%							
–	39.8	15700	–	0,468	36.7	40 10%							
–	–			0.631	49,5	s/m 8/5							
–	100	0,094											
–	63.1	9800			101								
1000	79.4	19700	180	3.5	191	s/m = 2/1.2							
–	–	–	–	2.85	156	s/m = 4/3 30 – 14%							
–	39.8	39400	–	0.473	51.7	s/m = 4/3 30 – 50%							
–	–	–	–	0.361	39.5	s/m = 4/3 n:30 – σ: 18%							
–	79.4	19700	–	1.97	108	s/m = 4/3 30 – 10%							
1260	79.4	31300	190	1.95	160	s/m = 4/3 50 – 15%							
–	39.8	62600	–	0.311	51	s/m = 4/3 50 – 34%							
–	–	–	–	0.194	32	s/m = 4/3 50 – 20%							
–	79.4	31300	–	1.33	109	s/m = 4/3 50 –							
1580	79.4	49300	200	1.61	198	54 – 20%							
–	–	–	–	1.57	193	50 – 14%							
–	39.8	98500	–	0.398	98	50 – 25%							
–	–	–	–	0.349	86	50 – 14							

Aths.:

Settum Fluke-mæli inn í straumtás sendis

„Fluke"inn sýnir 6 mV hærra en sjálfur mælirinn á 1000 mV skala

Aths. Af hverju lækkar spennumerkið þegar komið er á sendistinn

(The potential-electrode (east-side) has a bad contact)

Annar spennupóllinn í 79.4 m er uppi á hraunhrygg. (A-póllinn)

A P P E N D I X II

Samples of computer printouts of interpreted sounding data for the programs "Vidnam", "Circle2" and "Dim-2".

ORKUSTOFNUN UNU THK04
81-10-08 DRL

4 LAYERS

	H 1 = 0.68	RO 1 = 782.0000	
DY 1 = 0.68			R 1 = 15.5179
	H 2 = 71.00	RO 2 =12135.0000	
DY 2 = 71.68			R 2 = 0.1756
	H 3 = 125.00	RO 3 = 2131.0000	
DY 3 = 196.68			R 3 = 0.0267
		RO 4 = 57.0000	

DIST.	CALCUL. RHOAPP	LOG10
1.00	0.1143033E+04	3.06
1.26	0.1351754E+04	3.13
1.58	0.1630081E+04	3.21
2.00	0.1978719E+04	3.30
2.51	0.2397607E+04	3.38
3.16	0.2888342E+04	3.46
3.98	0.3452726E+04	3.54
5.01	0.4090026E+04	3.61
6.31	0.4794972E+04	3.68
7.94	0.5556501E+04	3.74
10.00	0.6357171E+04	3.80
12.59	0.7173311E+04	3.86
15.85	0.7978128E+04	3.90
19.95	0.8733537E+04	3.94
25.12	0.9412074E+04	3.97
31.62	0.9977703E+04	4.00
39.81	0.1039399E+05	4.02
50.12	0.1061685E+05	4.03
63.10	0.1058733E+05	4.02
79.43	0.1022918E+05	4.01
100.00	0.9465089E+04	3.98
125.89	0.8262524E+04	3.92
158.49	0.6695562E+04	3.83
199.53	0.4966483E+04	3.70
251.19	0.3338725E+04	3.52
316.23	0.2017972E+04	3.30
398.11	0.1083533E+04	3.03
501.19	0.5101050E+03	2.71
630.96	0.2174745E+03	2.34
794.33	0.1016701E+03	2.01
1000.00	0.6821018E+02	1.83
1258.93	0.6084213E+02	1.78
1584.89	0.5897373E+02	1.77
1995.26	0.5818680E+02	1.76

SAMPLE COMPUTER OUTPUT OF "VIDNAM" PROGRAM FOR FORWARD ONE-DIMENSIONAL MODELING.

ORKUSTOFNUN UNU THK04
81-10-08 DBL

COMPARISON OF CALCULATED AND MEASURED VALUES

DIST.	MEAS. RES.	LOG MEAS.	LOG CALC.	DIFF	WEIGHT
1.50	0.1260000E+04	3.10	3.19	-0.09	8.1633
3.00	0.2500000E+04	3.40	3.44	-0.04	8.1633
4.50	0.3300000E+04	3.52	3.58	-0.06	8.1633
6.00	0.4100000E+04	3.61	3.67	-0.05	8.1633
7.50	0.5350000E+04	3.73	3.73	0.00	8.1633
9.00	0.6350000E+04	3.80	3.78	0.03	8.1633
12.00	0.8650000E+04	3.94	3.85	0.09	8.1633
15.00	0.1020000E+05	4.01	3.89	0.12	8.1633
18.00	0.1050000E+05	4.02	3.92	0.10	8.1633
21.00	0.1075000E+05	4.03	3.95	0.08	8.1633
24.00	0.1090000E+05	4.04	3.97	0.07	8.1633
27.00	0.1070000E+05	4.03	3.98	0.05	8.1633
30.00	0.1150000E+05	4.06	3.99	0.07	8.1633
36.00	0.1150000E+05	4.06	4.01	0.05	8.1633
42.00	0.1210000E+05	4.08	4.02	0.06	8.1633
48.00	0.1200000E+05	4.08	4.02	0.05	8.1633
54.00	0.1200000E+05	4.08	4.03	0.05	8.1633
60.00	0.1190000E+05	4.08	4.03	0.05	8.1633
72.00	0.1150000E+05	4.06	4.02	0.04	8.1633
84.00	0.1080000E+05	4.03	4.00	0.03	8.1633
96.00	0.1020000E+05	4.01	3.98	0.03	8.1633
108.00	0.9500000E+04	3.98	3.96	0.02	8.1633
120.00	0.8300000E+04	3.92	3.93	-0.01	8.1633
144.00	0.6700000E+04	3.83	3.87	-0.04	8.1633
168.00	0.5800000E+04	3.76	3.80	-0.03	8.1633
192.00	0.5200000E+04	3.72	3.72	0.00	8.1633
216.00	0.4300000E+04	3.63	3.64	-0.01	8.1633
240.00	0.3500000E+04	3.54	3.56	-0.02	8.1633
264.00	0.2800000E+04	3.45	3.48	-0.03	8.1633
288.00	0.2700000E+04	3.43	3.40	0.03	8.1633
312.00	0.2100000E+04	3.32	3.32	0.00	8.1633
336.00	0.1600000E+04	3.20	3.24	-0.04	8.1633
360.00	0.1300000E+04	3.11	3.16	-0.05	8.1633
384.00	0.1000000E+04	3.00	3.08	-0.08	8.1633
408.00	0.1060000E+04	3.03	3.00	0.02	8.1633
456.00	0.6400000E+03	2.81	2.85	-0.04	8.1633
504.00	0.4500000E+03	2.65	2.70	-0.05	8.1633
552.00	0.3200000E+03	2.51	2.56	-0.05	8.1633
600.00	0.2200000E+03	2.34	2.42	-0.07	8.1633
648.00	0.1600000E+03	2.20	2.30	-0.09	8.1633
696.00	0.1500000E+03	2.18	2.19	-0.01	8.1633
744.00	0.1140000E+03	2.06	2.09	-0.03	8.1633
792.00	0.9200000E+02	1.96	2.01	-0.05	8.1633
840.00	0.7600000E+02	1.88	1.95	-0.06	8.1633
900.00	0.6800000E+02	1.83	1.90	-0.07	8.1633
1000.00	0.6500000E+02	1.81	1.83	-0.02	8.1633
1100.00	0.6300000E+02	1.80	1.79	0.01	8.1633
1200.00	0.6000000E+02	1.78	1.79	-0.01	8.1633
1300.00	0.5600000E+02	1.75	1.78	-0.03	8.1633
1400.00	0.6400000E+02	1.81	1.77	0.03	8.1633
1500.00	0.5900000E+02	1.77	1.77	0.00	8.1633

WEIGHTED MEAN DIFFERENCE OF MEASURED AND CALCULATED LOGVALUES = 0.05

ORKUSTOFNUN UNU THK04
81-10-08 DBL

LOG10 OF APPARENT RESISTIVITY VERSUS AB/2

X=CALCULATED I=MEASURED *=COINCIDENT

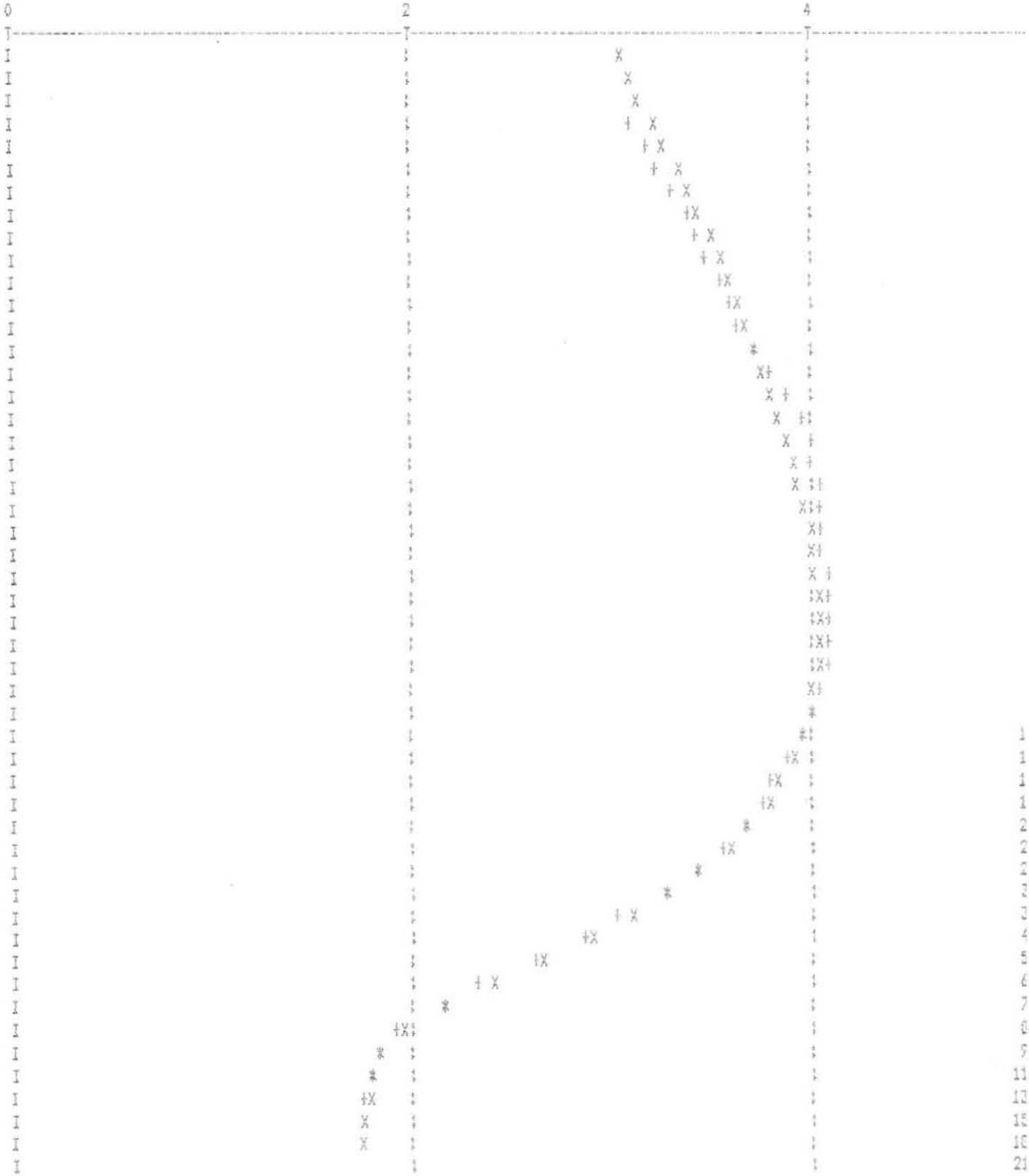

ORKUSTOFNUN UNU THK04
81-10-08 DBL

4 LAYERS

	H 1 = 0.36	RO 1 = 356.0000	
DY 1 = 0.36			R 1 = 50.1854
	H 2 = 33.00	RO 2 =17866.0000	
DY 2 = 33.36			R 2 = 0.2702
	H 3 = 115.00	RO 3 = 4828.0000	
DY 3 = 148.36			R 3 = 0.0120
		RO 4 = 58.0000	

DIST.	CALCUL. RHOAPP	LOG10
1.00	0.9433602E+03	2.97
1.26	0.1170873E+04	3.07
1.58	0.1450869E+04	3.16
2.00	0.1792129E+04	3.25
2.51	0.2204779E+04	3.34
3.16	0.2699344E+04	3.43
3.98	0.3285859E+04	3.52
5.01	0.3972715E+04	3.60
6.31	0.4765070E+04	3.68
7.94	0.5662818E+04	3.75
10.00	0.6658098E+04	3.82
12.59	0.7732363E+04	3.89
15.85	0.8853055E+04	3.95
19.95	0.9969728E+04	4.00
25.12	0.1100976E+05	4.04
31.62	0.1187439E+05	4.07
39.81	0.1243900E+05	4.09
50.12	0.1256621E+05	4.10
63.10	0.1214275E+05	4.08
79.43	0.1113882E+05	4.05
100.00	0.9656979E+04	3.98
125.89	0.7917806E+04	3.90
158.49	0.6165202E+04	3.79
199.53	0.4556931E+04	3.66
251.19	0.3143476E+04	3.50
316.23	0.1948939E+04	3.29
398.11	0.1036751E+04	3.02
501.19	0.4609904E+03	2.66
630.96	0.1835998E+03	2.26
794.33	0.8766410E+02	1.94
1000.00	0.6480582E+02	1.81
1258.93	0.6052832E+02	1.78
1584.89	0.5941468E+02	1.77
1995.26	0.5885289E+02	1.77

ORKUSTOFNUN UNU THK04
81-10-08 DBL

COMPARISON OF CALCULATED AND MEASURED VALUES

DIST.	MEAS. RES.	LOG MEAS.	LOG CALC.	DIFF	WEIGHT
1.50	0.1260000E+04	3.10	3.14	-0.04	8.1633
3.00	0.2500000E+04	3.40	3.41	-0.01	8.1633
4.50	0.3300000E+04	3.52	3.56	-0.04	8.1633
6.00	0.4100000E+04	3.61	3.66	-0.05	8.1633
7.50	0.5350000E+04	3.73	3.73	-0.01	8.1633
9.00	0.6350000E+04	3.80	3.79	0.01	8.1633
12.00	0.8650000E+04	3.94	3.87	0.06	8.1633
15.00	0.1020000E+05	4.01	3.93	0.08	8.1633
18.00	0.1050000E+05	4.02	3.98	0.05	8.1633
21.00	0.1075000E+05	4.03	4.01	0.02	8.1633
24.00	0.1090000E+05	4.04	4.03	0.00	8.1633
27.00	0.1070000E+05	4.03	4.05	-0.02	8.1633
30.00	0.1150000E+05	4.06	4.07	-0.01	8.1633
36.00	0.1150000E+05	4.06	4.09	-0.03	8.1633
42.00	0.1210000E+05	4.08	4.10	-0.01	8.1633
48.00	0.1200000E+05	4.08	4.10	-0.02	8.1633
54.00	0.1200000E+05	4.08	4.10	-0.02	8.1633
60.00	0.1190000E+05	4.08	4.09	-0.01	8.1633
72.00	0.1150000E+05	4.06	4.07	0.00	8.1633
84.00	0.1080000E+05	4.03	4.03	0.00	8.1633
96.00	0.1020000E+05	4.01	4.00	0.01	8.1633
108.00	0.9500000E+04	3.98	3.96	0.02	8.1633
120.00	0.8300000E+04	3.92	3.92	0.00	8.1633
144.00	0.6700000E+04	3.83	3.84	-0.01	8.1633
168.00	0.5800000E+04	3.76	3.76	0.00	8.1633
192.00	0.5200000E+04	3.72	3.68	0.03	8.1633
216.00	0.4300000E+04	3.63	3.61	0.03	8.1633
240.00	0.3500000E+04	3.54	3.53	0.01	8.1633
264.00	0.2800000E+04	3.45	3.46	-0.01	8.1633
288.00	0.2700000E+04	3.43	3.38	0.05	8.1633
312.00	0.2100000E+04	3.32	3.30	0.02	8.1633
336.00	0.1600000E+04	3.20	3.22	-0.02	8.1633
360.00	0.1300000E+04	3.11	3.14	-0.03	8.1633
384.00	0.1000000E+04	3.00	3.06	-0.06	8.1633
408.00	0.1060000E+04	3.03	2.98	0.04	8.1633
456.00	0.6400000E+03	2.81	2.81	-0.01	8.1633
504.00	0.4500000E+03	2.65	2.65	0.00	8.1633
552.00	0.3200000E+03	2.51	2.50	0.00	8.1633
600.00	0.2200000E+03	2.34	2.35	-0.01	8.1633
648.00	0.1600000E+03	2.20	2.22	-0.02	8.1633
696.00	0.1500000E+03	2.18	2.11	0.06	8.1633
744.00	0.1140000E+03	2.06	2.02	0.04	8.1633
792.00	0.9200000E+02	1.96	1.95	0.02	8.1633
840.00	0.7600000E+02	1.88	1.89	-0.01	8.1633
900.00	0.6800000E+02	1.83	1.86	-0.03	8.1633
1000.00	0.6500000E+02	1.81	1.81	0.00	8.1633
1100.00	0.6300000E+02	1.80	1.78	0.02	8.1633
1200.00	0.6000000E+02	1.78	1.79	-0.01	8.1633
1300.00	0.5600000E+02	1.75	1.78	-0.03	8.1633
1400.00	0.6400000E+02	1.81	1.77	0.03	8.1633
1500.00	0.5900000E+02	1.77	1.78	0.00	8.1633

WEIGHTED MEAN DIFFERENCE OF MEASURED AND CALCULATED LOGVALUES = 0.03

ORKUSTOFNUN UNU THK04
81-10-08 DBL

LOG10 OF APPARENT RESISTIVITY VERSUS AB/2

X=CALCULATED +=MEASURED *=COINCIDENT

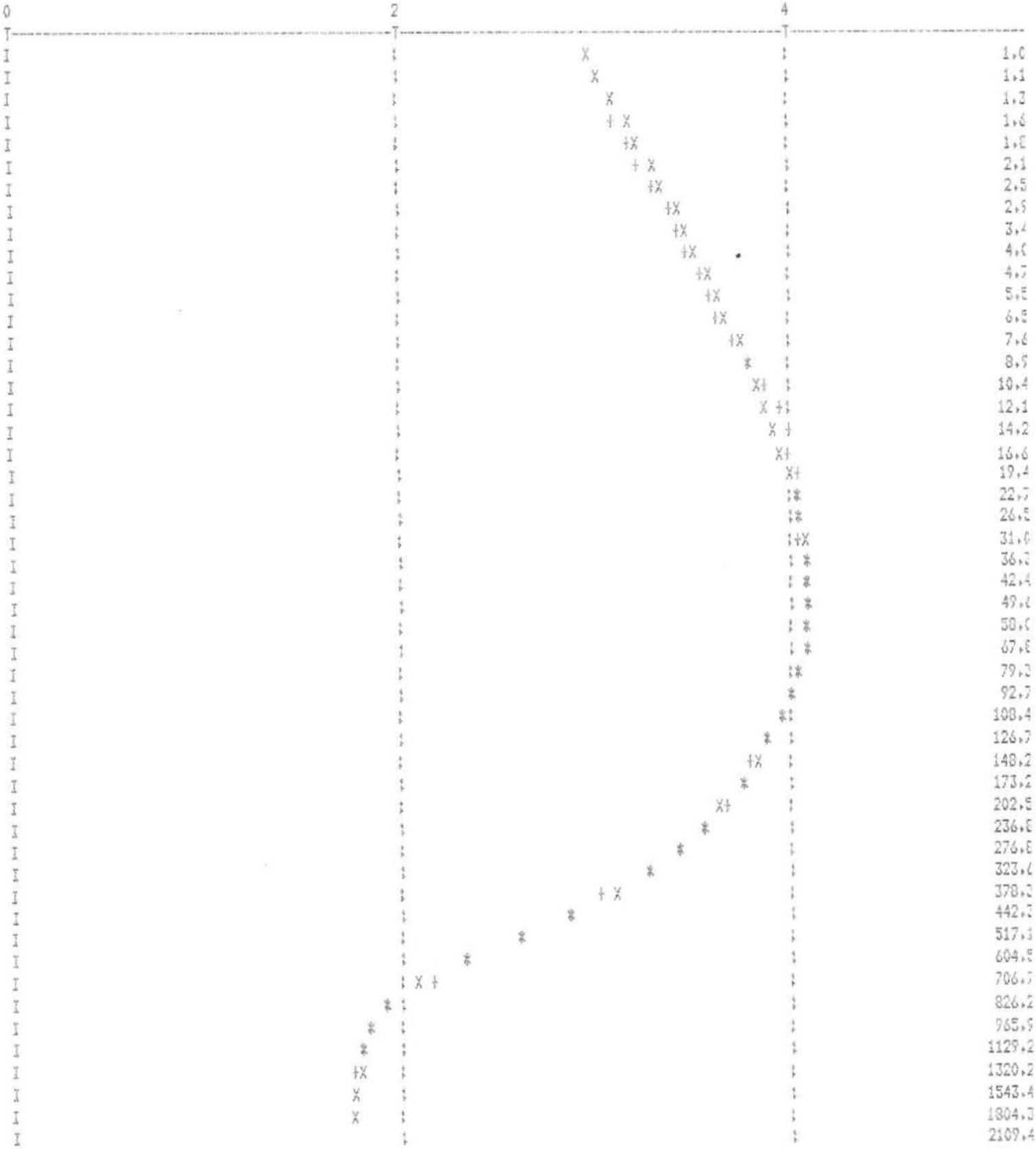

THK04

NUMBER OF DATA POINTS : 50
NUMBER OF LAYERS : 4
NUMBER OF VARIABLE PARAMETERS : 7

PROGRAM CONTROL PARAMETER : 41

THE FOLLOWING MEASUREMENTS ARE INCLUDED:

ID	TYPE	AB/2	RHO	ST.DEV
2	1	1.50	2500.00	3.50
3	1	2.25	3300.00	3.50
4	1	3.00	4100.00	3.50
5	1	3.75	5350.00	3.50
6	1	4.50	6350.00	3.50
7	1	6.00	8650.00	3.50
8	1	7.50	10200.00	3.50
9	1	9.00	10500.00	3.50
10	1	10.50	10750.00	3.50
11	1	12.00	10900.00	3.50
12	1	13.50	10700.00	3.50
13	1	15.00	11500.00	3.50
14	1	18.00	11500.00	3.50
15	1	21.00	12100.00	3.50
16	1	24.00	12000.00	3.50
17	1	27.00	12000.00	3.50
18	1	30.00	11900.00	3.50
19	1	36.00	11500.00	3.50
20	1	42.00	10800.00	3.50
21	1	48.00	10200.00	3.50
22	1	54.00	9500.00	3.50
23	1	60.00	8300.00	3.50
24	1	72.00	6700.00	3.50
25	1	84.00	5800.00	3.50
26	1	96.00	5200.00	3.50
27	1	108.00	4300.00	3.50
28	1	120.00	3500.00	3.50
29	1	132.00	2800.00	3.50
30	1	144.00	2700.00	3.50
31	1	156.00	2100.00	3.50
32	1	168.00	1600.00	3.50
33	1	180.00	1300.00	3.50
34	1	192.00	1000.00	3.50
35	1	204.00	1060.00	3.50
36	1	228.00	640.00	3.50
37	1	252.00	450.00	3.50
38	1	276.00	320.00	3.50
39	1	300.00	220.00	3.50
40	1	324.00	160.00	3.50
41	1	348.00	150.00	3.50
42	1	372.00	114.00	3.50
43	1	396.00	92.00	3.50
44	1	420.00	76.00	3.50
45	1	450.00	68.00	3.50
46	1	500.00	65.00	3.50
47	1	550.00	63.00	3.50
48	1	600.00	60.00	3.50
49	1	650.00	56.00	3.50
50	1	700.00	64.00	3.50
51	1	750.00	59.00	3.50

ITERATION NUMBER 1

LAYER	RHO	CORR.	ST.DEV.	THICKN.	CORR.	ST.DEV.	DEPTH

SAMPLE COMPUTER PRINTOUT OF "CIRCLE2" PROGRAM FOR INVERSE ONE-DIMENSIONAL MODELING.

1	1000,00	-240,494	18,449	0,50	-0,138	0,009	0,50
2	8800,00	1009,051	61,097	54,50	-7,964	0,184	55,00
3	764,00	1087,422	22,169	55,50	1,276	0,958	110,50
4	56,00	0,020	0,695				

MEANSQUARE= 0,2664D+04

ITERATION NUMBER 2

LAYER	RHO	CORR,	ST,DEV,	THICKN,	CORR,	ST,DEV,	DEPTH
1	759,51	22,754	13,793	0,36	-0,024	0,007	0,36
2	9809,05	2326,833	78,325	46,54	-10,580	0,195	46,90
3	1851,42	280,055	26,014	56,78	5,616	0,476	103,67
4	56,02	0,535	0,718				

MEANSQUARE= 0,5837D+03

ITERATION NUMBER 3

LAYER	RHO	CORR,	ST,DEV,	THICKN,	CORR,	ST,DEV,	DEPTH
1	782,26	-274,804	13,422	0,34	-0,100	0,006	0,34
2	12135,88	2777,591	105,348	35,96	-10,888	0,189	36,29
3	2131,48	2205,675	24,780	62,39	-6,874	0,375	98,69
4	56,55	1,254	0,697				

MEANSQUARE= 0,4757D+03

ITERATION NUMBER 4

LAYER	RHO	CORR,	ST,DEV,	THICKN,	CORR,	ST,DEV,	DEPTH
1	507,46	-69,479	7,623	0,24	-0,024	0,004	0,24
2	14913,47	1631,032	158,321	25,07	-6,167	0,187	25,31
3	4337,15	315,210	37,347	55,52	2,652	0,249	80,83
4	57,81	-0,057	0,697				

MEANSQUARE= 0,2240D+03

ITERATION NUMBER 5

LAYER	RHO	CORR,	ST,DEV,	THICKN,	CORR,	ST,DEV,	DEPTH
1	437,98	-37,280	6,315	0,22	-0,014	0,003	0,22
2	16544,51	943,282	195,900	18,90	-1,450	0,190	19,12
3	4652,36	46,985	38,016	58,17	-0,453	0,229	77,29
4	57,75	0,177	0,692				

MEANSQUARE= 0,1764D+03

ITERATION NUMBER 6

LAYER	RHO	CORR,	ST,DEV,	THICKN,	CORR,	ST,DEV,	DEPTH
1	400,70	-24,888	5,608	0,20	-0,011	0,003	0,20
2	17487,79	270,363	213,177	17,45	-0,537	0,184	17,65
3	4699,35	88,028	38,520	57,72	-0,087	0,224	75,37
4	57,93	0,080	0,684				

MEANSQUARE= 0,1759D+03

ITERATION NUMBER 7

LAYER	RHO	CORR,	ST,DEV,	THICKN,	CORR,	ST,DEV,	DEPTH
1	375,81	-19,580	5,224	0,19	-0,009	0,003	0,19
2	17758,15	108,043	219,537	16,91	-0,244	0,183	17,10
3	4787,37	41,474	39,025	57,63	-0,017	0,222	74,73
4	58,01	0,040	0,684				

MEANSQUARE= 0.1758D+03

ITERATION NUMBER 1

LAYER	RHO	CORR.	ST.DEV.	THICKN.	CORR.	ST.DEV.	DEPTH
1	356.23	0.000	4.939	0.18	0.000	0.003	0.18
2	17866.19	0.000	222.340	16.67	0.000	0.183	16.85
3	4828.85	0.000	39.252	57.61	0.000	0.221	74.46
4	58.05	0.000	0.684				

MEANSQUARE= 0.0000D+00

LOGARITHMIC EIGENVALUES

1	2	3	4	5	6	7
0.30D+03	0.11D+03	0.90D+02	0.72D+02	0.30D+02	0.10D+02	0.14D-01

ESTIMATED LOGARITHMIC SEMIAXES

0.33D-02	0.91D-02	0.11D-01	0.14D-01	0.33D-01	0.98D-01	0.70D+02

PARAMETER EIGENVECTORS

	1	2	3	4	5	6	7
RHO1	-0.105	0.456	-0.419	0.244	-0.198	-0.087	-0.707
D1	0.105	-0.456	0.419	-0.244	0.197	0.085	-0.708
RHO2	0.032	0.664	0.212	-0.296	0.543	0.361	-0.001
D2	0.256	0.305	0.345	-0.250	-0.125	-0.802	0.001
RHO3	0.388	0.188	0.316	-0.053	-0.709	0.458	0.000
D3	0.864	-0.074	-0.277	0.279	0.305	-0.006	0.000
RHO4	0.119	-0.100	-0.555	-0.806	-0.128	0.032	0.000

ACTUAL SEMIAXES OF 68 PERCENT CONFIDENCE ELLIPSOID
IN POSITIVE DIRECTION OF EIGENVECTOR

0.33D-02	0.91D-02	0.11D-01	0.14D-01	0.33D-01	0.96D-01	0.41D+01

IN NEGATIVE DIRECTION OF EIGENVECTOR

0.33D-02	0.91D-02	0.11D-01	0.14D-01	0.33D-01	0.92D-01	0.20D+01

EXTREME PARAMETER SETS

THE TWO MODELS EXTREMIZING RHO1 ARE:

	MAX	MIN
RHO1	1495.06	19.26
D1	0.76	0.01
DEPTH1	0.76	0.01
RHO2	17888.24	17814.17
D2	16.63	16.76
DEPTH2	17.39	16.77
RHO3	4831.08	4823.32
D3	57.62	57.60
DEPTH3	75.01	74.36
RHO4	0.58D+02	0.58D+02

THE TWO MODELS EXTREMIZING D1 ARE:

	MAX	MIN
RHO1	1494.73	19.26
D1	0.76	0.01
DEPTH1	0.76	0.01

RHO2	17898.02	17909.38
D2	16.62	16.76
DEPTH2	17.38	16.77
RHO3	4832.47	4822.64
D3	57.62	57.60
DEPTH3	75.00	74.37
RHO4	0.58D+02	0.58D+02

THE TWO MODELS EXTREMIZING RHO2 ARE:

	MAX	MIN
RHO1	372.22	285.95
D1	0.19	0.14
DEPTH1	0.19	0.14
RHO2	18591.80	17186.10
D2	15.58	17.79
DEPTH2	15.77	17.93
RHO3	4966.27	4704.65
D3	57.81	57.41
DEPTH3	73.58	75.34
RHO4	0.58D+02	0.58D+02

THE TWO MODELS EXTREMIZING D2 ARE:

	MAX	MIN
RHO1	291.95	370.74
D1	0.15	0.19
DEPTH1	0.15	0.19
RHO2	17272.52	18501.53
D2	17.96	15.43
DEPTH2	18.11	15.62
RHO3	4637.34	5036.71
D3	57.59	57.63
DEPTH3	75.70	73.25
RHO4	0.58D+02	0.58D+02

THE TWO MODELS EXTREMIZING RHO3 ARE:

	MAX	MIN
RHO1	360.80	332.39
D1	0.18	0.17
DEPTH1	0.18	0.17
RHO2	18270.00	17498.26
D2	15.62	17.74
DEPTH2	15.80	17.91
RHO3	5076.34	4599.80
D3	57.30	57.94
DEPTH3	73.10	75.84
RHO4	0.58D+02	0.58D+02

THE TWO MODELS EXTREMIZING D3 ARE:

	MAX	MIN
RHO1	361.42	332.09
D1	0.18	0.17
DEPTH1	0.18	0.17
RHO2	18078.80	17657.23
D2	16.63	16.71
DEPTH2	16.82	16.87
RHO3	4717.49	4943.43
D3	58.29	56.94
DEPTH3	75.10	73.82
RHO4	0.58D+02	0.58D+02

THE TWO MODELS EXTREMIZING RHO4 ARE:

	MAX	MIN
RHO1	356.60	353.76
D1	0.18	0.18
DEPTH1	0.18	0.18
RHO2	17939.37	17802.99
D2	16.42	16.90
DEPTH2	16.60	17.08
RHO3	4906.69	4755.45
D3	57.33	57.89
DEPTH3	73.94	74.97
RHO4	0.59D+02	0.57D+02

THE TWO MODELS EXTREMIZING DEPTH1 ARE:

	MAX	MIN
RHO1	1494.73	19.26
D1	0.76	0.01
DEPTH1	0.76	0.01
RHO2	17898.02	17809.38
D2	16.62	16.76
DEPTH2	17.38	16.77
RHO3	4832.47	4822.64
D3	57.62	57.60
DEPTH3	75.00	74.37
RHO4	0.58D+02	0.58D+02

THE TWO MODELS EXTREMIZING DEPTH2 ARE:

	MAX	MIN
RHO1	459.27	137.67
D1	0.23	0.07
DEPTH1	0.23	0.07
RHO2	17288.16	18447.83
D2	17.93	15.52
DEPTH2	18.16	15.59

RHO3	4640.44	5023.45
D3	57.59	57.62
DEPTH3	75.75	73.22
RHO4	0.58D+02	0.58D+02

THE TWO MODELS EXTREMIZING DEPTH3 ARE:

	MAX	MIN
RHO1	449.99	146.42
D1	0.23	0.07
DEPTH1	0.23	0.07
RHO2	17447.51	18293.83
D2	17.77	15.65
DEPTH2	18.00	15.72
RHO3	4608.80	5056.73
D3	57.92	57.32
DEPTH3	75.91	73.04
RHO4	0.58D+02	0.58D+02

THE FULL SET OF EIGENVALUES AND EIGENVECTORS:

LOGARITHMIC EIGENVALUES

1	2	3	4	5	6	7
0.30D+03	0.11D+03	0.90D+02	0.72D+02	0.30D+02	0.10D+02	0.14D-01

ESTIMATED LOGARITHMIC SEMIAXES

0.33D-02	0.91D-02	0.11D-01	0.14D-01	0.33D-01	0.98D-01	0.70D+02

PARAMETER EIGENVECTORS

	1	2	3	4	5	6	7
RHO1	-0.105	0.456	-0.419	0.244	-0.198	-0.087	-0.707
D1	0.105	-0.456	0.419	-0.244	0.197	0.085	-0.708
RHO2	0.032	0.664	0.212	-0.296	0.543	0.361	-0.001
D2	0.256	0.305	0.345	-0.250	-0.125	-0.802	0.001
RHO3	0.388	0.188	0.316	-0.053	-0.709	0.458	0.000
D3	0.864	-0.074	-0.277	0.279	0.305	-0.006	0.000
RHO4	0.119	-0.100	-0.555	-0.806	-0.128	0.032	0.000

DATA EIGENVECTORS

-0.02	0.23	-0.23	0.15	-0.26	-0.30	-0.72
-0.02	0.23	-0.21	0.14	-0.22	-0.22	-0.10
-0.01	0.22	-0.19	0.13	-0.18	-0.16	0.14
-0.01	0.22	-0.18	0.11	-0.15	-0.11	0.24
-0.01	0.22	-0.17	0.10	-0.12	-0.06	0.28
-0.01	0.21	-0.15	0.08	-0.06	0.02	0.27
-0.01	0.21	-0.13	0.07	-0.02	0.08	0.22
-0.01	0.21	-0.11	0.05	0.02	0.13	0.15
-0.01	0.21	-0.10	0.04	0.05	0.17	0.09
-0.01	0.20	-0.08	0.02	0.08	0.19	0.04
0.00	0.20	-0.07	0.01	0.10	0.21	-0.01
0.00	0.20	-0.05	0.00	0.12	0.22	-0.05
0.00	0.20	-0.03	-0.02	0.16	0.21	-0.11
0.00	0.20	-0.01	-0.04	0.18	0.18	-0.14
0.01	0.20	0.02	-0.06	0.19	0.14	-0.15
0.01	0.20	0.04	-0.08	0.20	0.09	-0.15
0.01	0.19	0.06	-0.09	0.20	0.04	-0.13
0.02	0.19	0.09	-0.12	0.19	-0.06	-0.08
0.03	0.19	0.12	-0.14	0.17	-0.15	-0.03

0,03	0,18	0,15	-0,15	0,13	-0,21	0,02
0,04	0,17	0,17	-0,16	0,09	-0,25	0,05
0,05	0,16	0,19	-0,17	0,05	-0,26	0,08
0,06	0,14	0,20	-0,16	-0,04	-0,23	0,10
0,08	0,13	0,20	-0,15	-0,11	-0,15	0,09
0,09	0,11	0,20	-0,12	-0,17	-0,06	0,06
0,11	0,09	0,18	-0,10	-0,21	0,02	0,03
0,12	0,08	0,17	-0,07	-0,22	0,08	0,01
0,14	0,07	0,15	-0,05	-0,22	0,13	-0,02
0,16	0,05	0,13	-0,02	-0,21	0,15	-0,03
0,18	0,04	0,11	0,00	-0,19	0,16	-0,04
0,20	0,03	0,10	0,02	-0,17	0,16	-0,05
0,22	0,03	0,08	0,05	-0,14	0,15	-0,05
0,24	0,02	0,06	0,06	-0,10	0,13	-0,04
0,25	0,01	0,05	0,08	-0,07	0,11	-0,04
0,28	-0,01	0,02	0,11	0,00	0,05	-0,03
0,31	-0,02	-0,02	0,12	0,07	-0,01	0,00
0,32	-0,03	-0,05	0,13	0,12	-0,06	0,01
0,31	-0,04	-0,08	0,10	0,15	-0,09	0,02
0,30	-0,05	-0,11	0,07	0,16	-0,12	0,02
0,27	-0,05	-0,14	0,02	0,16	-0,13	0,02
0,23	-0,05	-0,16	-0,03	0,14	-0,11	0,03
0,19	-0,05	-0,17	-0,09	0,10	-0,09	0,03
0,15	-0,05	-0,18	-0,15	0,06	-0,06	0,04
0,10	-0,04	-0,19	-0,21	0,01	-0,03	0,03
0,06	-0,04	-0,19	-0,26	-0,04	0,01	-0,02
0,04	-0,03	-0,18	-0,29	-0,08	0,05	-0,06
0,02	-0,03	-0,18	-0,31	-0,10	0,06	-0,04
0,02	-0,03	-0,18	-0,31	-0,11	0,07	-0,01
0,02	-0,03	-0,18	-0,31	-0,11	0,07	0,01
0,02	-0,03	-0,18	-0,32	-0,11	0,08	0,00

THEORETICAL DATA

1	1	1.50	2574.333127899	3.50
2	1	2.25	3633.004821942	3.50
3	1	3.00	4576.435887495	3.50
4	1	3.75	5422.224188113	3.50
5	1	4.50	6183.887209826	3.50
6	1	6.00	7495.730035810	3.50
7	1	7.50	8575.874998741	3.50
8	1	9.00	9468.480541623	3.50
9	1	10.50	10205.938791508	3.50
10	1	12.00	10812.058813126	3.50
11	1	13.50	11305.496813318	3.50
12	1	15.00	11701.581881827	3.50
13	1	18.00	12248.102785375	3.50
14	1	21.00	12530.585581087	3.50
15	1	24.00	12607.377624438	3.50
16	1	27.00	12526.608745613	3.50
17	1	30.00	12325.845393612	3.50
18	1	36.00	11687.236716842	3.50
19	1	42.00	10875.443747530	3.50
20	1	48.00	10009.241112136	3.50
21	1	54.00	9156.214099361	3.50
22	1	60.00	8352.694629329	3.50
23	1	72.00	6941.655650237	3.50
24	1	84.00	5792.223404173	3.50
25	1	96.00	4856.609494473	3.50
26	1	108.00	4084.109522320	3.50
27	1	120.00	3438.464394510	3.50
28	1	132.00	2892.460825557	3.50
29	1	144.00	2427.352599762	3.50
30	1	156.00	2031.259187184	3.50
31	1	168.00	1695.259090987	3.50
32	1	180.00	1410.710071182	3.50
33	1	192.00	1169.530003143	3.50
34	1	204.00	968.859038027	3.50
35	1	228.00	664.102031136	3.50
36	1	252.00	454.663148215	3.50
37	1	276.00	317.989899736	3.50
38	1	300.00	226.947237204	3.50
39	1	324.00	167.704023677	3.50
40	1	348.00	129.410080193	3.50
41	1	372.00	105.719461583	3.50
42	1	396.00	90.305242785	3.50
43	1	420.00	79.796694980	3.50
44	1	450.00	71.279322855	3.50
45	1	500.00	64.830762237	3.50
46	1	550.00	62.255281784	3.50
47	1	600.00	60.887922449	3.50
48	1	650.00	60.208036126	3.50
49	1	700.00	59.953942158	3.50
50	1	750.00	59.669854006	3.50

```
-1,1,0.,0.,0.
 -1.
 41  15
  4
  0.356D+03,V,   0.180D+00,V
  0.179D+05,V,   0.167D+02,V
  0.483D+04,V,   0.576D+02,V
  0.580D+02,V
  0
  0
```

```
THK33-DIM-01
 113   16    9   1.00000   1.00000  50.00000
 1000.00    100.00     20.00      4.00      1.00      1.00      1.00      1.00
    1.00      1.00      1.00      1.00      1.00      1.00      1.00      1.00
    1.00      1.00      1.00      1.00      1.00      1.00      1.00      1.00
    1.00      1.00      1.00      1.00      1.00      1.00      1.00      1.00
    1.00      1.00      1.00      1.00      1.00      1.00      1.00      1.00
    1.00      1.00      1.00      1.00      1.00      1.00      1.00      1.00
    1.00      1.00      1.00      1.00      1.00      1.00      1.00      1.00
    1.00      1.00      1.00      1.00      1.00      1.00      1.00      1.00
    1.00      1.00      1.00      1.00      1.00      1.00      1.00      1.00
    1.00      1.00      1.00      1.00      1.00      1.00      1.00      1.00
    1.00      1.00      1.00      1.00      1.00      1.00      1.00      1.00
    1.00      1.00      1.00      1.00      1.00      1.00      1.00      1.00
    1.00      1.00      1.00      1.00      1.00      1.00      1.00      1.00
    1.00      1.00      1.00      1.00      4.00     20.00    100.00   1000.00
    1.00      1.00      1.00      1.00      2.00      2.00      2.00      2.00
    2.00      2.00      4.00      4.00      8.00     64.00    512.00
0.600E-02 0.900E-02 0.200E-01 0.500E-01 0.900E-01 0.150E+00 0.300E+00 0.600E+00
0.125E+01
   20     2    57 0.00
   15    19    23    27    31    35    39    43
   47    51    63    67    71    75    79    83
   87    91    95    99
   1.0192    1.0095    1.0043    0.9973    0.9877    0.9758    0.9617    0.9457
   0.9277    0.9075
   55    59
   4
   2
     6.0     200.0
    12.0
 -1000.0
   3
  6500.0     100.0
   700.0     100.0
     8.0
   200.0
   3
  6500.0     100.0
   700.0     200.0
     8.0
  1400.0
   4
 17000.0     100.0
  3800.0      50.0
   450.0     350.0
  1500.0
```

SAMPLE COMPUTER PRINTOUT OF "DIM-2" FINITE DIFFERENCE PROGRAM FOR TWO-DIMENSIONAL MODELING.

THK33-DIM-01

INPUT VALUES

NO. OF X-POINTS= 113 NO. OF Z-POINTS= 16 NO. OF FILTERP.= 9

XSCAL= 1.00 ZSCAL= 1.00 UNIT=50.00

DISTANCES BETWEEN LINES

IN X-DIRECTION (DX) :

1000.00	100.00	20.00	4.00	1.00	1.00	1.00	1.00
1.00	1.00	1.00	1.00	1.00	1.00	1.00	1.00
1.00	1.00	1.00	1.00	1.00	1.00	1.00	1.00
1.00	1.00	1.00	1.00	1.00	1.00	1.00	1.00
1.00	1.00	1.00	1.00	1.00	1.00	1.00	1.00
1.00	1.00	1.00	1.00	1.00	1.00	1.00	1.00
1.00	1.00	1.00	1.00	1.00	1.00	1.00	1.00
1.00	1.00	1.00	1.00	1.00	1.00	1.00	1.00
1.00	1.00	1.00	1.00	1.00	1.00	1.00	1.00
1.00	1.00	1.00	1.00	1.00	1.00	1.00	1.00
1.00	1.00	1.00	1.00	1.00	1.00	1.00	1.00
1.00	1.00	1.00	1.00	1.00	1.00	1.00	1.00
1.00	1.00	1.00	1.00	1.00	1.00	1.00	1.00
1.00	1.00	1.00	1.00	4.00	20.00	100.00	1000.00

IN Z-DIRECTION (DZ) :

1.00	1.00	1.00	1.00	2.00	2.00	2.00	2.00
2.00	2.00	4.00	4.00	8.00	64.00	512.00	

VALUES OF FILTERPOINTS:

0.006	0.009	0.020	0.050	0.090	0.150	0.300	0.600
1.250							

NO. OF TRANSMITTING POINTS= 20 NO. OF RECEIVING POINTS= 2
X-NUMBER OF CENTER OF ARRAY= 57 ANGLE = 0.0 DEGREES

X-NUMBERS OF TRANSMITTING POINTS (ITX) :

15	19	23	27	31	35	39	43
47	51	63	67	71	75	79	83
87	91	95	99				

COEFFICIENTS FOR HOMOGENEOUS EARTH :

1.019	1.010	1.004	0.997	0.988	0.976	0.962	0.946
0.928	0.908						

X-NUMBERS OF RECEIVING POINTS (IRX) :

55	59

RESISTIVITY STRUCTURE

NO. OF X-BLOCKS : 4

NO. OF LAYERS : 2

LAYER	1	RESISTIVITY :	6.0	THICKNESS :	200.0	DEPTH :	200.0
LAYER	2	RESISTIVITY :	12.0				

X-BOUNDARY 1 : -1000.0

NO. OF LAYERS : 3

LAYER	1	RESISTIVITY :	6500.0	THICKNESS :	100.0	DEPTH :	100.0
LAYER	2	RESISTIVITY :	700.0	THICKNESS :	100.0	DEPTH :	200.0
LAYER	3	RESISTIVITY :	8.0				

X-BOUNDARY 2 : 200.0

NO. OF LAYERS : 3

LAYER	1	RESISTIVITY :	6500.0	THICKNESS :	100.0	DEPTH :	100.0
LAYER	2	RESISTIVITY :	700.0	THICKNESS :	200.0	DEPTH :	300.0
LAYER	3	RESISTIVITY :	8.0				

X-BOUNDARY 3 : 1400.0

NO. OF LAYERS : 4

LAYER	1	RESISTIVITY :	17000.0	THICKNESS :	100.0	DEPTH :	100.0
LAYER	2	RESISTIVITY :	3800.0	THICKNESS :	50.0	DEPTH :	150.0
LAYER	3	RESISTIVITY :	450.0	THICKNESS :	350.0	DEPTH :	500.0
LAYER	4	RESISTIVITY :	1500.0				

CALCULATED CURVE

AB/2= 300.00	RHOAPP= 2000.9755
AB/2= 500.00	RHOAPP= 389.2675
AB/2= 700.00	RHOAPP= 91.4225
AB/2= 900.00	RHOAPP= 30.0276
AB/2= 1100.00	RHOAPP= 14.0080
AB/2= 1300.00	RHOAPP= 11.0127
AB/2= 1500.00	RHOAPP= 10.6473
AB/2= 1700.00	RHOAPP= 10.7133
AB/2= 1900.00	RHOAPP= 11.0184
AB/2= 2100.00	RHOAPP= 11.3071

```
THK33-DIM-01
    1     1          300.00     2000.975463867          0.00
    1     1          500.00      389.267547607          0.00
    1     1          700.00       91.422477722          0.00
    1     1          900.00       30.027557373          0.00
    1     1         1100.00       14.007988930          0.00
    1     1         1300.00       11.012730598          0.00
    1     1         1500.00       10.647270203          0.00
    1     1         1700.00       10.713265419          0.00
    1     1         1900.00       11.018385887          0.00
    1     1         2100.00       11.307141304          0.00
   -1     1            0.00        0.000000000          0.00
  4
  2
      6.0      200.0
     12.0
  -1000.0
  3
   6500.0      100.0
    700.0      100.0
      8.0
    200.0
  3
   6500.0      100.0
    700.0      200.0
      8.0
   1400.0
  4
  17000.0      100.0
   3800.0       50.0
    450.0      350.0
   1500.0
```